JPC 419

Report Number
F-66-2

Mass Transfer in Annular, Two-Phase Flow

by

G. R. Schneiter

Final Report
NSF Grant G-21976

February 1966

JET PROPULSION CENTER
PURDUE UNIVERSITY
SCHOOL OF MECHANICAL ENGINEERING
LAFAYETTE, INDIANA

JPC-419 Report Number F-66-2

PURDUE UNIVERSITY

AND

PURDUE RESEARCH FOUNDATION

Lafayette, Indiana

MASS TRANSFER IN ANNULAR, TWO-PHASE FLOW

by

G. R. **Schneiter**

Final Report

NSF **Grant** G-21976
NASA **Contract** NsG 592

Jet Propulsion Center
Purdue University

February 1966

ACKNOWLEDGMENTS

The research reported herein was sponsored for three years by the National Science Foundation, Contract No, G-21976, and for two months by the National Aeronautics and Space Administration, Contract No. NsG 592. Reproduction of this document in whole are in part is permitted for any purpose of the United States Government,

The author wishes to express his gratitude to Dr. M. J. Zucrow, Director of Jet Propulsion Center, and also to Dr. M. R. L'Ecuyer, for their valuable suggestions and recommendations throughout the course of the research program and during the writing of the report.

The assistance of many associates, particularly Messrs. Mezey, Anderson, Bennett, Navarro, and Bottura, is gratefully acknowledged. Gratitude is also expressed to the service and clerical staffs of the Jet Propulsion Center, and to the Aluminum Company of America, which donated material for part of the experimental apparatus. The National Science Foundation Graduate Fellowship and the Donnan Scholarship Award held by the author during the course of the research program are gratefully acknowledged.

TABLE OF CONTENTS

Page

LIST OF TABLES vi

LIST OF ILLUSTRATIONS vii

ABSTRACT x

1 INTRODUCTION. 1

2 REVIEW OF THE LITERATURE, ... 4

2.1 Introduction 4

2.2 Mass Transfer. 5

2.3 Surface Characteristics. 17

2.4 Entrance Region, ... 24

2.5 Experimental' Techniques for Measuring Surface Characteristics 27

2.5.1 Light Absorption Technique. 28
2.5.2 Fluorescence-Spectrometer Method. 32
2.5.3 Miscellaneous Techniques. 33

2.6 Summary. 34

3 EXPERIMENTAL RESULTS. 36

3.1 Mass Transfer Experiments. 36

3.1.1 Description of the Mass Transfer Experiments. 36
3.1.2 Method of Correlation of the Data 40
3.1.3 Results of the Mass Transfer Experiments. 48

3.2 Surface Characteristics Experiments. 60

3.2.1 Description of the Surface Characteristics Experiments. 60

3.2.2 Results of the Surface Characteristics Experiments, ... 65

Page

4 DISCUSSION OF RESULTS. 73

5 CONCLUSIONS AND RECOMMENDATIONS. 84

5.1 Conclusions 84

5.2 Recommendations 85

LIST OF REFERENCES, ... 87

APPENDIX A--NOMENCLATURE. 93

APPENDIX B--DESCRIPTION OF THE EXPERIMENTAL APPARATUS . . 97

B.1 Air Flow System 97

B.2 Water Supply System 100

B.3 Test Section Assembly 103

B.3.1 Injector Assembly. 103
B.3.2 Glass Tube 107
B.3.3 Collector Assembly 108

B.4 Temperature Measurement 110

B.5 Pressure Measurement. 111

B.6 Humidity Measuring Stations 111

6.7 Optical System and Associated Equipment, ... 113

APPENDIX C–EXPERIMENTAL PROCEDURE. 120

C.1 Mass Transfer Experiments 120

C.2 Experiments Concerned with the Film Surface Characteristics, ... 125

APPENDIX D–ANALYSIS GF THE MASS TRANSFER DATA. 131

D.1 Calculation of the Measured Value of Sh 131

D.2 Calculation of the Analytical Value of Sh 133

Page

D.2.1 Introduction. 133
D.2.2 Assumptions 134
D.2.3 Model 135
D.2.4 Equations 135
D.2.5 Application of the Equations to the Calculation of the Heat and Mass Transfer in One Increment of the Test Section . . . 141
D.2.6 Calculation of Sh 143

D.3 Determination of the Correlation Coefficients. . . 145

D.4 Illustration of the Effect of the Water Inlet Temperature on the Over-All Sherwood Number. . . . 146

APPENDIX E--METHOD OF MEASUREMENT OF THE SURFACE CHARACTERISTICS 149

E.1 Film Thickness 149

E.2 Wave Velocity. 154

E.3 Surface Area 156

APPENDIX F--SAMPLE CALCULATIONS. 160

F.1 Measured Sherwood Number 160

F.2 Calculated Sherwood Number 165

F.3 Mean Film Thickness. 165

F.4 Wave Velocity. 167

F.5 Surface Area 167

APPENDIX G--TABULATED DATA 169

LIST OF TABLES

Table		Page
1	Results of the Surface Characteristics Experiments	69
2	Data for Mass Transfer Experiments.	170

LIST OF ILLUSTRATIONS

Figure		Page
1	Schematic Diagram of the Experimental Apparatus	38
2	Effect of x/d on Local Nusselt and Sherwood Numbers	45
3	Mass Transfer Group as a Function of Liquid Reynolds Number for the 8.5 in. Test Section	49
4	Mass Transfer Group as a Function of Liquid Reynolds Number for the 16.5 in. Test Section,	50
5	Mass Transfer Group as a Function of Liquid Reynolds Number for the 23.5 in. Test Section.	51
6	Mass Transfer Group as a Function of Liquid Reynolds Number for the 32.4 in. Test Section.	52
7	Mass Transfer Group as a Function of Liquid Reynolds Number for the 39.9 in. Test Section.	53
8	Sherwood Number Ratio as a Function of Liquid Reynolds Number for the 8.5 in. Test Section	55
9	Sherwood Number Ratio as a Function of Liquid Reynolds Number for the 16.5 in. Test Section.	56
10	Sherwood Number Ratio as a Function of Liquid Reynolds Number for the 23.5 in. Test Section.	57
11	Sherwood Number Ratio as a Function of Liquid Reynolds Number for the 32.4 in. Test Section.	58
12	Sherwood Number Ratio as a Function of Liquid Reynolds Number for the 39.9 in. Test Section,	59
13	Sherwood Number Ratio as a Function of Liquid Reynolds Number.	61

Figure		Page
14	Schematic Diagram of the Optical System	62
15	Typical Oscillograph-Record Camera Traces	
	(a) x = 5.3% in., ...	66
	(b) x = 33.94 in.	68
16	Mean Film Thickness as a Function of Liquid Reynolds Number	71
17	Average Wave Velocity as a Function of Liquid Reynolds Number	72
18	Comparison ot Present Mass Transfer Results with Results of Kafesjian, Plank, and Gerhard (39)	76
19	Comparison of Present Film Thickness Results with Results of Charvonia (11).	79
20	Comparison of Present Wave Velocity Results with Results of Greenberg (27).	82
21	Schematic Diagram of the Air Flow System.	98
22	Schematic Diagram of the Water Flow System. . . .	101
23	Diagram of the Test Section Assembly.	104
24	Photograph of the Test Section Assembly and the Optical System.	105
25	Photograph of the Humidity Measuring Stations . .	112
26	Schematic Diagram of the Optical System	114
27	Schematic Diagram of the Electronic Apparatus . .	115
28	Photograph of the Film Divider.	116
29	Schematic Diagram of the Model Employed in the Analysis.	136
30	Schematic Diagram of an Increment of the Model Employed in the Analysis.	137

Figure Page

31 Effect of the Liquid Reynolds Number on the Mass Transfer Group as Determined by the Analysis. 148

32 Schematic Diagram of an Oscillograph-Record Camera Trace. 155

ABSTRACT

This report discusses an experimental investigation of the mass transfer (evaporation) occurring during the annular, two-phase **flow** of air and water in a vertical pipe, Measurements are made of the mass transfer (evaporation) occurring during the annular, two-phase flow of air and water in a vertical pipe. Measurements were made of the **mass** transfer rate and the surface characteristics of the air-water interface as a function of the following **flow** parameters:

Water Reynolds number:	23 to 1350
Air inlet temperature:	110 to 350 F
Test section length:	8 to 40 in.

All experiments were conducted **at** an air velocity *of* 48 fps in 1.5 in, I.D. glass test sections, The mass transfer rate was determined ,by measuring the increase in the specific humidity of the air stream as it passed through the test section. The surface characteristics (liquid film thickness, wave velocity, and surface area) were measured employing a light absorption technique.

The mass transfer data were correlated satisfactorily **by** the following equations for the local heat and mass transfer:

$$Nu_x = 0{,}0205 \left[1 + \left(\frac{0.588}{x/d}\right)^{0.75}\right] Re_G^{0.8} Pr^{0.33}$$

$$Sh_x = 0.0138 \left[1 + \left(\frac{0.588}{x/d}\right)^{0.75}\right] Re_G^{0.83} Sc^{0.44}$$

When the data were correlated by the aforementioned equations, the water Reynolds number was shown to have no effect on the dimensionless mass transfer coefficient (Sherwood number).

There was a negligible increase in the area of the air-water interface due to the presence of waves on the surface of the liquid film. The measured film thickness and wave velocity values agreed with those of previous investigators employing a 2.5 in. I.D. test section,

1. INTRODUCTION

For the past several decades there has been considerable interest in the two-phase flow of a gas and a liquid through a channel of circular cross section. The regularity and homogeneity of such a flow depends upon such factors as the size and inclination of the channel, the properties and flow rates of the two fluids, and the method employed for injecting the fluids. Certain regimes of flow have been fairly well defined, including the bubbly, slug, stratified, annular, and mist regimes. Also, combinations of regimes such as annular-mist may exist.

The annular regime of flow, in which the pure liquid phase continuously wets the inside surface of a tube and the pure gas phase passes through the core of the tube, has received considerable attention for several reasons. The geometry of the flow pattern is convenient for mathematical analysis, due to the axial symmetry of the flow. Also, a considerable amount of research on the pressure drop, heat transfer, and mass transfer in single-phase pipe flow has been conducted, and many of those results may be applied to annular, two-phase flow, whereas such is not the case in other regimes of two-phase flow.

In addition to the usefulness of the annular flow geometry in making comparisons with theoretical two-phase flow analyses and the experimental results of single-phase systems, it is prevalent in many industrial processes. Perhaps the predominant example of annular, two-phase flow is currently found

in nuclear reactor techno1ogy, where two-phase flow occurs in heat exchanging equipment. Another application of annular, two-phase flow is in the film cooling of the combustion chambers and nozzles of rocket motors. It was the latter application which led to the interest in annular, two-phase flow at the Jet Propulsion Center.

The research reported herein concerns the evaporation of liquid from the film wetting the wall of a tube into the gas stream. The evaporation process is driven by the interaction between the two phases, and is independent of conditions external to the tube (e.g., heat transfer through the wall of the tube).

In the case of an evaporation process, as opposed to, say, the absorption of gas by the liquid phase, the rate of mass transfer is primarily controlled by the properties and rate of flow of the gas phase. Thus the process is said to be gas-film controlled. Nearly all of the investigations of mass transfer in annular, two-phase flow systems have been for the most part concerned with the effects af the gas flow and the properties of the fluids on the rates of mass transfer. Only recently has the effect of the liquid flow rate been included in the analysis of observed rates of mass transfer.

The subject investigation was initiated to determine the effect of the 1iquid flow rate, and particularly the surface characteristics of the liquid film, on the mass transfer process. The system investigated comprised a vertical test section with downward, concurrent flow of the two phases, air and water.

Since the driving force for mass transfer in such a system is the difference between the partial pressure of the vapor in the gas phase and

the vapor pressure of the liquid at the surface of the liquid film, and the latter is a strong function of the temperature of the surface of the film, it is apparent that heat transfer plays an important role in the mass transfer process. It was necessary, therefore, also to investigate the effects of the heat transferred from the gas to the liquid. Accordingly the temperature difference between the gas and the liquid was varied from 40 F to 280 F.

It was also of importance to study the variation in the local rates of heat and mass transfer along the tubular channel; those rates were highest near the entrance region of the channel. Such entrance effects are particularly important in film-cooling applications, where the length-to-diameter ratio of the film-cooled section is usually quite small, The subject investigation was conducted, therefore, employing tubular test sections of different lengths; the L/d values ranged from 5.7 to 26.6.

Correlation of the data was accomplished employing equations for the local values of heat and mass transfer along the length of the test section. The form of the equations was such that the variations in the mass transfer caused by variations in the liquid, and the length of the test section were accounted for,

Simultaneously with the mass transfer studies, a program was conducted to determine experimentally the characteristics of the liquid film, including the film thickness, the wave velocity, and the surface area of the gas-liquid interface.

2. REVIEW OF THE LITERATURE

2.1 Introduction

The rate of growth of the literature concerned with two-phase, gas-liquid flow has increased enormously in recent years, due for a large part to the increasing need for the information necessary for analyzing and designing fluid flow systems in which part or all of the flowing medium is a two-phase flow. Probably the major impetus has come from the design of heat exchangers for nuclear reactors, although other applications such as liquid film cooling, ablation, refrigeration, and chemical processing have also required considerable progress in the understanding of two-phase, gas-liquid flow systems.

Many reviews of the literature have appeared in recent years concerned with various aspects of two-phase flow. Recently a comprehensive index to the literature was published covering practically all aspects of gas-liquid two-phase flow (24,25)*. The author hopes that the index will be kept up-to-date since it provides an excellent starting point for a review of the literature. As pointed out by Gouse (25), if the present rate of growth of the literature on two-phase flow continues, approximately 750 papers will appear in the literature for 1965.

Among the recent reviews of the literature are those of Bennett (5), Charvonia (10), and Govier (26), the last of which is concerned with vertical flow only. Also, an excellent review article by Fulford (22),

---

* Numbers in parentheses refer to items in the Bibliography

which is concerned nominally with the flow of thin films, spends a considerable amount of time on thin films flowing in the presence of a gas stream, as in the case of annular, two-phase flow. Fulford's article contains a useful chronological resumé of papers on film flow and related topics.

The research described herein is concerned with the mass transfer occurring in annular, two-phase flow, and different factors which influence that mass transfer. Two factors of particular interest are the characteristics of the gas-liquid interface, and the effect of the entrance region. Consequently, the literature review presented herein was restricted to that literature pertinent to the aforementioned two factors. The literature review is presented under the following subject headings: Mass transfer, surface characteristics, entrance effects, and experimental techniques.

2.2 Mass Transfer

The classical work concerned with mass transfer in annular, two-phase flow was published over 30 years ago by Gilliland and Sherwood **(23).** Due to the importance of that work, it is reviewed in somewhat greater detail than are other references. The investigation included an extensive experimental program, during which measurements were made of the rates of evaporation of nine different liquids into air flowing in a vertical wetted-wall column. Both laminar and turbulent air flow .conditionswere investigated, with both countercurrent and concurrent flow. The test section was a vertical pipe, 1.05 in. I. D. and 46 in. long. In all of the experiments the liquid volumetric flow rate was approximately 43 cu in. per min. (For the experiments with water that flow rate correspdnded to a liquid Reynolds

number of from 750 to 1200, depending on the temperature.) The air flow rate was varied over a range of Reynolds numbers from 2000 to 27,000, and the static pressure was varied from 2.13 to 45.1 psia, The Schmidt numbers for the different liquids ranged from 0.60 to 2.26. The temperature of the air was within 6 F of the liquid inlet temperature in nearly all of the runs, varying from 79 to 133 F. Consequently the heat transfer between the two phases was negligible.

Evaporation rates were determined by measuring the rate of decrease of the volume of the recirculating liquid in the flow system, the liquid flow system being closed except for the liquid which evaporated in the test section and was carried out by the air stream. Also, in the case of water, the evaporation rates were determined from the difference in the humidity of the air stream entering and leaving the test section; wet-bulb and dry-bulb temperature measurements were employed for determining the humidity of the flowing air. The results obtained by the two methods for determining the evaporation of the liquid were in good agreement.

The data were correlated by dimensionless equations similar to those employed in heat transfer correlations. The following equation gave the best correlation of the data for the case of turbulent flow (23). Thus

$$\frac{d}{x_D} = 0.023 \left(\frac{\rho V d}{\mu}\right)^{0.83} \left(\frac{\mu}{\rho D}\right)^{0.44} \qquad (1)$$

where d = inside diameter of the column, ft

x_D = effective film thickness of the gas, ft

V = mean gas velocity, fps

ρ = gas density, slugs/ft^3

μ = gas dynamic viscosity, lb-sec/ft^2

D = diffusion coefficient for the vapor-gas system, ft^2/sec

The effective film thickness of the gas x_D is defined by Gilliland and Sherwood as that imaginary thickness of stagnant gas which would offer the same resistance to diffusion as the resistance actually measured for the flowing gas. It can be shown that in equation 1, the term on the left hand side is equivalent to the following (3). Thus

$$\frac{d}{x_D} = \frac{h_M d}{D}\left(\frac{p_{BM}}{P}\right) \qquad (2)$$

where p_{BM} = log mean partial pressure of the gas through which the vapor diffuses, psia

P = static pressure of the gas-vapor misture, psia

h_M = mass transfer coefficient, fps

The mass transfer coefficient, h_M, is defined by

$$W_{ev} = h_M A(\Delta C_m) \qquad (3)$$

where W_{ev} = weight rate of evaporation, lb/sec

A = interfacial area, ft^2

ΔC_m = log mean difference between the concentration of the vapor in the gas stream and the concentration of the vapor at the interface, lb/ft^3

Substituting equations 2 and 3 into equation 1 yields

$$\frac{h_M d}{D}\left(\frac{p_{BM}}{P}\right) = 0.023\left(\frac{\rho V d}{\mu}\right)^{0.83}\left(\frac{\mu}{\rho D}\right)^{0.44} \qquad (4)$$

Let

Sh = Sherwood number = $h_M d/D$

Re_G = Reynolds number for the flowing gas = $\rho Vd/\mu$

Sc = Schmidt number = $\mu/\rho D$

Substituting the above relationships into equation 4, one obtains

$$Sh\left(\frac{p_{BM}}{P}\right) = 0.023 \quad Re_G^{0.83}\ Sc^{0.44} \qquad (4a)$$

If the partial pressure of the diffusing vapor is very small compared with the static pressure of the gas mixture P, then $p_{BM}/P \approx 1$, and that ratio can be omitted from equation 4.

Experiments where the gas flow was turbulent indicated that the velocity of the downward moving liquid film had no influence upon the rate of mass transfer; the same results were obtained with the air flowing either upward or downward. Because the test section was relatively short, the aforementioned results were explained by the velocity profile of the gas stream not having sufficient time to adjust significantly to the velocity of the surface of the film. It was also observed that the presence of the liquid film had no effect upon the pressure drop, across the test section, due to wall friction.

Chilton and Colburn (13) correlated the mass transfer data of several investigators, including Gilliland and Sherwood (23), by means of the so-called j-factors, which they had shown to be useful for correlating heat

transfer data with wall friction data. The j-factor for mass transfer, j_D, is defined by (13)

$$j_D = \frac{Kp_{BM}}{(G/M_m)} \left(\frac{\mu}{\rho D}\right)^{0.56} \quad (5)$$

where G = mass velocity, lb/hr-ft^2

K = molar mass transfer coefficient, lb moles/hr-ft^2-atm

M_m = mean molecular weight

p_{BM} = log mean partial pressure of the inert component, atm

A plot of the j-factor for mass transfer as a function of gas Reynolds number, Re_G, was shown to be approximately similar to the plot of the wall friction factor (1/2) f as a function of Re_G. By definition

$$(1/2)\ f = \frac{(\Delta P)g}{\rho V^2} \left(\frac{S}{A}\right) \quad (6)$$

where ΔP = pressure drop, psf

g = gravitational constant, ft/sec^2

V = linear velocity, fps

S = flow cross sectional area, ft^2

A = surface area, ft^2

Chilton and Colburn point out that the exponent 0.56 in equation 5 is based upon the correlation equation due to Gilliland and Sherwood (equation 1). They also point out that the exponent 0.67 determined empirically applying the analog between heat transfer and fluid friction,

slightly improves the correlation of the data for water, but slightly decreases the-agreement in the case of data for organic liquids. Subsequent investigators generally adopted the exponent 0.67 instead of 0.56.

Considerable experimental data, for example those of Barnet and Kobe (3), and Jackson and Ceaglske (36), have established the validity of the correlations discussed above. In many cases, however, there are disagreements in magnitudes of the empirically determined coefficients. Some of those discrepancies are discussed later in the present section.

An extensive discussion of the different equations employed for correlating the data obtained for mass transfer processes are presented in the text of Sherwood and Pigford (56), and others.

Two papers by Cairns and Roper (8,9) describe experiments on the heat and mass transfer in a wetted-wall column where the flowing air had large values of humidity. The object of those experiments was to determine the validity of the inclusion of the term p_{BM}/P on the left-hand side of equation 4. In the experiments discussed up to this point the concentration of the diffusing medium was so small that $p_{BM}/P \simeq 1.0$. Accordingly, Cairns and Roper varied the mole fraction of the diffusing medium from 0.03 to 0.85 and determined the influence of varying p_{BM}/P upon the correlation of the data by equation 4. Their experimental results indicated equation 4 correlated the data for the mass transfer from the gas to the liquid if the ratio p_{BM}/P is replaced by (p_{BM}/P) 0.83

Two important contributions were made by Linton and Sherwood (44) in their-work concerning the rate of solution of cast materials in water under various conditions of flow and geometry.

The materials investigated were benzoic acid, cinnamic acid, and betanaphtol; the variation in the Schmidt number ranged from 1000 to 3000, approximately 1000 times the values previously investigated by Gilliland and Sherwood (23). The results indicated that the exponent on the Schmidt number, in the Chilton-Colburn correlation equation (equation 5), should be 0.67. Reference 44 also investigated the variation of the rate of mass transfer with the distance from the entrance to the test section. Those results will be discussed in Section 2.4

Schwarz and Hoelscher (54) conducted experiments in a 3.33 in. I. D. by 4 ft long wetted-wall column; and measured the vapor concentration profiles at 4 distances from the inlet to the column. From their results they calculated values for the eddy diffusivities of momentum and mass, and the local rates of mass transfer. Rippling of the liquid film was eliminated by adding a wetting agent to the water. Somewhat similar experiments were conducted by Dhanak (19) in a horizontal, 1.925 in. by 12 in. rectangular channel 3 ft long, in which one or both of the longer walls, which were covered with felt, could be wetted. Measurements of velocity and concentration profiles and turbulence correlations were employed for calculating values of the eddy diffusivities of momentum and mass; the diffusivity of mass was found to be significantly higher (about 75 per cent) than that of momentum.

McCarter and Stutzman (46) conducted experiments in a 7.5 cm I. D. vertical glass tube with the object of determining if the eddy diffusivity had a significant influence upon the total resistance to mass transfer, They calculated the thicknesses of the laminar and buffer layers in the

gas phase, applying fluid mechanics considerations, and compared the calculated thicknesses with calculated values of effective film thickness based on mass transfer data. Reasonable agreement was found between the laminar layer thicknesses and the effective film thicknesses. The results obtained from their experiments wherein the length of the column was varied from 14 to 40 in. indicated that the length of the column had no effect on the effective film thickness.

Several investigators of mass transfer in annular, two-phase flow have noticed that there are inconsistencies in published results of different investigators. Kafesjian, Plank, and Gerhard **(39)** analyzed those inconsistencies and concluded that in most cases they could be satisfactorily explained by considerations pertinent to the conditions of the liquid film. They analyzed the data for the evaporation of water into air reported by eight different investigators. They classified the experiments into two cases: (a) rippling films, and (b) non-rippling films. Plots were made of the mass transfer group $Sh(p_{BM}/P)Re_G^{-0.83}$ as a function of liquid Reynolds number, Re_L, for (a) rippling films, and (b) non-rippling films; the liquid Reynolds number, Re_L, is defined by

$$Re_L = \frac{4\,G'}{g\mu_L} \tag{7}$$

where G' = inlet peripheral liquid flow rate, lb/sec-ft

g = gravitational constant, ft/sec^2

μ_L = dynamic viscosity of the liquid, $lb\text{-}sec/ft^2$

The gas Reynolds number, Re_G, was based upon the velocity of the gas relative to the pipe for the case of rippling films, and on the velocity of the gas relative to the surface of the film for the case of non-rippling films. No dependence of the mass transfer group on liquid Reynolds number was noted for the case of non-rippling films. The results obtained for rippling films, however, showed a definite increase in the mass transfer group with liquid Reynolds number; the logarithmic plot of the mass transfer group $Sh(p_{BM}/P)Re_G^{-0.83}$ as a function of the liquid Reynolds number, (see equation 7), could be approximated by a straight line. Accordingly, reference 39 proposed the following equation for correlating the data for mass transfer involving rippling films. Thus

$$Sh\left(\frac{p_{BM}}{P}\right) = 0.0065\ Re_G^{0.83}\ Re_L^{0.15} \qquad (8)$$

(The Schmidt number was not included because it varied only a few per cent in the subject experiments.)

With the exception of approximately half of the data of Gilliland and Sherwood (23), all of the data mentioned in this chapter, as well as those analyzed by Kafesjian, et al., were obtained under conditions of countercurrent flow; that is, the liquid was introduced at the top of the column and the gas entered at the bottom. Kafesjian, et al., state that equation 8 may be utilized for correlating the data based on concurrent flow obtained by Gilliland and Sherwood, because it does not involve the Reynolds number based upon the velocity of the gas relative

to the surface velocity of the liquid. Although the logarithmic plot of the data for concurrent flow, due to Gilliland and Sherwood, also may be represented by a straight line, the range of liquid Reynolds number for those data is much too small compared with its scatter to warrant a conclusion regarding the application of equation 8 as a general correlation equation for mass transfer with concurrent flow.

As a possible explanation of the results of their analysis, Kafesjian, et al. (30), suggest that an increase in the surface area of the film may be at least partly responsible for the results noted, but do not go into any detail on that subject. Kafesjian (38), however, did give considerable attention to that matter, based upon the work of Tailby and Portalski (59), which apparently came to his attention following the submission of reference 39. Those considerations are discussed in Section 2.3.

An experimental program concerned with mass transfer in concurrent, annular, two-phase flow was conducted at the Jet Propulsion Center by Merey (48) as a part of the subject research program. Mezey's work comprised a systematic investigation of mass transfer in a 1.502 in. I. D. vertical glass tube over the following ranges of parameters:

Gas (air) Reynolds number	15,500 to 228,000
Liquid (water) Reynolds number	91 to 515
Inlet gas temperature	104 to 355 F
Test section length	8.5 to 40.5 in.

The results obtained were presented in the form of a correlation equation, similar to equation 8, for each tube length investigated. The plots presented the Sherwood number as a function of the gas and the liquid

Reynolds numbers. Due to certain shortcomings of the experimental apparatus a satisfactory energy balance was not obtained, and although the over-all results are generally valid, they are not sufficiently reliable to permit conclusions regarding the effect of liquid flow rate on tne mass transfer coefficient.

Anderson, Bollinger, and Lamb (2) conducted studies of the absorption of ammonia for the concurrent flow of air and water in a horizontal pipe, primarily in the annular-mist regime, Their measurements allowed calculations to be made of the rates of interchange of droplets from the film into the air stream and back to the film. The results were correlated in terms of j-factors which were found to be functions of the gas and liquid Reynolds numbers. Since the subject investigation is concerned with annular flow without droplets present in tne gas core, no details of the work discussed in reference 2 will be presented; it is cited because it presents data under conditions arising from increasing either the liquid or the gas flow rate to values higher tnan those investigated by the author. It should also be noted that considerable work on annular-mist flow has been and is being conducted at several laboratories, and certain aspects of that work are also applicable to annular, two-phase flow; an excellent review of tnat work has been presented by Silvestri (57).

Russian investigators of heat and mass transfer from flat plates (21, 45) recomniend the inclusion of the Gukhman number, Gu, in Nusselt-type heat and mass transfer correlation equations. By definition

$$Gu = (T_a - T_b)/T_a \qquad (9)$$

where

T_a = temperature of the surrounding medium (free stream temperature), R

T_b = temperature of the state of adiabatic air saturation (wet-bulb temperature corresponding to free stream conditions), R

The Russian investigators claim that by including the Gukhman number, to an appropriate power, in the correlation equations the peculiarities of heat and mass transfer in liquid-evaporation processes is taken into account; it accounts for the variations in the free stream temperature and also the effect of the humidity of the free stream air., In their correlations the Russian investigators evaluate the transfer coefficients at the free stream temperature, as opposed to the mean temperature of the boundary 1ayer.

In the literature concerned with annular, two-phase flow that has been reviewed thus far, the correlation of the data on rates of mass transfer has been accomplished by assuming that the driving force is the prevailing concentration gradient; that is, the difference between (a) the vapor pressure of the liquid film and (b) the partial pressure of the vapor in the gas stream, usually a bulk or mixing cup value of the partial pressure. Such a method of correlation, however, requires an accurate knowledge of the suface temperature of the liquid film, since the vapor pressure is usually a strong function of temperature. Most of the experiments reported were conducted with the two media at near room temperatures and with relatively large liquid flow rates, so that there was no appreciable change in the liquid temperature.

Liquid film-cooling experiments, on the other hand, for example as

reported in references 20 and 41, have generally been conducted with the gas stream temperatures much higher than the boiling point of the liquid film; that is, the saturation temperature corresponding to the local static pressure. In such cases it is generally assumed that the temperature of the liquid film is that corresponding to the local boiling point, and the driving force for the mass transfer process is the rate of heat transfer from the gas stream to the film. The amount of mass transfer, the evaporation of liquid which occurs, is that corresponding to the equality between the heat of vaporization for the liquid and the heat transferred to the film from the hot gas stream.

Knuth (42) points out that the temperature of the liquid film is actually somewhat below that of the boiling point of the film, due to the heat absorbed in the evaporation process. The difference, however, has no significant effect on the evaluation of the driving force (temperature difference); the temperature difference between the gas stream and the film greatly exceeds the difference between the actual and assumed (boiling point) temperature of the film. Hence, for the gas temperatures occurring in rocket motors, it is satisfactory to assume that the film temperature is the same as the boiling point temperature for the liquid.

2.3 Surface Characteristics

As pointed out in Section 2.2 experiments concerned with the problems pertinent to mass transfer in annular, two- phase flow have been conducted for more than 30 years. The roughness of the liquid film, generally referred to as rippling, has been noted by practically all of the investigators. It is only recently, however, that quantitative experiments concerned with the

configuration of the surface of the liquid have been conducted. For the most part, the investigations of the surface characteristics of the films have been concerned with determining the effect of the roughness of the surface on the pressure drop experienced by the gas phase. The results of such investigations, up to 1958, were reviewed by Charvonia (10), and subsequent experiments have been reported by Charvonia (11), Chien and Ibele (12), and others.

Stirba and Hurt (58) suggested that an increase in the surface area, due to rippling, might be at least partly responsible for the increase in the absorption in the case of rippling films. Based upon visual observation and photographs, they estimated that the increase in surface area due to rippling was probably less than 50 per cent.

Lilleleht and Hanratty **(43)** employed a light absorption technique in their investigation of the interfacial structure of a moving surface of water over which a stream of air was blown. They presented measurements of the root-mean-square displacement of the surface and its frequency spectrum. No information was reported on surface area.

Several papers have been presented reporting the work of Portalski (52). Two of them are of particular interst here.

Tailby and Portalski (59) extended the theoretical study of wave motion due to Kapitsa in an effort to predict (a) the liquid Reynolds number at the inception of waves, and (b) the increase in surface area due to the presence of waves. These theoretical developments are supported by experimental studies conducted on a vertical flat plate down which a film of liquid flowed. The apparatus was designed so that a stream of air could

flow across the free surface in either an upward or downward direction. The heights of waves were measured by means of capacitance probes, the heads of which were 2 mm by 4.5 mm. The probes were mounted a small distance from the flat plate. The presence of the liquid film on the plate changed the capacitance between the probe and the plate, and by proper calibration the output from the probe could be related to the thickness of the liquid film. The resulting wave profiles were recorded on a strip chart recorder, No mention was made of either the speed of the strip chart or how that speed was determined. The only reference made to the chart speed was that a "synchronized paper feed'.' was employed, As is pointed out in Appendix E of the present report, it is important to know the scale in the direction of film flow on a film thickness profile. That scale must be based upon the wave velocity, which was available to the authors.

Considerable percentage increases in the surface area were predicted by theory. For example, it was predicted that the surface area of a water film flowing at a Reynolds number of 1000 experiences approximately a 19 per cent increase., Furthermore, for a Reynolds number of only 700 the increase in surface area for a film of 2-propanol is nearly 150 per cent, In support of the theory one experimental point was compared with the theory (3.3 per cent increase in surface area) for the flow of 82% glycerin solution at a Reynolds number of 12.0. Two methods were employed for measuring the length of the recorded thickness-time trace. The ratio of the measured length of the trace to the straight line distance over which the length was measured was assumed equal to the ratio of the areas of the rippled and smooth films. The methods employed were (a) an opisometer

(as used for measuring distances on maps), and (b) fitting a thread on the curve. The increases calculated by the two methods fell on opposite sides of the theoretical line. It is Unfortunate that experimental results were not given for more than one datum point, since agreement at some of the more extreme conditions would have given strong support to the theory.

In his discussion of the paper of Tailby and Portalski (59) Sawistowski points out the wide discrepancies between the results of Tailby and Portalski and those of Brauer (7). He raised the questions of whether Brauer's results were completely wrong, or whether Kapitza's theory perhaps did not apply over the range of viscosities included in Brauer's work. (Brauer measured the increase in the surface area of films flowing down the outside of a vertical cylinder under the influence of gravity by analyzing silhouette photographs of the cylinder.) According to Portalski the photographic technique of Brauer was quite inadequate, the troughs of the surface waves at the boundary of the photographic image were always masked by the crests of waves closer to the camera, and it was not surprising that Brauer's results for the increase in surface area were very low. Portalski did not comment on the question regarding the applicability of Kapitza's theory.

Examination of the papers of Brauer (7) and Belkin, MacLeod, Monrad, and Rothfus (4), who employed similar techniques for the measurement of wave profiles, indicates that Portalski's criticism is somewhat justified, for there is some masking of the wave troughs by the adjacent crests. The effect of such masking on the determination of the wave geometries is, however, not nearly as large as was indicated by Portalski. It is the opinion

of the writer that in most cases the aforementioned masking would not have a significant effect upon the determination of the surface area of the film. Consequently, the results of Brauer should not be discounted.

Fulford (22) points out that the theory of Kapitsa is valid only if the wavelength is more than 13.7 times the film thickness; the corresponding liquid Reynolds number is approximately 200. On the other hand, the relationship for the film surface area developed by Tailby and Portalski (59) was claimed to be valid up to a liquid Reynolds number of approximately 1200.

Finally, it should be noted that the theory set forth by Tailby and Portalski (59) applies only to wavy laminar film flow, and no account is taken for the effect of a gas stream flowing in either direction past the vertical free surface.

In another paper reporting Portalski's research (52), Tailby and Portalski (60) present the results of experiments conducted on a vertical flat plate down which a liquid flowed, and over which was passed a vertical stream of flowing air, Measurements were made of the so-called "depth of wave inception" (the distance from the knife edge at the top of the plate where the liquid flowed onto the plate to the point where waves first appeared on the film) as a function of liquid (water) Reynolds number, gas (air) Reynolds number, and the direction of the air flow. At all water Reynolds numbers, the depth of wave inception was less for the cases with air flow than for those without air flow. Increasing the air flow rate in a given direction decreased the depth of wave inception, And in all cases, for given values of air and water Reynolds numbers, concurrent (downward) air

flow resulted in a smaller depth of wave inception than countercurrent (upward) air flow.

Kafesjian (38) attempted to correlate the increase in surface area of the film with the physical properties of the flowing liquid. He introduced certain simplifying approximations in the expression due to Tailby and Portalski (59), and developed the following expression for the fractional increase in surface area ΔA. Thus

$$\Delta A = 4{,}2\ (10)^{-6}\ \frac{(g\nu)^{\frac{1}{3}}\mu}{\sigma}\ \ Re_L^{5/3} \qquad (10)$$

where

g = gravitational constant force, ft/sec^2

ν = kinematic viscosity of the liquid, ft^2/sec

μ = dynamic viscosity of the liquid, $lb\text{-}sec/ft^2$

σ = dynamic surface tension of the liquid, lb/ft

Re_L = liquid Reynolds number

The general relation for mass transfer in annular, two phase flow then became (38)

$$Sh\ \frac{p_{BM}}{p} = 0.0175\ [1+4.2\ (10)^{-6}\ \frac{(g\nu)^{\frac{1}{3}}\mu}{\sigma}\ \ Re_L^{5/3}]\ Re_G^{0.83}\ \ Sc^{1/2} \qquad (11)$$

Equation 11 was recommeded by Kafesjian for calculating the mass transfer in the absence of experimental data.

The motion and frequency of large disturbance waves in the upward, annular, two-phase flow of air-water mistures were studied by Hal1,

Taylor, Hewitt, and Lacey (28). An extension of that work was reported by Nedderman and Shearer (50). Large disturbance waves are characterized by a milky appearance, the ripping of droplets from the crests, and the fact that the waves keep their identity for the entire length of the test section. Such waves occur only in the annular-mist regime (when droplets are present in the flowing gas stream); no further consideration will be given to them.

In addition to his comments on Portalski's conclusions, Fulford (22) includes in his review of thin film flow a brief discussion of the increase of interfacial area due to waves. Most of the references cited indicated that the increases in the surface area are much smaller than those predicted by Tailby and Portalski (59). Fulford concludes that although there must be a measurable increase in the interfacial area due to the waviness of the surface to the film, it is unlikely that the increase in that area is of practical importance, An important phenomenon in the applications of film flow, according to Fulford, is the mixing effect promoted by the surface waves. He cites numerous references to different theoretical and experimental studies that indicate, in general, that the waves cause flow fields which would otherwise be laminar to become turbulent. The resulting increase in the mixing due to the waves increases the rates of heat and mass transfer. Much of the work cited includes studies utilizing dye injection; observation is made of the breakup of a stream of dye in an attempt to visualize the regions of laminar and turbulent flow.

2.4 Entrance Region

Consider a fluid of uniform temperature and species concentration, and having a fully developed velocity profile as it flows through a channel. At a certain cross-section of the channel the transfer of heat or mass begins due to a change in the temperature of the wall, or a change in the concentration of a species at the wall. The region immediately following that cross-section is termed the entrance region.

Both theoretical and experimental investigations have substantiated the fact that heat and mass transfer coefficients are considerably larger in the entrance region. The increases in the values of those coefficients are due to the fact that the rate of heat or mass transfer is proportional to the gradient of the driving force, and at the cross-section of the channel where the heat or mass transfer begins, there is a discontinuity in the driving force at the wall of the channel, so that the gradient becomes infinite. Consequently, the local rate of transfer and the local transfer coefficient based upon that rate of transfer are also infinite. As either the temperature or concentration field develops downstream from the entrance, the gradient at the wall decreases, and finally approaches a constant value as the field becomes fully developed.

The analysis of Deissler (17) extended previous work on fully developed flow to the entrance region of pipe flow and enabled the prediction of the Nusselt number as a function of Reynolds number and x/d.

Good agreement is shown between Deissler's theory and the heat transfer experiments with air of Boelter, Young, and Iversen (6). Subsequent

extensions of that analysis by Deissler to include mass transfer and the effects of high Schmidt and Prandtl number are reported in reference 18.

Wolf (62) extended Deissler's analysis to obtain a better representation of the variation of the physical properties of the flowing fluid for the case of heat transfer in the entrance region of a pipe. Included in that work is a review of the pertinent literature up to 1957, Experimental studies employing air and carbon dioxide show good agreement with the theory (62).

Hartnett (30) experimented with water and with oil flowing in a 0.652 in. I.D. tube, and obtained good agreement with the analysis due to Deissler. He found that the local heat ransfer coefficient decreased to within one per cent of the fully developed value about 15 diameters from the cross-section where heating began.

Davey (16) conducted experiments on the cooling of air in a 2 in, I.D. copper tube and also obtained good agreement with Deissler's analysis. Davey correlated this data over the range $1 < x/d < 8$ by the equation

$$Nu_x = 0.036\ Re_G^{0.8}\ Pr^{0.4}\ \left(\frac{x}{d}\right)^{-0.2}\ \left(\frac{T_G}{T_W}\right)^{0.18} \qquad (12)$$

where

Nu_x = local Nusselt number

T_G = bulk gas temperature, R

T_W = wall temperature, R

Experiments indicated that for s/d less than 1, values of the heat transfer

coefficient were at least 50 per cent larger than the largest value determined for x/d greater than 1.

Relatively little work has been done concerning local values of mass transfer. As can be noted from Section 2.2, most of the data obtained for mass transfer in tubes have been from studies of essentially fully developed mass transfer, i.e., in tubes of relatively large L/d ratios. As mentioned above, the analysis due to Deissler (18) also applies to the case of mass transfer. In fact, he presents identical curves for heat and mass transfer; they differ only by the substitution of the Sherwood and Schmidt numbers for the Nusselt and Prandtl numbers, respectively, for the case of mass transfer.

Linton and Sherwood (44) conducted experiments on mass transfer in which they measured the rate of solution of cast pipes made of benzoic acid, cinnamic acid, and betanaphtol into the water flowing through the pipes. The pipes were constructed from several short cylinders attached together. Mass transfer in turbulent flow was calculated from measurements of the decrease in the weight of the cylinders over a period of time during which water flowed through the pipe. Thus the effect of L/d could be determined by noting the different values of the mass transfer coefficients for the different sections. The authors noted a slightly smaller decrease in mass transfer coefficient with increased L/d than was reported by Boelter, Young, and Iversen (6). The data were correlated by j_D (see equation 5), and it was stated that the effect of tube length on j_D was negligible for values of L/d greater than approximately 6.

Schwarz and Hoelscher (54) in their wetted-wall column studies measured the mass flux of water vapor in the air stream at 4 different elevations of their vertical test section; they computed local rates of mass transfer at each of those elevations. The results indicated that the rate of mass transfer was approximately the same at all of the elevations investigated, including elevations from 5.6 to 25.5 diameters from the gas inlet. They concluded, therefore, that the rate of mass transfer was constant for values of $L/d > 6$, approximately.

McCarter and Stutzman (46), based on their wetted-wall column investigations, found no appreciable difference in rates of mass transfer obtained in two columns of L/d values of 4.7 and 13.3. Their data presented in graphical form, do indicate, however, that there are differences amounting to as much as 25 per cent for some of the liquids they investigated,

2.5 Experimental Techniques for-Measuring Surface Characteristics

A broad coverage of experimental methods employed in two-phase flow experiments is given in a survey article by McManus (47). In that article he discusses the methods which are applicable to making measurements in the different regimes encountered in gas-liquid flow in pipes, including the annular regime discussed herein,

Of more pertinence to the experimental investigations of the writer are several articles written by staff of the Atomic Energy Research Establishment, Harwell, (14,31,32,33) which are concerned with studies of films in annular, two-phase flow. Discussions are presented of several

methods for measuring film thickness, including conductance probes, contact probes, light absorption, and a recently developed fluorescence-spectrometer method. For detailed discussions of the several other experimental techniques, the reader is referred to the afprementioned works and their cited references. The discussion herein will be limited to the light-absorption method, the fluorescence-spectrometer method, and two other methods which were published recently.

2.5.1 Light Absorption Technique

The light absorption technique for obtaining an instantaneous measurement of film thickness, the method employed in the subject investigation, was developed by Greenberg (27) at the Jet Propulsion Center, Purdue University. It was subsequently employed by Charvonia (11), Ammann (1), and Miller (49) also at that laboratory. The underlying principle of the light absorption technique is Beer's law (29). According to that law the absorption of light by a solution of a solute in a liquid solvent and may be written in the form

$$I = I_o e^{-bct} \tag{13}$$

where I_o = intensity of the incident light

I = intensity of the transmitted light

b = absorption coefficient for unit concentration of the solute

c = concentration of the solute

t = distance the light passes through the solution

In the experiments conducted at the Jet Propulsion Center, the solute (Nigrosine dye) was dissolved in the solvent (water or a mixture of glycerine and water) which was the liquid phase of the two-phase flow system. The light intensities were detected by means of a photo-multiplier tube, and the product bc determined by ,calibration. Detailed descriptions of the theory governing the light absorption technique are presented in references 11 and 27.

Recently some criticism of the light absorption technique has appeared in the literature, The following comments are, therefore, pertinent. McManus (47) commented that, since with vented air-liquid systems liquid evaporation is appreciable, constancy of dye strength is a problem, He stated that in a critical investigation of the light absorption technique, Hewitt and Lovegrove (32) concluded that light scattering effects were of such magnitude that the method was unsuitable for use where thin films are involved, Actually McManus incorrectly generalized the conclusions of Hewitt and Lovegrove, who stated (32) "Although this general method has been reported as satisfactory with falling films, the sharp wave profiles and presence of spray in the climbing film regime of interest were found to introduce gross refraction and scattering effects which swamped other signals," In other words, the method appeared unsuitable for the study of upwards annular flow,

Obviously, then, there are situations under which the light absorption technique gives invalid results. The validity of the method can be established rather simply, as was done by Charvonia (11). Employing the same method as

Hewitt and Lovegrove, Charvonia demonstrated that the technique could be applied to the system he investigated. The system is operated with clear liquid rather than dyed liquid, and the resulting output from the photomultiplier tube is observed. Ideally that output should remain constant and be equal to that corresponding to no liquid flow. In practice, however, the technique is considered to be satisfactory if the fluctuations in the output of the photomultiplier tube are very small compared with the fluctuations observed when a dyed liquid is flowing. That the technique satisfied the aforementioned criterion was indicated by Charvonia (11), as well as in the subject investigation.

The question of the effect of evaporation of the liquid upon the concentration on the dye in the liquid film again depends upon the operating conditions. Whether or not a significant change in dye concentration occurs depends upon what percentage of the liquid film evaporated between the point of injection (where the dye concentration is known) and the point where the film thickness is being measured. In most instances of the flow of air and water at approximately room temperatures the percentage evaporation is so small that the change in dye concentration is negligible. On the other hand, when the air is at an elevated temperature, and particularly when the air velocity is high, the tube length long, and the liquid flow rate small, an appreciable fraction of the entering liquid evaporates, and consideration of the change in dye concentration is essential to avoid serious errors in the determination of film thickness. In previous experiments in which the light absorption technique was employed the dye concentration was essentially constant. In the subject research, however,

the change in dye concentration was significant and was taken into account, by calculating the amount of evaporation which occurred between the point of injection and the point of film thickness measurement, and adjusting the value of dye concentration accordingly.

One of the objectives of the subject investigation was the determination of the geometry of the gas-liquid interfacial surface. As will be demonstrated later, that geometry may be determined from film thickness-time traces, such as obtained from instantaneous film thickness measurements employing the light absorption technique, provided the velocities of the waves which are present are known. The methods most commonly employed for determining wave velocities are measuring the time required for waves to travel a known distance with a stopwatch, and photographing the system with a high-speed motion picture camera. Miller (49) employed the light absorption technique with two optical systems, displaced 4 5/8 in. vertically, in his investigations of film thickness in downward, concurrent, annular, two-phase flow. He attempted to determine the wave velocity by measuring the time taken for a wave to travel from one optical system measuring station to the other. His efforts were successful, however, because in most cases the waves in question did not maintain their identify sufficiently to be recognized at the two stations. He also reported that the character of the waves was significantly different at the two stations, hypothesizing that the presence of the filtn divider required for the upper optical system disturbed the flow downstream from the film divider. Both of the shortcomings of Miller's system mentioned above may be overcome by placing the two beams of light much closer together, as was accomplished in the subject research.

2.5.2 Fluorescence-Spectrometer Method

A new technique for the local measurement of liquid film thickness has been developed at Harwell during the past few years (14,33). This technique, denoted as the fluorescence-spectrometer method, shows considerable potential for applications to film thickness measurement. The principle of operation will now be described. A fluorescent dyestuff is mixed with the liquid prior to its injection into the test section, At the point where the film thickness is to be measured, an incident beam of light of a certain wave length is' directed into the liquid film. The incident light excites a fluorescence of a different frequency in the liquid film, and the fluorescence is detected by an appropriately filtered photomultiplier device. The amount of fluorescent light detected is a function of the thickness of the film, increasing with the film thickness. The method is claimed to overcome the many disadvantages of other methods, such as placing some foreign object inside the tube and, as in the case of the light absorption method, having part of the transmitted light go undetected by the photomultiplier tube due to scattering and reflection losses. It was not stated in reference 14 whether the incident light intensity was such that the fluorescence was saturated, i. e,, the intensity of the emitted light was independent of the intensity of the incident light for a given concentration of dye and a given film thickness. If it were not, errors could be produced by the fluorescence of the dye caused by incident light which reflected from the gas-liquid interface and passed through the film a second time, Alignment of the system was said to be very critical, and also the calibration of

the device; the latter is accomplished by employing a film of known thickness in a mockup similar to the experimental setup. If the field viewed by the photomultiplier tube can be made sufficiently small compared to the dimensions of the waves being studied, the fluorescence-spectrometer technique appears to be an attractive method for measuring instantaneous film thickness at one location on the tube.

2.5.3 Miscellaneous Techniques

Two recently published papers describe techniques employed for making different measurements of interest in annular, two-phase flow, and are mentioned briefly in the following paragraphs.

Persson (51) employed a photographic technique for measuring the mean velocity, velocity distribution, and thickness of a thin (0.1 to 0.9 mm) liquid film. Small (20 to 40 μm) aluminum particles were uniformly distributed in the film, which was photographed by a camera mounted with its optical axis perpendicular to the film. The length of the streaks made on the film by the particles indicated the spectrum of velocities in the film. Assuming that the velocity distribution was monotonic with the larger velocities being farther from the solid wall, and employing the continuity equation, the aforementioned parameters were calculated. The effect of air blowing across the surface of the film at velocities up to 30 m per sec had no effect on the film velocity profile, Good agreement was found between the calculated film thickness and that determined by a needle contact technique. The above technique is limited to the flow of films having a constant thickness over the field of the photograph during all of the exposures

made for a given determination of parameters. (It was indicated that at least 5 such photographs were necessary per determination.)

Jacowitz and Brodkey (37) devised a method for photographing a cross-section of the liquid film flowing on the inside of a glass tube for horizontal, annular, two-phase flow. One difficulty encountered in taking such a photograph is the distortion of the image caused by the refraction and often by the total reflection of the light rays when they pass through the curved glass-air and glass-liquid interfaces. According to reference 37 those problems were solved by approximately matching the index of refraction of the medium outside the glass tube with the index of refraction of the glass tube; the tube was surrounded by a bath of turpentine. The section of the film to be photographed was illuminated from one side of the tube and was photographed from the opposite side with a Fastax camera through a microscope, which yielded a very shallow depth of field, In this manner a photograph of the section of the film in focus, including the gas-liquid interfacial profile, was obtained. There were many difficulties encountered, among them blurring due to the relatively high surface velocity, distortion of the image due to air bubbles, and, as in the case of the photographs of Brauer (7) and Belkin, et al. (4), some interference with the profile in the plane of focus due to the troughs of waves closer to the camera.

2.6 Summary

As the result of substantial research in the area of annular, two-phase flow much is known concerning the process of mass transfer in such

a system. The effects of the concentration of the diffusing vapor (as expressed by the ratio p_{BM}/P), the Reynolds number of the gas phase, and the Schmidt number have been fairly well established for both countercurrent and concurrent fully developed flow. Also the effect on the mass transfer of the liquid Reynolds number has been determined for the case of countercurrent flow.

However, the case of concurrent flow has received considerably less attention than has countercurrent flow. In fact, the effect of the liquid Reynolds number has not been investigated for concurrent flow. Also, little work has been done concerning mass transfer in the entrance region of the flow, and heat transfer from the gas to the liquid and its relationship to the mass transfer process has received little attention. Finally, although some investigations have been conducted to determine the characteristics of the free liquid surface in single and two-phase flows, there has been no attempt to measure those characteristics in a system experiencing significant mass transfer and to relate those characteristics to the observed rates of mass transfer.

The subject investigation was initiated for the purpose of providing the information required for increasing the available knowledge of mass transfer in annular, two-phase flow.

3. EXPERIMENTAL RESULTS

The purpose of the experimental investigation of annular two-phase flow discussed herein was to obtain information concerning the following:

1. The effect of the liquid flow rate upon the rate of mass transfer.
2. The effect of heat transfer from the hot flowing gas to the annular liquid film upon the rate of mass transfer.
3. The rate of mass transfer in the entrance region of the channel,
4. The characteristics of the gas-liquid interface and their effect upon the rate of mass transfer.

Section 3.1 discusses the experiments concerned with the first three of the aforementioned topics; Section 3.2 discusses the experiments for determining the characteristics of the interfacial surface.

3.1 Mass Transfer Experiments

3.1.1 Description of the Mass Transfer Experiments

The mass transfer experiments were conducted to determine (a) the effect of the liquid flow rate upon the rate of mass transfer in annular, two-phase flow, and (b) the effect of the entrance region upon the local rate of mass transfer. The effects of the gas flow rate, as represented by the gas Reynolds number, and the Schmidt number on the rate of mass transfer in annular, two-phase flow have been well established by previous work. It was, therefore, decided not to investigate those aspects of the problem,

so that the attention could be concentrated upon the aforementioned objectives.

Since few investigations have been reported in which the gas temperature was equal to or greater than the boiling point of the liquid, the gas temperature was varied to determine whether or not the correlation equations currently employed were satisfactory for correlating the results obtained from experiments wherein the gas temperature was varied,

The experiments were conducted with test sections having different lengths; all of them were constructed from (precision bore) borosilicate glass tubing having an inside diameter of 1.502 in. A detailed description of the experimental apparatus is presented in Appendix B, and only a brief description is presented here.

Figure 1 is a schematic diagram of the apparatus. Air and deionized water were the gas and liquid media, respectively.

Heated air from the high pressure supply tanks, after passing through a 6 ft long approach section having an I. D. of 1.495 in., entered the test section. Water from a pressurized supply tank was injected at the top of the test section onto the inside wall of the test section, through a narrow (0.018 in.) slot in the injector. At the bottom of the test section, the water which did not evaporate into the air stream flowed into the collector; the air was exhausted through a duct to the outside atmosphere. The temperatures of the air and water entering and leaving the test section were measured with chromel-alumel thermocouples, and recorded on a strip recorder. The water flow rate was regulated with globe valves, and measured by means of calibrated Fischer & Porter Flowrators. The

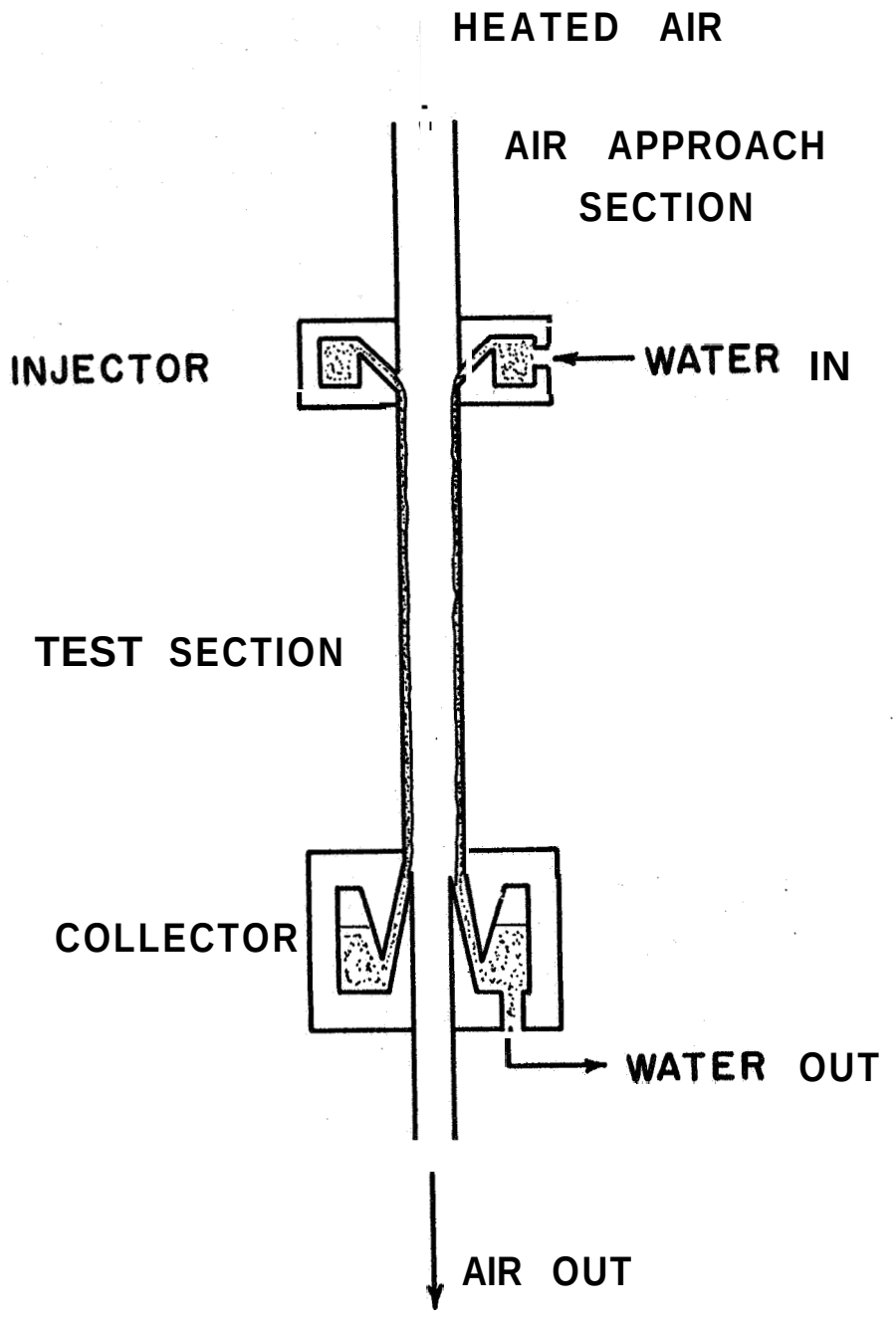

Fig. 1 Schematic Diagram of the Experimental Apparatus

air temperature was automatically held at a preset value by means of a pneumatic controller, which regulated the fraction of the air passing through a propane furnace. A pneumatically controlled regulating valve controlled the air flow rate; the latter was measured with a thin plate orifice. The humidity of the air entering and leaving the test section was measured continuously by psychrometric means, and from those measurements the rates of mass transfer were calculated. A water seal in the collector prevented air from escaping at that location.

Five different test section lengths, ranging from 8 to 40 in., were employed; each of them had the same I.D. (1.502 in.). Three different inlet air temperatures were investigated, 110, 230, and 350 F. Since the static pressure in the test section was practically atmospheric, the aforementioned temperatures corresponded to values below, approximately equal to, and above the boiling point of the liquid film.

In all of the experiments the inlet air velocity was 48 fps. It was desirable to have the air velocity as large as possible to improve the accuracy of the measurements. The air velocity was, however, limited by the following considerations. It was desired to operate over a range of parameters such that no droplets were entrained in the gas stream, Preliminary experiments indicated that at velocities higher than 48 fps droplet entrainment did occur at the higher liquid flow rates investigated. Also, the collector was found to operate unsatisfactorily (water spilled over the inlet to the collector) at higher air flow rates. Depending on the air temperature, the gas Reynolds number varied from 19,800 to 36,500. The liquid flow rate was varied from 0.00152 to 0.0718 lb per sec, which

corresponded to peripheral liquid flow rates of 0.000322 to 0.0152 lb per sec-in., and liquid Reynolds numbers ranging from 23 to 1350.

The air approach section, injector, and test section were all insulated to prevent heat loss from the system. After the flow conditions were set to the desired values, the system was allowed to reach equilibrium before readings were taken of the pertinent parameters.

3.1.2 Method of Correlation of the Data

The raw data obtained in the mass transfer experiments enabled the calculation of the mass transfer which occurred between the inlet and exit sections of the test section, and also the parameters describing the prevailing flow conditions for the water and the air,

The method employed for correlating the data was based upon the well known Nusselt-type equations, which enable calculating a dimensionless heat or mass transfer coefficient when the Reynolds and Prandtl or Schmidt numbers are known. Such an equation was first employed for the correlation of mass transfer data by Gilliland and Sherwood (23), and their equation is

$$Sh = 0.023\ Re_G^{0.83}\ Sc^{0.44} \qquad (14)$$

Equation 14 is based on the over-all transfer coeficient, and since it was obtained from experiments employing a tube of large L/d ratio (L/d = 44), it would be expected that it would apply for the case of essentially fully developed mass transfer, and not for tubes of small L/d. In equation 14,

the Sherwood number is defined by

$$Sh = \frac{h_M d}{D}$$

where

h_M = mass transfer coefficient

d = diameter of the test section

D = molecular diffusivity of the vapor in the gas

In general, the mass transfer coefficient h_M is defined by an expression of the following type. Thus

$$h_M = \frac{W_{ev}}{A\ \Delta C_m}$$

where

W_{ev} = rate of evaporation (mass transfer)

A = surface area

ΔC_m = driving force for the mass transfer process, represented by a difference in concentrations

The concentration gradient is usually taken as the difference between (a) the bulk (mixing cup) concentration of the diffusing species in the gas stream, and (b) the concentration of the diffusing species at the surface where the mass transfer occurs. In the case of evaporation, the latter concentration is based upon the vapor pressure of the liquid corresponding to the surface temperature of the liquid. A problem arises in that the concentration difference does not remain constant with the distance from

the inlet to the test section. The usual practice is to employ a log mean concentration difference, based on the difference in the concentrations at the outlet and inlet cross-sections. which is analogous to the log mean temperature difference commonly employed in the design and analysis of heat excnangers. Such a representation is satisfactory, providing that the changes in concentration difference are small. If, however, there is a significant change in concentration difference between the inlet and the outlet, the extent to which the long mean concentration difference gives a satisfactory representation depends upon the manner in which the concentration difference varies with distance from the inlet section of the test section. In the case of evaporation from an annular liquid film into a gas stream flowing in a tube, the manner in which the vapor pressure (a strong function of temperature) varies alonq the tube depends upon the liquid flow rate, as well as such parameters as the gas temperature, velocity, etc. For example, suppose the gas temperature and the flow rate are such that the liquid is heated as it flows in a film along the tube wall. If the liquid flow rate is large. the film will be slowly heated at a fairly uniform rate. On the other hand, if the liquid flow rate is small, the film will be rapidly heated to its equilibrium temperature (approximately the wet-bulb temperature corresponding to the gas stream temperature) within a short distance from the inlet and then remain at approximately that temperature thereafter, as it flows in the tube. Obviously a log mean concentration difference based upon the inlet and outlet conditions will give a fairly goad representation of the conditions in the first (large rate of flow of liquid) case, but might give a poor

representation of the conditions in the second (small rate of flow of liquid) case.

The aforementioned limitation on the application of a correlation based upon the log mean concentration difference (which is treated in more detail in Appendix D) necessitated a method of treatment of the data that took into account the variation in the driving force with the distance from the inlet. The method employed was the application of a correlation for the local mass transfer coefficient,

Since the heat transfer from the gas to the liquid plays an important role in determing the temperature of the film as a function of distance from the inlet, it was necessary to include the heat transfer in the equation for correlating the data., The heat transfer correlation employed was also based upon the local heat transfer coefficient. The manner in which the data obtained from the experiments were correlated is described briefly in the following paragraphs; a more detailed description is presented in Appendix D.

The basis for the correlations were the Nusselt-type equations for the local rates of heat and mass transfer, Thus

(a) Heat Transfer:

$$Nu_x = C_1 F_1(x/d) Re_G^{C_2} Pr^{C_3} \quad (17)$$

(b) Mass Transfer:

$$Sh_x = C_4 F_2(x/d) Re_G^{C_5} sc^{C_6} \quad (18)$$

In equations 17 and 18 the symbols C_1 through C_6 represent constants, and F_1 and F_2 are functions of x/d. Previous work by other investigators has established the effect of the Reynolds, Prandtl, and Schmidt numbers upon the heat and mass transfer coefficients. No attempt was made, therefore, in the subject research to vary those parameters. Rather, the previously established exponents were assumed to apply (3). Hence, equations 17 and 18 can be rewritten in the form

$$Nu_x = C_1 F_1(x/d) Re^{0.80} Pr^{0.33} \quad (19)$$

$$Sh_x = C_4 F_2(x/d) Re^{0.83} Sc^{0.44} \quad (20)$$

It was assumed that the functions F_1 and F_2 were identical functions of x/d, as indicated by Deissler (18). Finally, a form of the function F_1 was assumed. Figure 2 (solid line) presents the ratio Nu_x/Nu_{fd} as a function of x/d for Re = 30,000 and Pr = 1 as determined analytically by Deissler (18). Nu_{fd} represents the Nusselt number for fully developed flow. The dashed line in Fig. 2 represents the equation

$$Nu_x/Nu_{fd} = 1 + \left(\frac{0.15}{x/d}\right)^{0.75} \quad (21)$$

which is seen to give a good representation of Deissler's results. A function of the form of equation 21 was, therefore, chosen for the function F_1. Thus

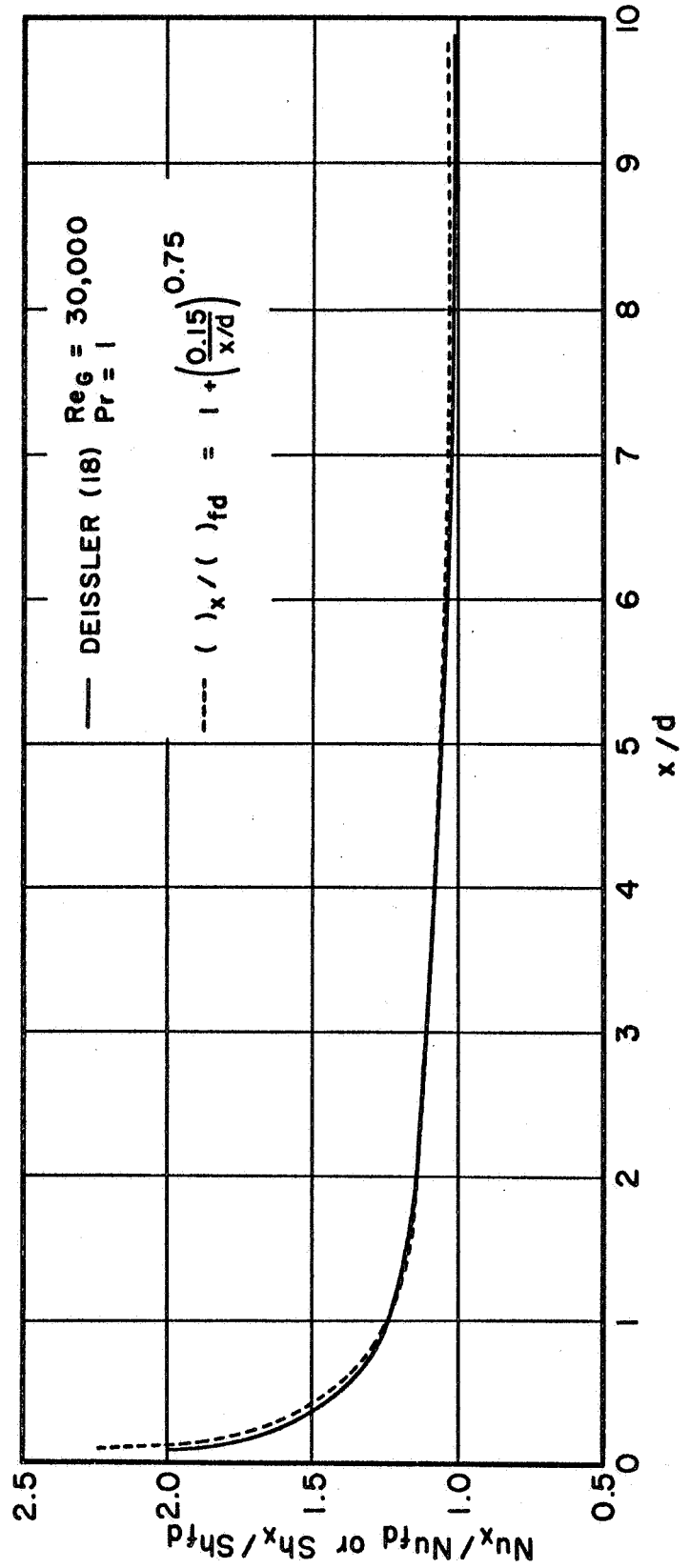

Fig. 2 Effect of x/d on Local Nusselt and Sherwood Numbers

$$F_1 = F_2 = 1 + \left(\frac{I}{x/d}\right)^{0.75} \qquad (22)$$

Hence, the expressions for correlating the experimental data are equations 19 and 20, with equation 22 relating the functions F_1 and F_2 with x/d. There are three empirical constants; C_1, C_4, and I.

The method employed for selecting the constants C_1, C_4, and I is presented below. Measurements were made of the rates of mass transfer as a function of the following parameters (nominal values are given):

a. test section length: 8, 16, 24, 32, and 40 in.

b. air inlet temperature: 100, 230, and 350 F

c. water weight flow rate:

0.001 52
0.001 88
0.00285
0.0041 8
0.00609
0.00996
0.01573
0.02649
0.04355
0.071 82 lb/sec

The inlet air velocity was 48 fps for all of the experiments. A total of 138 experimental runs was made including nearly all possible combinations of the above parameters; the data obtained for the 40 in. tube at 110 F were discarded because a faulty thermocouple. For each experimental run, the "measured" over-all Sherwood number, Sh, was calculated based upon the inlet and outlet conditions, employing the log mean concentration difference as the driving force. (The details of the data reduction and the correlation procedures are presented in Appendix D, and only a short description is presented here.) The value of the measured over-

all Sherwood number was then compared with a "calculated" over-all Sherwood number, Sh_{calc}. The following paragraph describes the procedure for determining the calculated over-all Sherwood number.

Values of the constants C_1, C_4 and I were initially chosen based upon the experience of other investigators., Equations 19 and 20 were employed for calculating the local heat and mass transfer occurring in successive 0.25 in. increments along the test section from the inlet to the exit. The measured values of the inlet air flow rate, temperature, and humidity and the inlet water flow rate and temperature were used as the initial conditions for that calculation. Based upon those conditions, the heat and mass transfer occurring in the first 0.25 in. from the inlet of the test section were calculated, yielding conditions 0.25 in. from the inlet. A calculation was then made of the heat and mass transfer in the second 0.25 in. from the inlet of the test section, yielding conditions 0.50 in. from the inlet. A calculation of the heat and mass transfer in the third increment was made, etc., until the outlet of the test section was reached. The calculation procedure gave the calculated values of the pertinent parameters at the exit of the test section, as well as the total mass transfer which had occurred between the inlet and outlet, From those results the calculated over-all Sherwood number, Sh_{calc}, was computed based upon the measured inlet and the calculated outlet conditions, again employing the log mean concentration difference as the driving force.

From the measured over-all Sherwood number Sh and the calculated oyer-all Sherwood number Sh_{calc}, the Sherwood number ratio R_{Sh} was computed. Thus

$$R_{Sh} = Sh/Sh_{calc}$$

If equations 19 and 20 with the chosen values of constants C_1, C_4 and I, correlated the experimental results satisfactorily, then the Sherwood number ratio would have the value unity. In practice, the Sherwood number ratio was either slightly larger or smaller than ,unity.

The value of R_{Sh} was calculated for each experimental run and the results analyzed, Adjustments were then made to the values of C_1, C_4 and I, based upon that analysis of results, and the calculations were repeated. The procedure was repeated until satisfactory agreement was obtained between the calculated and measured values of Sherwood numbers, and in addition the calculated total mass transfer corresponded to that obtained in the experiments.

The variation for liquid temperature with distance from the inlet was approximately the same for the actual and the calculated cases. Therefore, the effect of changes in the concentration gradient with distance from the inlet upon the over-all mass transfer coefficient, was the same for both the measured and the calculated cases,

An IBM-7094 digital computer was employed for making the aforementioned calculations, including the initial reduction of the experimental data,

3.1.3 Results of the Mass Transfer Experiments

Figures 3 through 7 present the mass transfer group $Sh/Re_G^{0.83}\ Sc^{0.44}$ as a function of liquid Reynolds number Re_L for test section lengths of 8.5, 16.5, 23.5, 32.4, 39.9 in., respectively. Each graph includes data taken at the different temperatures investigated, The temperatures are

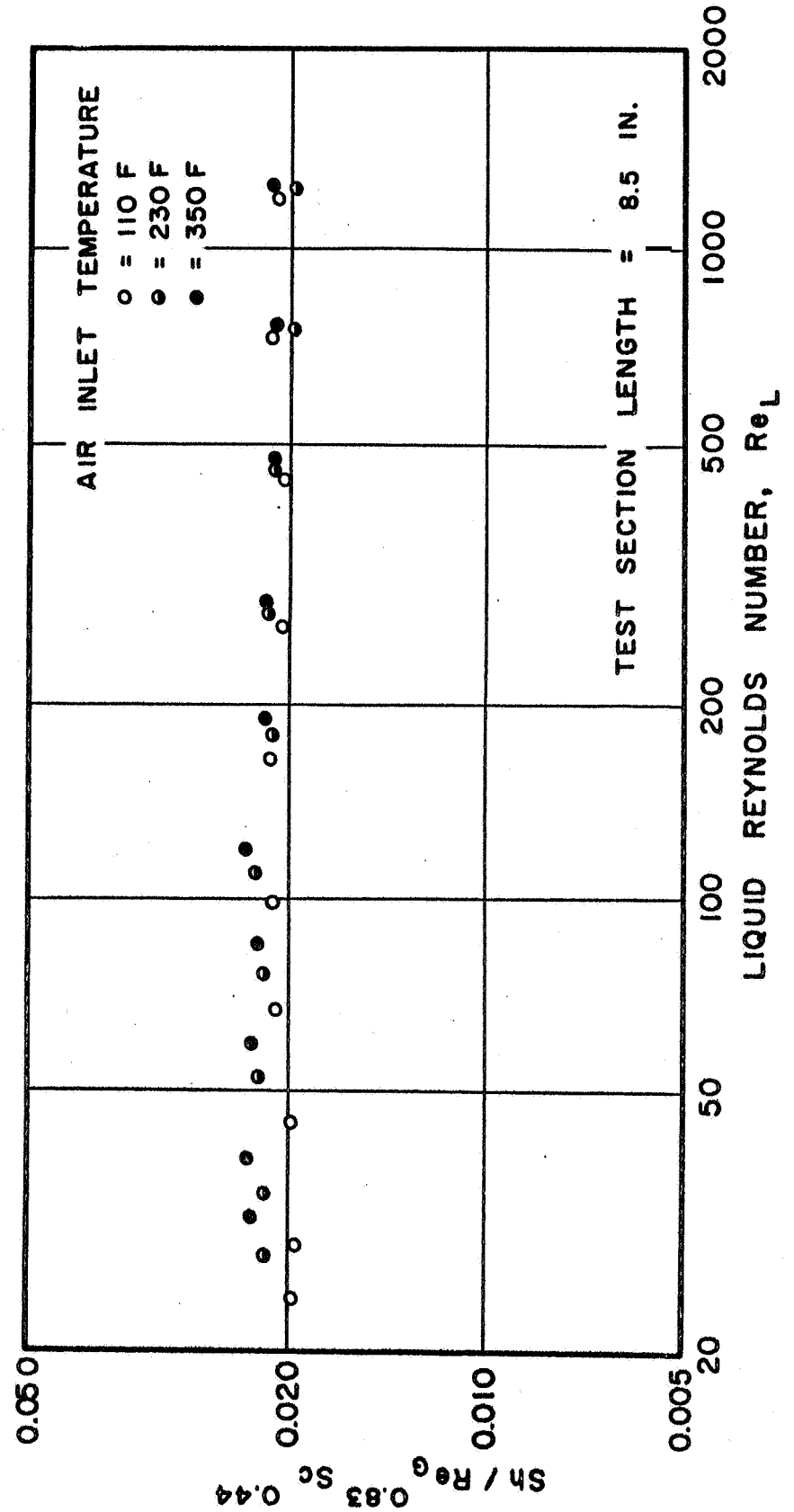

Fig. 3 Mass Transfer Group as a Function of Liquid Reynolds Number for the 8.5 in. Test Section

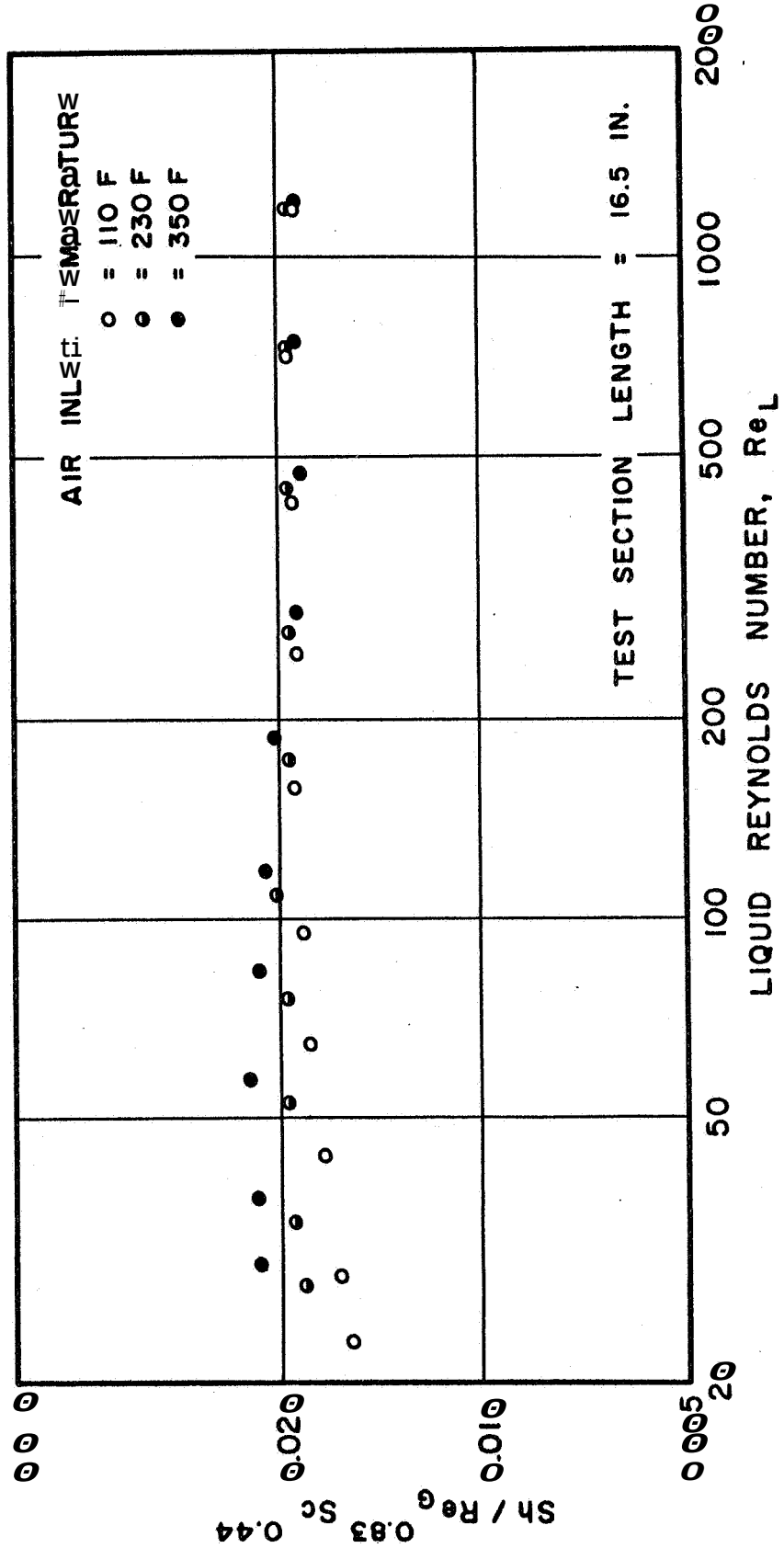

Fig. 4 Mass Transfer Group as a Function of Liquid Reynolds Number for the 16.5 in. Test Section

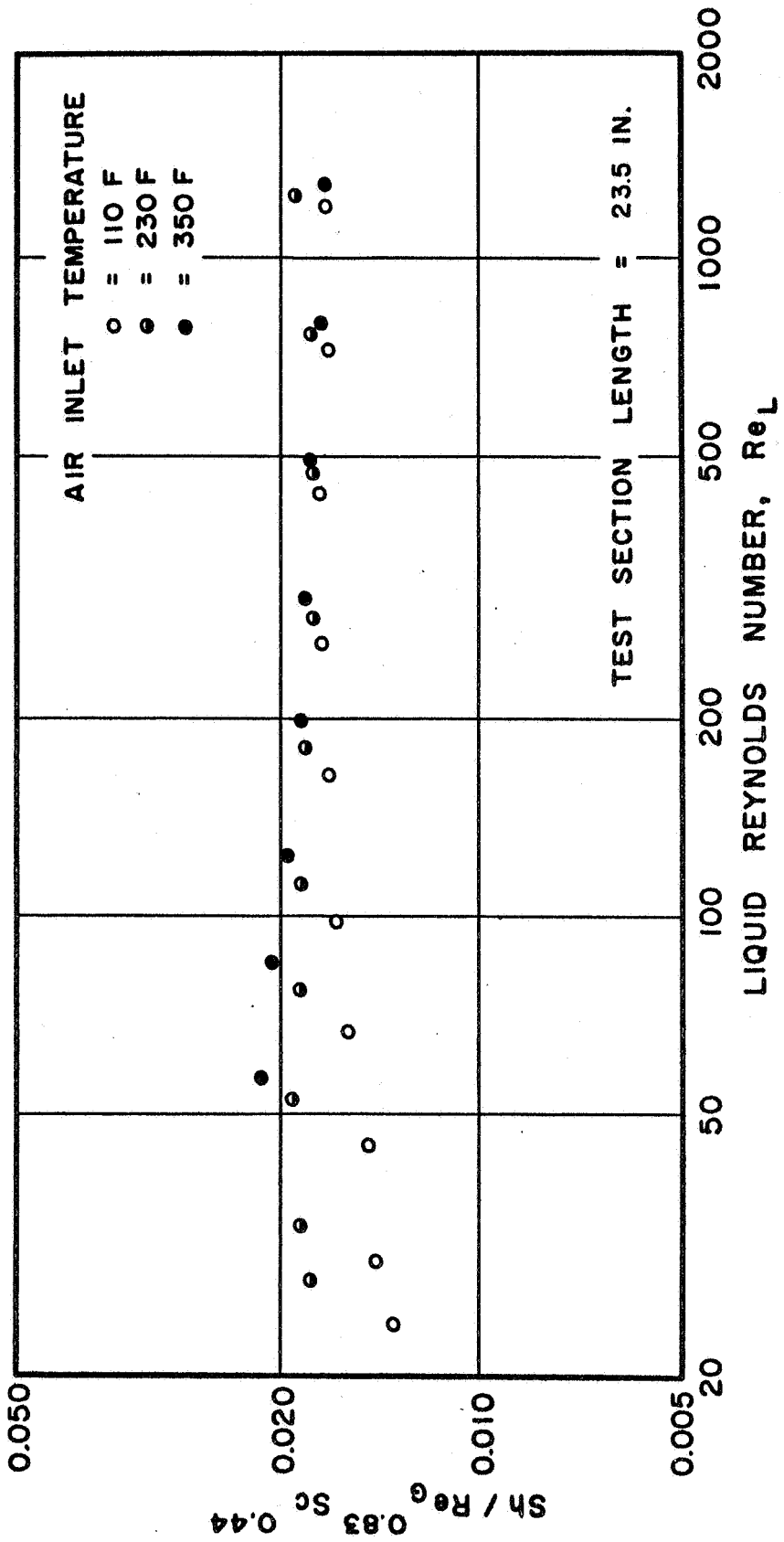

Fig. 5 Mass Transfer Group as a Function of Liquid Reynolds Number for the 23.5 in. Test Section

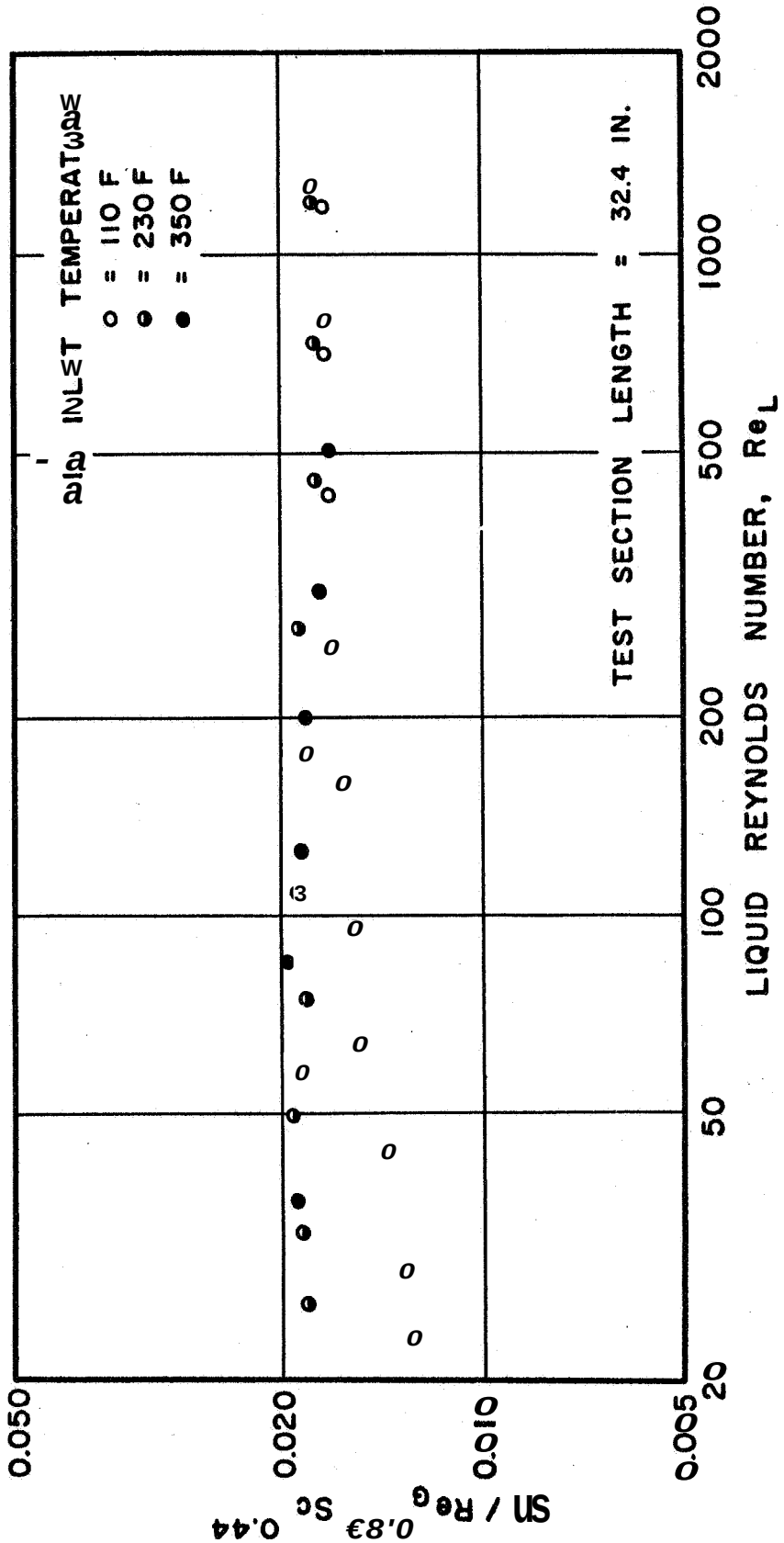

Fig. 6 Mass Transfer Group as a Function of Liquid Reynolds Number for the 32.4 in. Test Section

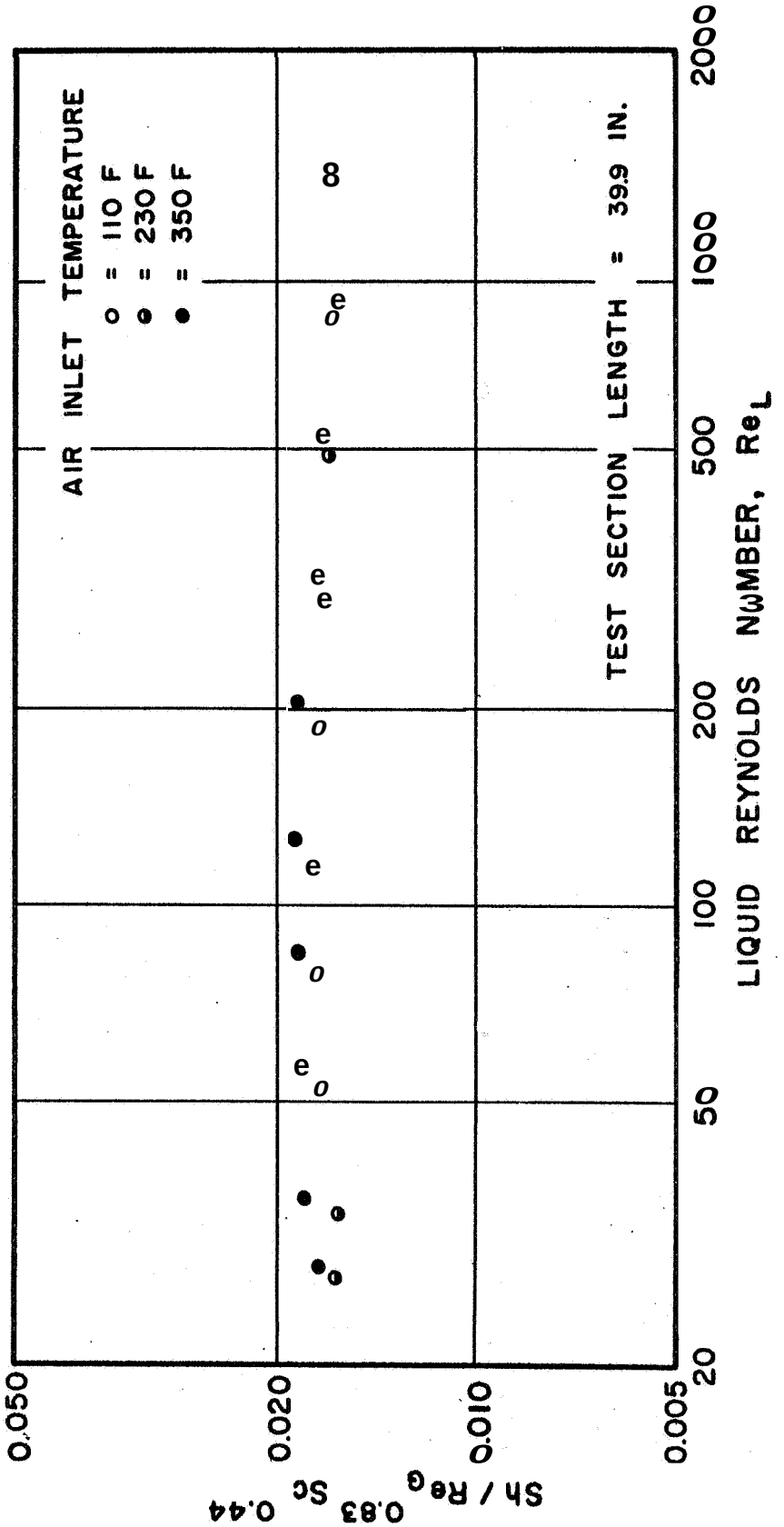

Fig 7 Mass Transfer Group as a Function of Liquid Reynolds Number for the 39.9 in. Test Section

noted on the graphs. The considerable scatter in the data, as well as the variation in the mean value of the mass transfer group with test section length, shows the inadequacy of such a correlation for satisfactorily describing the mass transfer process.

Figures 8 through 12 present the Sherwood number ratio $R_{Sh}=Sh/Sh_{calc}$ as a function of liquid Reynolds number Re_L for the same set of test section lengths, Again each graph includes all temperatures investigated. The calculated Sherwood number Sh_{calc} was determined by a numerical calculation of heat and mass transfer from the inlet to the exit of the test section employing the following equations for local heat and mass transfer:

$$Nu_x = 0.0205\ F_1\ Re_G^{0.8}\ Pr^{0.33} \tag{24}$$

$$Sh_x = 0.0138\ F_1\ Re_G^{0.83}\ Sc^{0.44} \tag{25}$$

where

$$F_1 = \begin{cases} 1 + \left(\frac{0.588}{x/d}\right)^{0.75} & \text{for } x/d > 0.166 \\ 5.51 - 11.6\,(x/d) & \text{for } x/d \le 0.166 \end{cases} \tag{26}$$

(see Section D.2.6 for an explanation of equation 26)

The average values of the ordinates and the standard deviations from those average values are presented below.

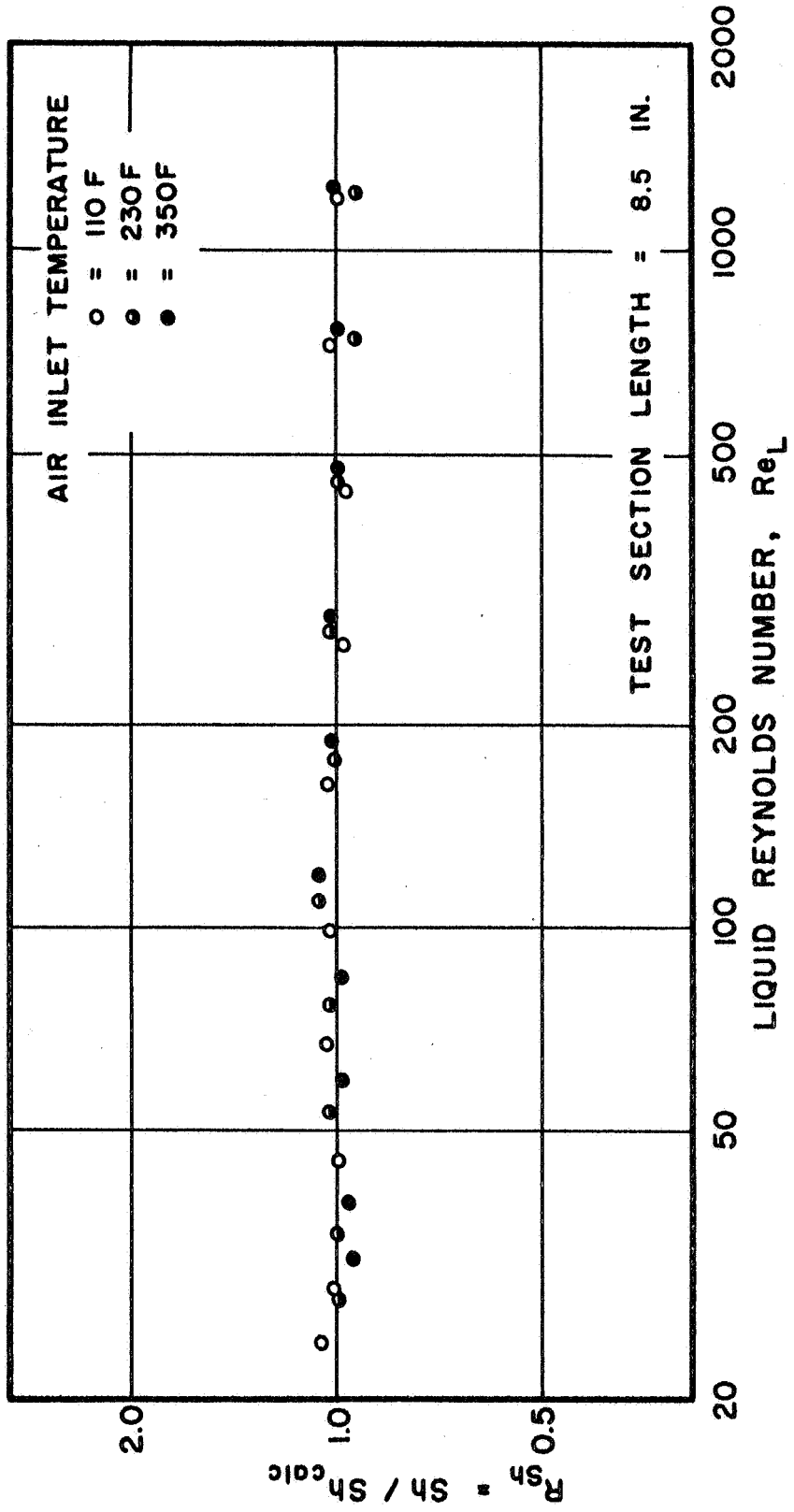

Fig. 8 Sherwood Number Ratio as a Function of Liquid Reynolds Number for the 8.5 in. Test Section

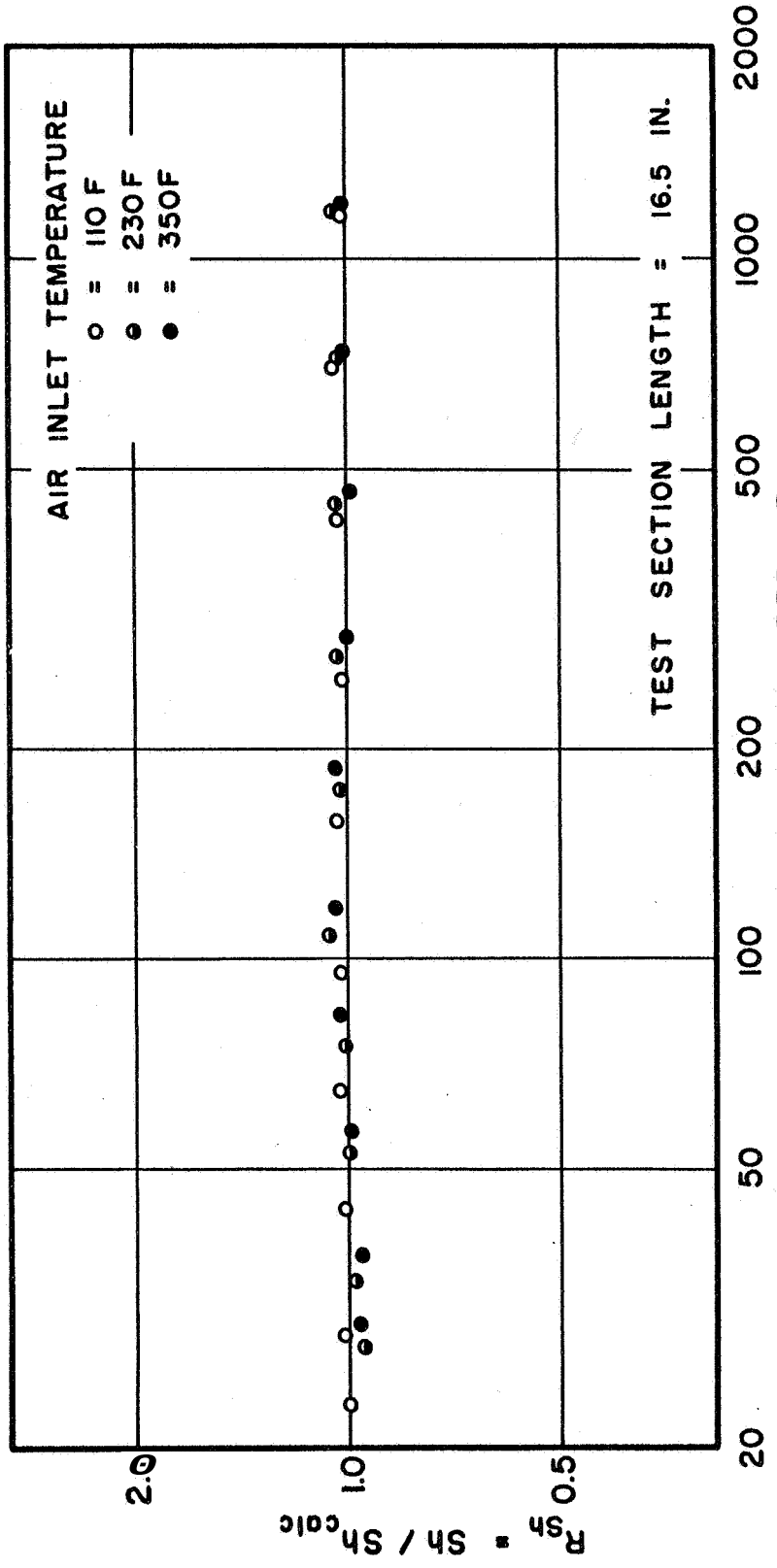

Fig. 9 Sherwood Number Ratio as a Function of Liquid Reynolds Number for the 16.5 in. Test Section

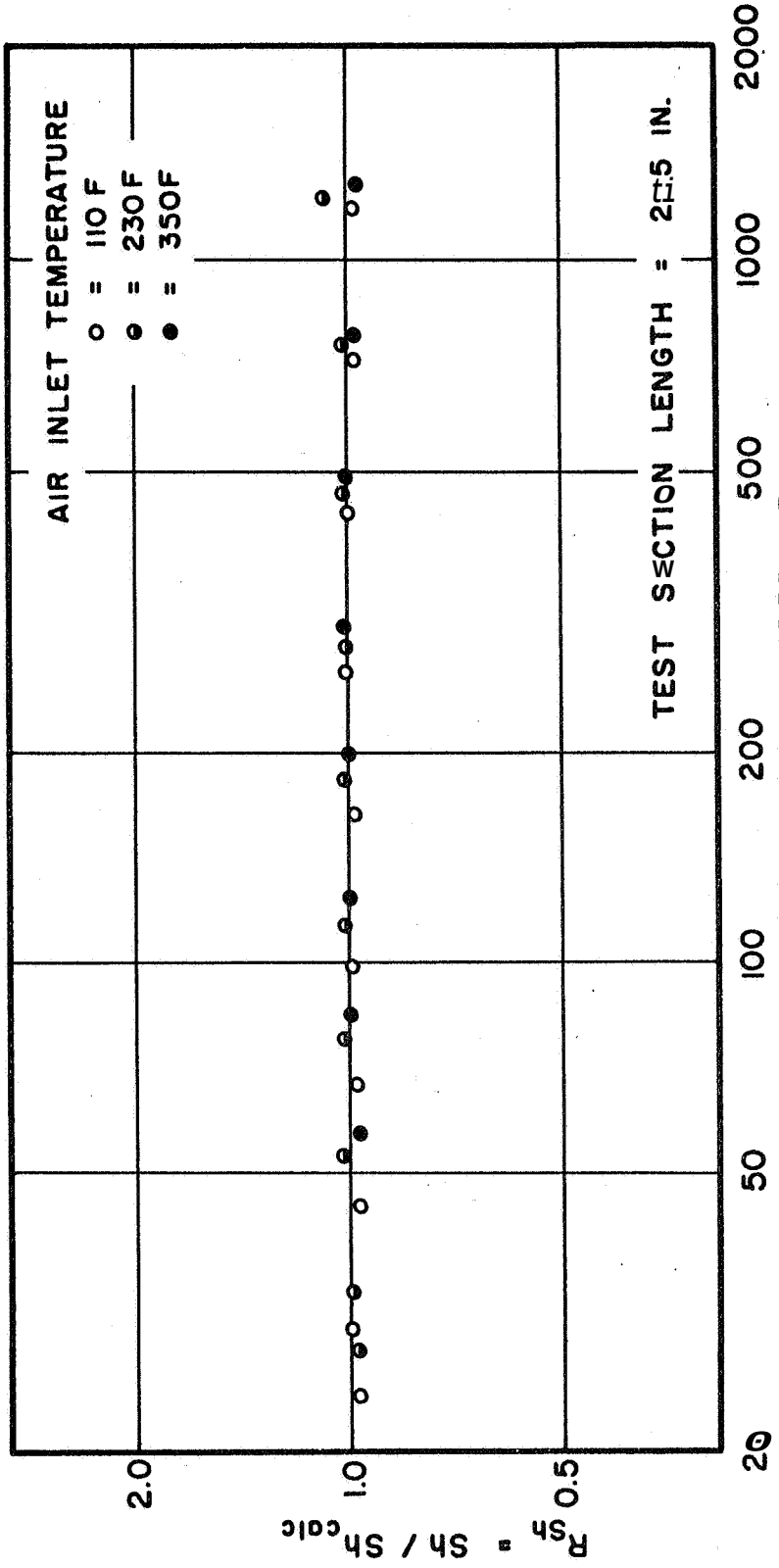

Fig. 10 Sherwood Number Ratio as a Function of Liquid Reynolds Number for the 23.5 in. Test Section

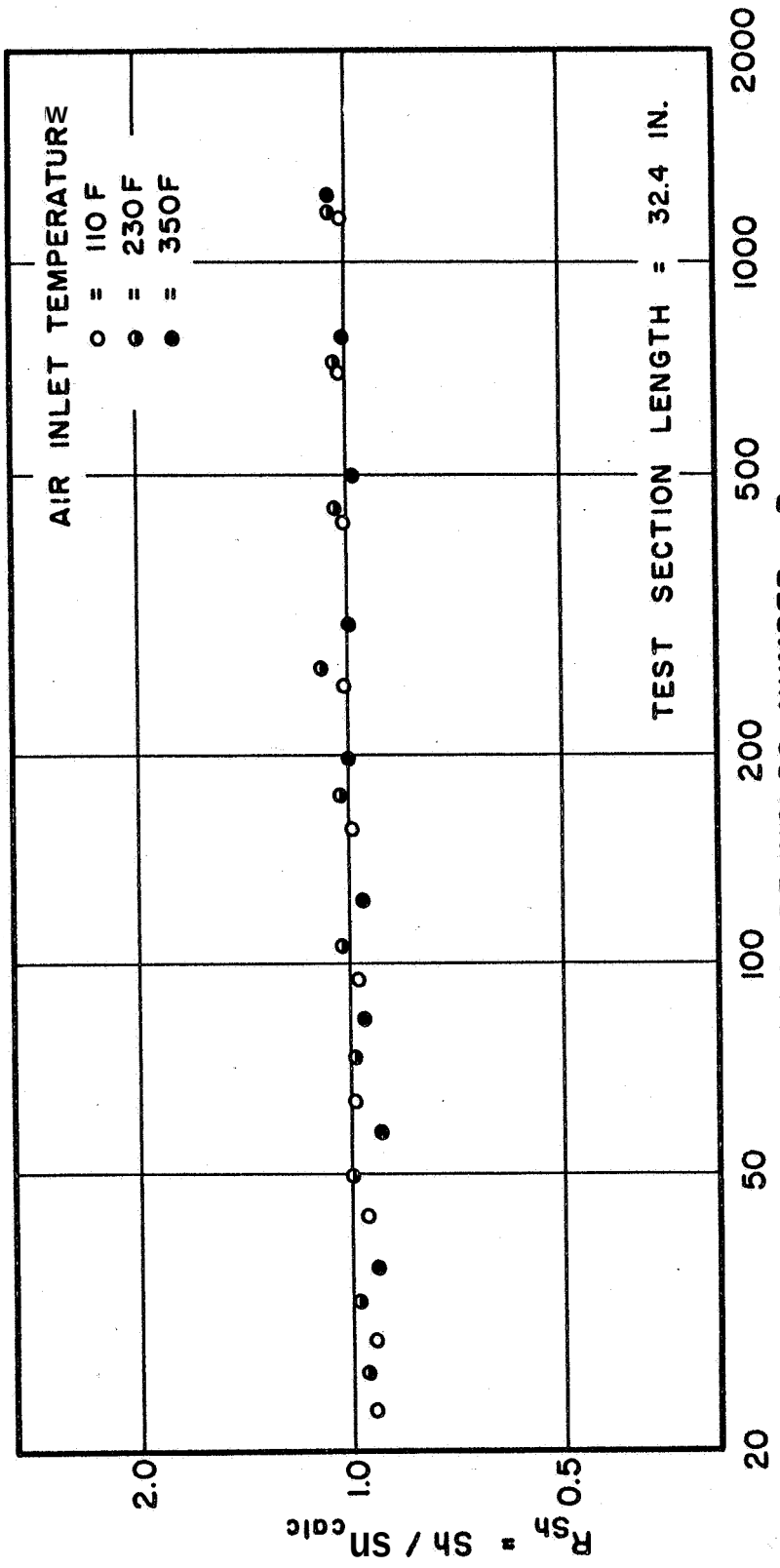

Fig. 11 Sherwood Number Ratio as a Function of Liquid Reynolds Number for the 32.4 in. Test Section

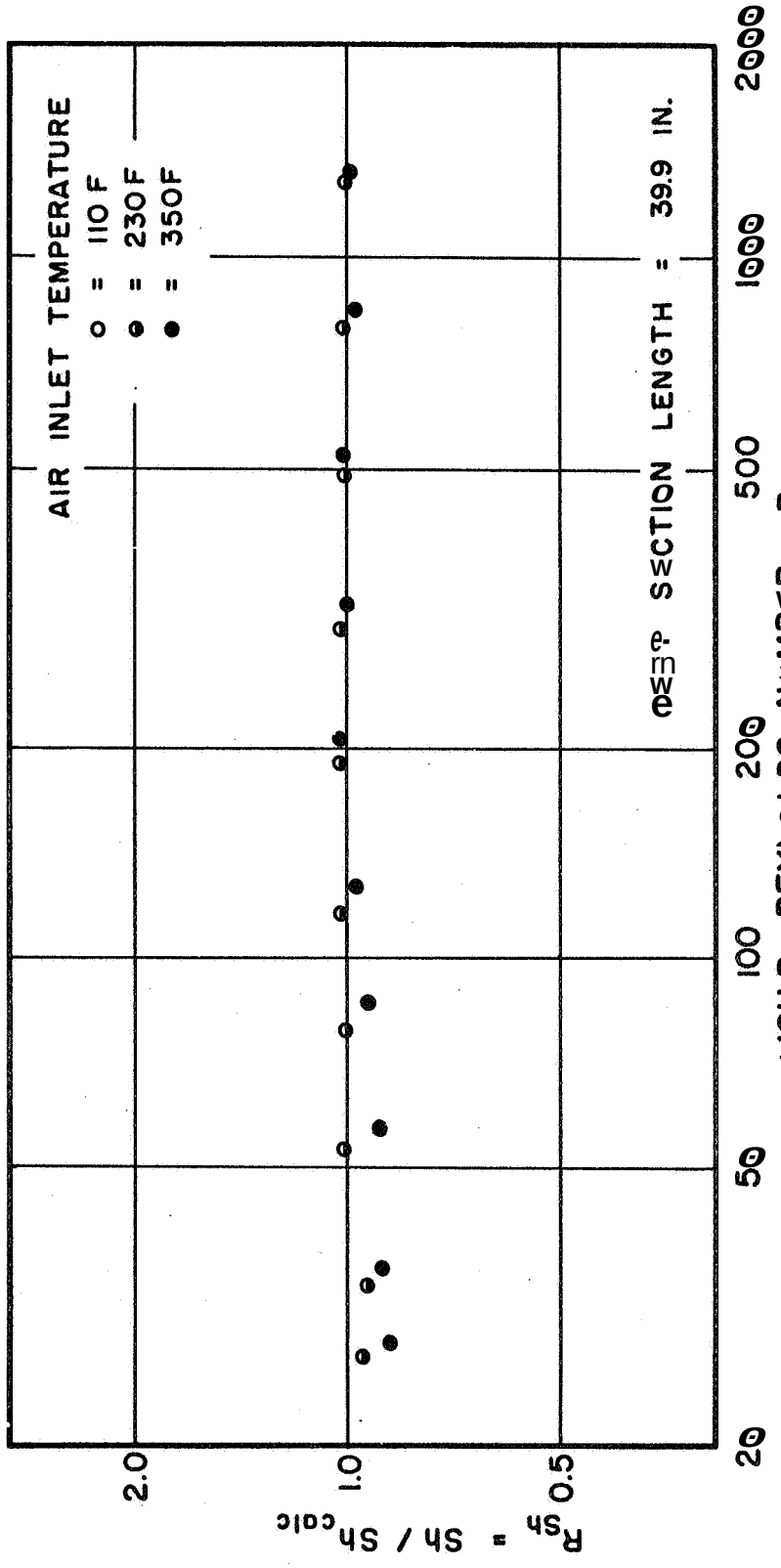

Fig. 12 Sherwood Number Ratio as a Function of Liquid Reynolds Number for the 39.9 in. Test Section

Test Section Length (in.)	L/d	Average K_{Sh}	Standard Deviation (per cent)
8.5	5.7	1.000	3.1
16.5	11.0	1.013	2.8
23.5	15.7	1.000	2.4
32.4	21.6	1.001	4.2
39.9	26.5	0.980	4.5

Figure 13 combines Fig. 8 through 12 into a single graph. The average value of the Sherwood number ratio is 1.000 with a standard deviation of 3.6 percent. (The correlation constants were so chosen that the average value of the Sherwood number ratio was close to unity, as discussed in the preceding section and in Appendix D.)

Appendix G presents a tabulation of the data obtained from the mass transfer experiments.

3.2 Surface Characteristics Experiments

3.2.1 Description of the Surface Characteristics Experiments

The primary purpose of the experiments concerned with the investigation of the surface characteristics of the liquid film was the determination of the surface area of the film under the conditions which prevailed in the experiments concerned with the mass transfer measurements. Since the measurements required for determining the surface area of the film also enabled calculating the mean film thickness and the velocity of the waves on the surface of the film, those characteristics were also determined as functions of the flow parameters.

Figure 14 presents a schematic diagram of the apparatus, which is described in detail in Appendix B. The primary component of the apparatus

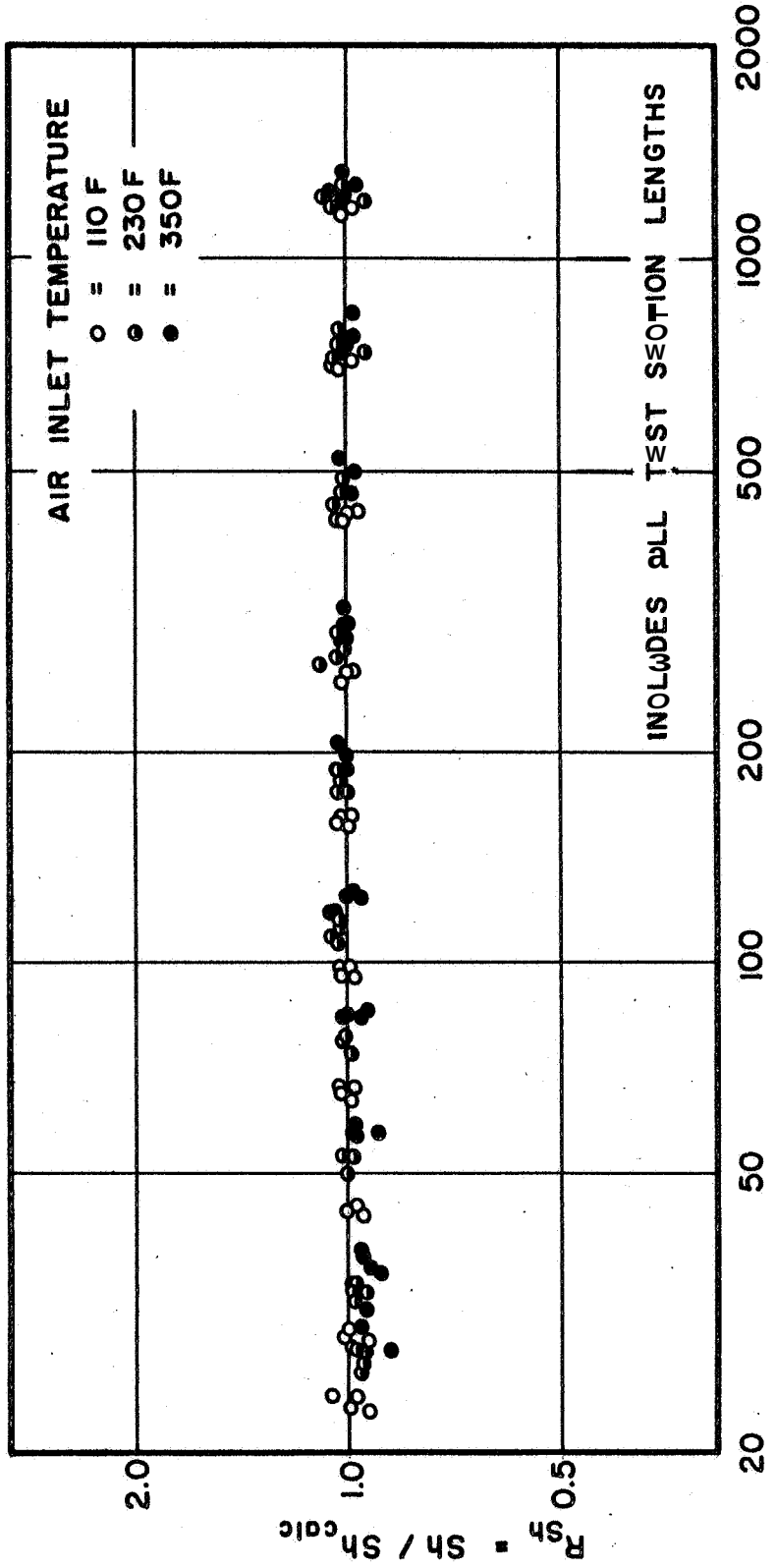

Fig. 13 Sherwood Number Ratio as a Function of Liquid Reynolds Number

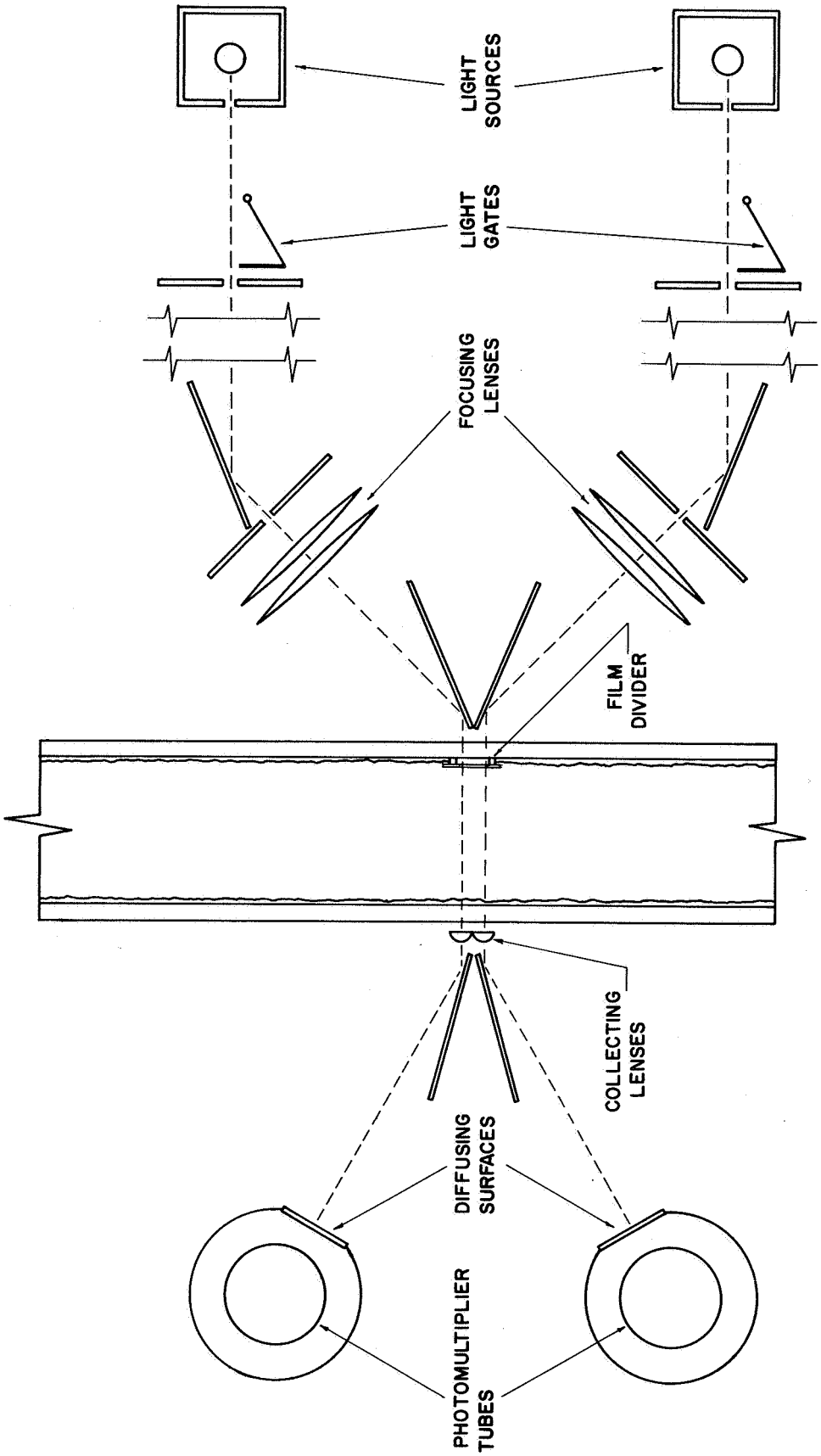

Fig. 14 Schematic Diagram of the Optical System

a

was a dual optical system, by means of which the instantaneous thickness of the liqaid film could be measured simultaneously at two locations in the test section, one location being 0.25 in. above the other. Since the two sets of equipment comprising the dual optical system are identical, the description of one of them will suffice.

Light from an incandescent bulb passes through a series of apertures, mirrors, and lenses and is brought to focus at a point approximately 0.01 in. from the inside surface of the test section where the film thickness is to be measured. A small streamlined piece of bakelite, called a film divider, is located on the opposite side of the test section where the light beam enters the tube; the film divider causes the film to break and flow on either side of the film divider. The incident beam of light passes through a hole in the center of the film divider. The light beam passes, therefore, through only the single thickness of the liquid film located where the incident light beam is focused on the opposite side of the test section, The intensity of the light transmitted through the film is measured by a photomultiplier tube. A lens between the point of measurement and the photomultiplier tube helps direct any divergent rays so that they fall on the surface of the photomultiplier unit. The output of the photomultiplier tube is displayed on a dual-beam oscilloscope, and the mean value of the current flowing through the photomultiplier tube is measured with a mirror galvanometer, placed in series with the photomultiplier tube.

Since a negligible amount of the incident light is absorbed by a film of clear water, it is necessary to add a dye to the water, so that small

changes in film thickness might be detected. Nigrosine dye, which has been shown to have a negligible effect on the physical properties of water (48), was used in the ratio of approximately 0,0005 pound dye per pound of water, The actual concentration of dye in the water entering the test section was determined by calibrating the optical system with samples of the dyed water taken periodically during the experiments.

As was pointed out in the Review of the Literature, the dye Concentration is a function of the fraction of the liquid evaporated after its injection into the test section; some of the water evaporates but not the dye. The change in concentration was calculated for each experimental run, employing the correlation technique described in the previous section and the measured inlet conditions for the experimental run. The dye concentration at the point of measurement is given by

$$c = c_i \frac{W_{Li}}{W_L} \qquad (27)$$

where c = dye concentration at point of measurement, lb/lb

c_i = dye concentration at inlet, lb/lb

W_L = weight rate of liquid flow at point of measurement, lb/sec

W_{Li} = weight rate of liquid flow at inlet, lb/sec

Experiments for the measurement of film surface characteristics were conducted for the nominal values for the system parameters presented below.

a. test section length to point of measurement: 5, 20, **34** in,

b. air inlet temperature: 110, 230, and 350 F

c. water weight flow rate: 0.00152
0.00188
0.00418
0.00996
0.02649
0.07182 lb/sec

In all of the experiments, the inlet air velocity was 48 fps. A total of 41 experimental runs was made, covering nearly all of the possible combinations of (a), (b), and (c), with the exception of the data taken at a water temperature of 350 F with the 24 in. test section; these data were not obtained due to breakage of the 24 in. long test section.

During each experimental run the following data were taken:

a. the measurements for determinating the inlet flow conditions

b. the reading of the mirror galvanometer

c. the photographic record of the film profile; obtained by photographing the dual-beam oscilloscope

Also, a sample of the dyed water was taken during each series of runs; a series comprised the runs made with a given test section at a given inlet temperature, The samples were used for calibrating the optical system.

3.2.2 Results of the Surface Characteristics Experiments

Figure 15(a) presents some typical oscillograph-record camera strips obtained during the investigation of the surface characteristics of the liquid film. The records shown are for liquid Reynolds numbers of 35, 185, and 1290, respectively. The pertinent parameters of the gas streams were approximately: inlet air temperature = 226 F, air velocity = 48 fps, air Reynolds number = 25,900. The distance from the point of liquid

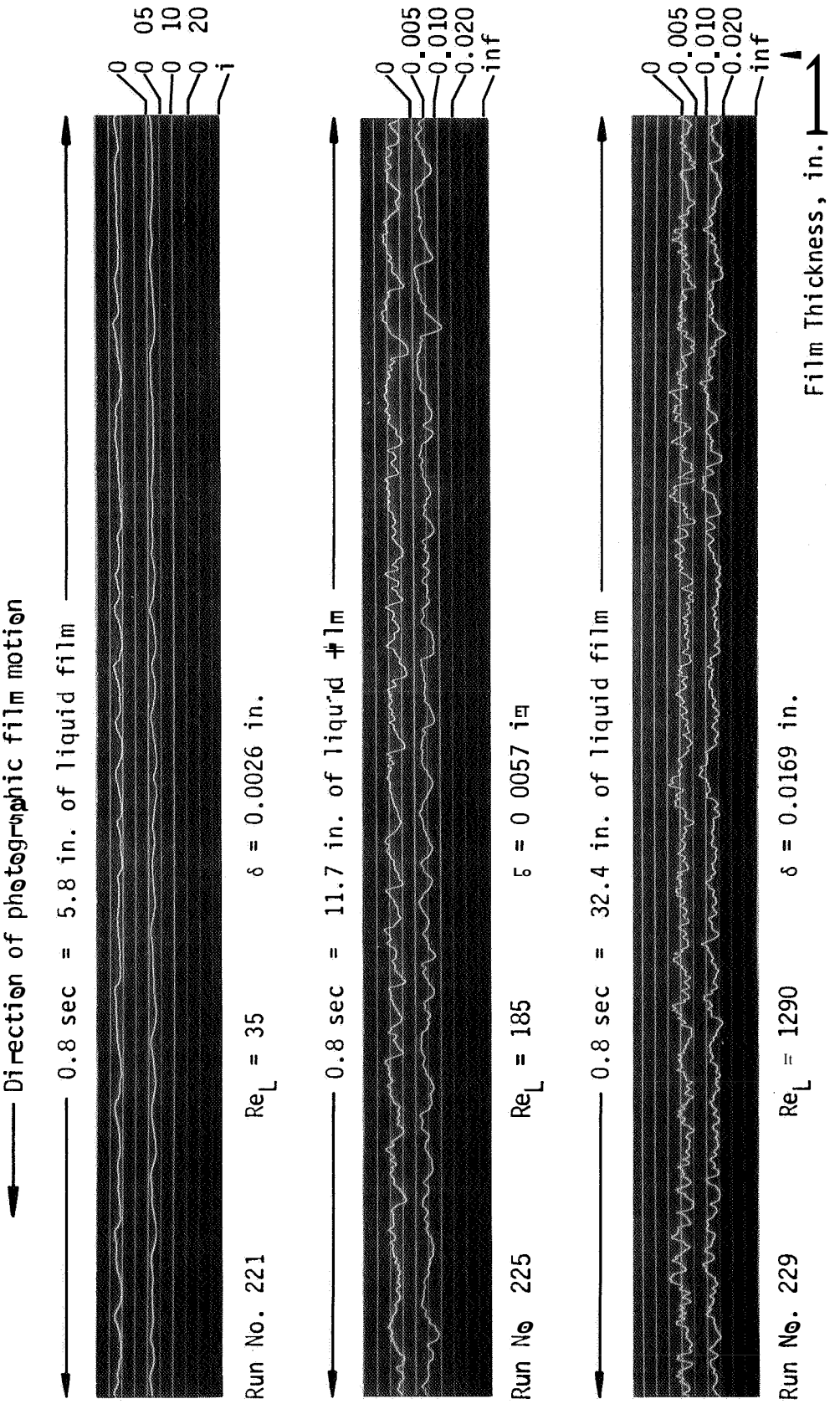

Fig. 15(a) Typical Oscillograph-Record Camera Traces for x = 5 38 in

injection to the point-of measurement was 5.38 in. Figure 15(b) presents strips taken under approximately the same conditions, but with the point of measurement 33.94 in. from the point of injection. The photographic film speed was 600 in./min. Appropriate time and liquid film thickness scales are shown for the lower trace.

Visual observation of the traces obtained for the different experimental runs indicated that there was essentially no difference between the traces obtained with the different air temperatures. Consequently, due to the relatively large amount of labor required for complete reduction of the data, the detailed results were computed only for the runs where the inlet air temperature was approximately 230 F. Three test section lengths were investigated, and three water flow rates were analyzed for each length of test section.

An oscillograph-record camera strip approximately 12 in. long, was obtained for each combination of length of test section and water flow rate. Three typical lengths of film 1 in. long were chosen from each strip for analysis. From the measurements made from each of those three lengths, the mean film thickness, the average wave velocity, and the surface area factor (calculated surface area of rough film divided by surface area of equivalent smooth film) were calculated. A detailed description of the method employed in the calculations is presented in Appendix E. It is sufficient to say here that the traces on the film were numerically analyzed to yield the geometry of the surface of the film, from which the desired parameters were calculated.

Table 1 presents the results of the calculations. In the runs included

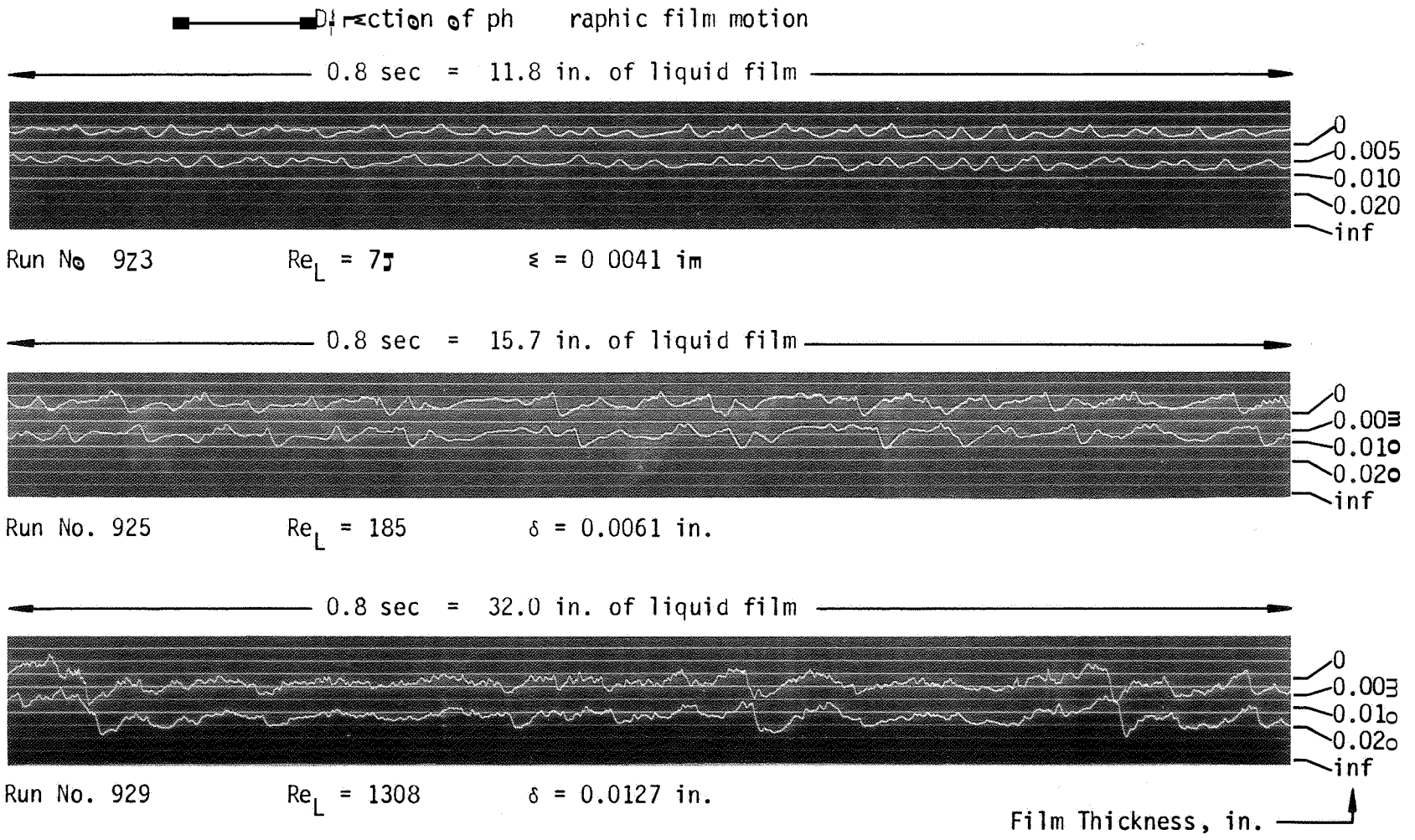

Fig. 15(b) Typical Oscillograph-Record Camera Traces for x = 33.94 in.

TABLE I

Results of the Surface Characteristics Experiments

Run No.	Distance from Injection	Water Reynolds Number	Mean Film Thickness (calc) (in.)	Mean Film Thickness (galvo) (in.)	Wave Velocity (fps)	Average Wave Velocity (fps)	Surface Area Factor	Average Surface Area Factor
S221a	5.38	35	,0024	.0026	.58	.60	1,0001	1.0001
b			.0026		.65		1.0001	
c			.0023		.57		1.0001	
S225a	5.38	185	.0053	.0057	1.05	1.22	1.0008	1.0008
b			.0056		1.31		1.0009	
c			.0053		1.30		1.0007	
S229a	5.38	1290	.0162	.0169	3.73	3.37	1.0005	1.0006
b			.0164		3.2%		1.0006	
c			.0149		3.09		1.0007	
S521a	20.25	35	,0037	,0038	.74	.77	1.0001	1.0001
b			.0043		.77		1.0002	
c			.0031		.80		1.0000	
S525a	20.25	188	.0059	.0059	1.48	1.45	1.0005	1.0004
b			.0055		1.36		1.0004	
c			.0064		1.52		1.0003	
S529a	20.25	1315	.0135	.0136	3.02	3.57	1.0005	1.0003
b			,0159		4.19		1.0002	
c			.0134		3.49		1.0003	
S923a	33.94	77	.0042	.0041	1.08	1.12	1.0002	1.0003
b			.0049		1.11		1.0003	
c			.0057		1.18		1.0005	
S925a	33.94	185	.0056	.0061	1.62	1.64	1.0004	1.0004
b			.0067		1.59		1.0004	
c			.0065		1.72		1.0004	
S929a	33.34	1308	.0123	.0127	3.45	3.33	1.0004	1.0005
b			.0098		3.01		1.0006	
c			.0146		3.54		1.0004	

in that table the air velocities ranged from 46.8 to 48.2 fps and the inlet air temperature ranged from 225 to 242 F. The mean film thicknesses presented in the column headed "mean film thickness (galvo)" were determined from the galvanometer readings, whereas the values in the column headed "mean film thickness (calc)" were obtained by analyzing the oscillograph-record camera strips.

Figure 16 presents a logarithmic plot of the mean film thickness, as determined from the galvanometer readings, as a function of the water Reynolds number for three test section lengths (x/d = 36. 13.5, and 22.6) at a nominal air inlet temperature of 230 F.

Figure 17 presents the average value of wave velocity (average of a, b, and c calculations far each run) as a function of the water Reynolds number for the three test section lengths at'a nominal air inlet temperature of 230 F.

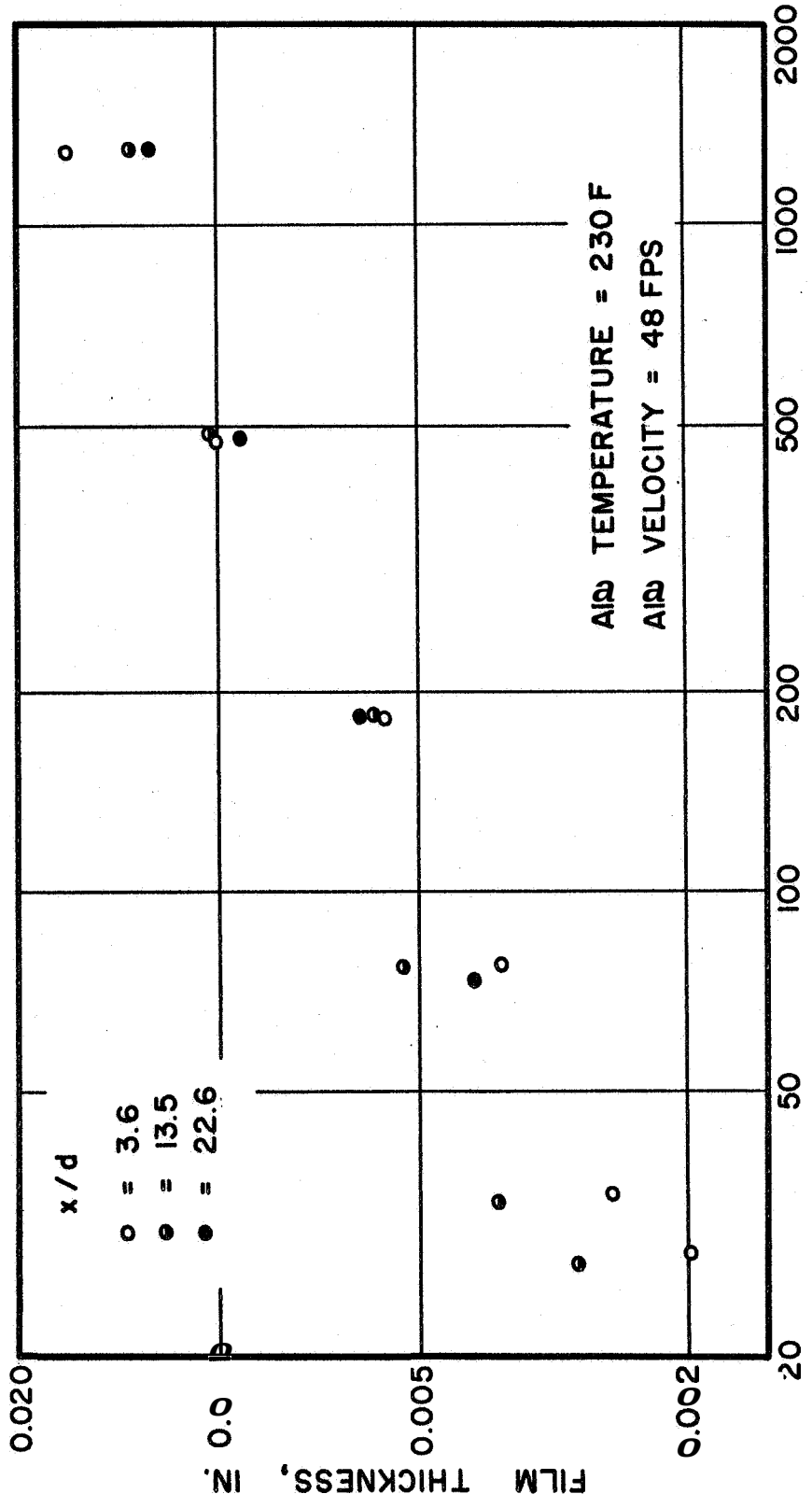

Fig. 16 Mean Film Thickness as a Function of Liquid Reynolds Number

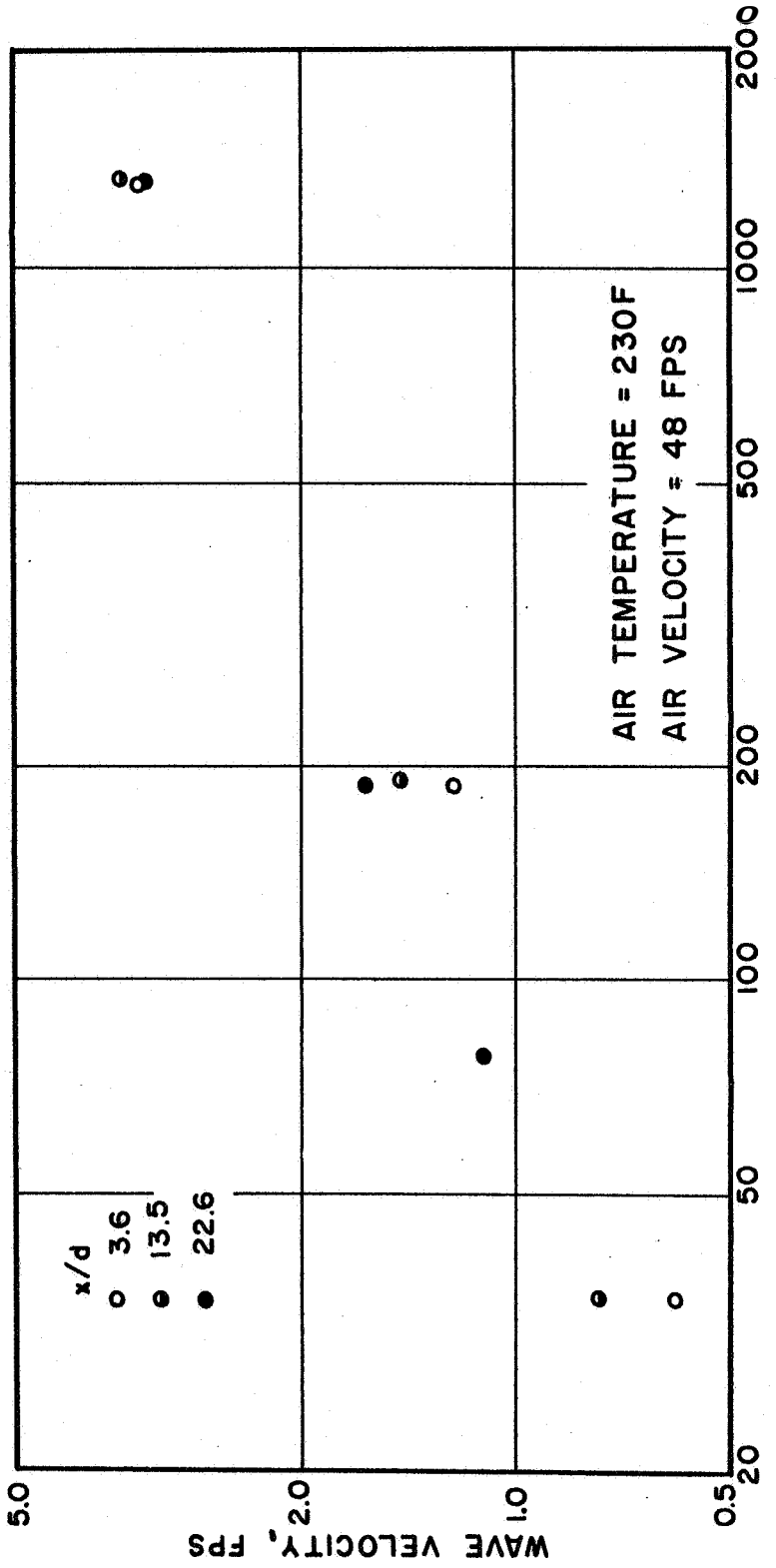

Fig. 17 Average Wave Velocity as a Function of Liquid Reynolds Number

4. DISCUSSION OF RESULTS

Figures 3 through 7 demonstrate that the experimental mass transfer data cannot be correlated by means of the conventional correlation equation (equation 14) based on the inlet and outlet conditions. It is worth noting here that in the preliminary attempts to correlate the data the transport properties were evaluated at the average value of the inlet and outlet air temperature, and the scatter of the data was increased; those obtained at the highest temperature falling far below the other data. It appeared that changes in the liquid flow rate affected the mass transfer group in an inconsistent manner for the different inlet ais temperatures; the effects were probably caused by variations in the water inlet temperature (see Appendix D).

When the data were correlated by the technique described in the preceding section, however, the effects of both the air inlet temperature and the water flow rate were eliminated (see Fig. 13), as may be seen by the greatly reduced scatter and the nearly horizontal slope of the curve. Also, the proper selection of a function describing the variation in heat and mass transfer coefficients with distance from the inlet to the test section made it possible to correlate the exprimental results with a single curve, for the different test sections (L/d varying from 5.7 to 26.5).

a

When the F_1 terms in equations 24 and 25 are replaced by unity, the equations then apply to the case for fully developed flow; i.e., with x/d approaching infinity. The latter case is approximated experimentally by employing a test section having a large L/d. Since most of the experimental work published in the literature is for test sections with large values of L/d (approximately L/d = 40), by setting $F_1 = 1$ in equation 25, the following equation is obtained for comparing the experimental results reported herein with those of other investigators. Thus

$$Sh = 0.0138\ Re_G^{0.83}\ sc^{0.44} \qquad (28)$$

(Actually, for L/d = 40, setting F_1 equal to approximately 1.1 would be a more nearly correct representation, because $F_1 = 1$ is valid only for the case where L/d = ∞. Such a substitution would result in slightly better agreement between the results reported herein and the nonrippling case of reference 39, as will be seen later.)

As noted in the Review of the Literature (see Section 2.2), Kafesjian, Plank, and Gerhard (39) analyzed all of the available data, including their own, and concluded that the following two correlation equations were applicable to (a) rippling and (b) nonrippling films, respectively. Thus

(a) Rippling film: $Sh\ (p_{BM}/P) = 0.0065\ Re_G^{0.83}\ Re_L^{0.15}$ (29)

(b) Nonrippling film: $Sh\,(p_{BM}/P) = 0.013\ Re'^{0.83}_{G}$ (30)

The prime on the gas Reynolds number in equation **30** indicates that the gas velocity upon which the Reynolds number is based is the velocity relative to the surface of the liquid film. To compare equation **28** with equations **29** and **30,** the substitutions Sc = 0.60 and $p_{BM}/P = 1$ are introduced into equations **28, 29,** and 30; the latter substitutions closely approximate the conditions prevailing in the subject experimental investigation. The results of that investigation are denoted by JPC results. Accordingly, one obtains

JPC results: $Sh = 0.0110\ Re_G^{0.83}$ (31)

Rippling **(39):** $Sh = 0.0065\ Re_G^{0.83}\ Re_L^{0.15}$ (32)

Nonrippling **(39):** $Sh = 0.013\ Re'^{0.83}_{G}$ (33)

Figure **18** presents a logarithmic graph of equations **31** through **33,** plotted with $Sh/Re_G^{0.83}$ as a function of the liquid Reynolds number Re_L. The length of the individual curves correspond to the range of liquid Reynolds number investigated in the pertinent experiments.

The JPC results are seen to lie on a curve parallel to and about **15** per cent below the curve for the results of Kafesjian, et **al.,** for nonrippling films. The JPC data are in approximate agreement with the Kafesjian curve for rippling films at low liquid Reynolds numbers, but at other liquid Reynolds numbers they do not agree with the

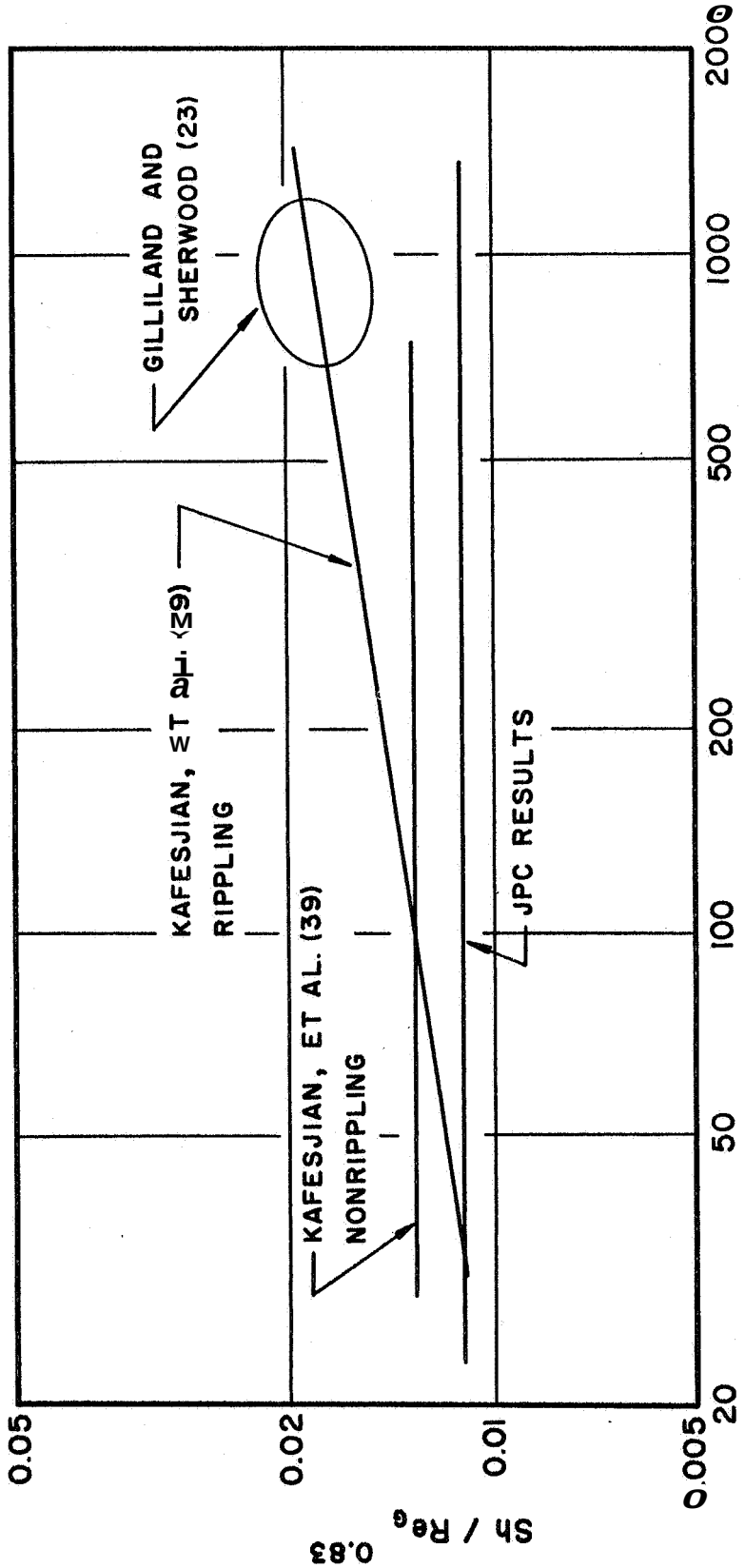

Fig. 18 Comparison of Present Mass Transfer Results with Results of Kafesjian, Plank, and Gerhard (39)

Kafesjian curve; the JPC data do not show the pronounced increase in Sherwood number with increasing liquid Reynolds number,

With the exception of approximately half of the data due to Gilliland and Sherwood (23), all of the data analyzed by Kafesjian, et al., were obtained for the case of countercurrent flow (39); that is, with the liquid flowing downward and the air flowing upward. The estimates of the percentage increase in the surface area of the liquid film ranged from negligible to more than 20 per cent. There are no reliable data, however, for substantiating those estimates of the increase in the surface area of the film under the flow conditions investigated by the author.

It is seen in Fig. 18 that the curve correlating the JPC results is substantially parallel to the correlation curve for nonrippling films. This is not surprising in view of the results obtained at the JPC in the experiments for determining the surface area of the liquid film under different flow conditions. Those results (see Table 1, Section 3.2.2) show that in all cases the percentage increase in surface area was less than 1 per cent.

The data of Gilliland and Sherwood for concurrent flow (23) lie within the ellipse drawn in Fig. 18. The countercurrent data also fall in the same area; no significant difference can be observed between the two sets of data. The range of liquid Reynolds numbers investigated was of the same order of magnitude as the scatter of the data, precluding any meaningful determination of the slope of the data for the two types of flow. No explanation can be given for

the disagreement between Gilliland's results for concurrent flow and those of the author. The experiments due to Gilliland were conducted at near room temperature, and there was little change in the liquid temperature due to the relatively large liquid flow rate. The method of correlation he employed, therefore, based upon inlet and outlet conditions, was satisfactory.

The results of the measurements of surface area indicated that there was a negligible increase in the surface area under the conditions investigated by the author. The measured increase in surface area ranged from 0.01 to 0.08 per cent. Due to the large amount of labor required for reading the photographic records, only a limited amount of the experimental data was reduced. Consequently, the consistency of the results was unsatisfactory. The increase in the amount of data that would have to be reduced to achieve consistency would be at least an order of magnitude. The limited amount of data that was reduced was sufficient, however, to establish that under all of the conditions investigated the increase in the surface area was negligible. Hence, it was concluded that the analysis of additional data would not yield a significant increase in meaningful information.

Figure 19 compares the mean film thicknesses measured in the subject investigation with those measured by Charvonia (11). The thickness parameter employed by Charvonia, is defined by

$$TP = \delta \left[\frac{1}{\sigma} \left(\frac{\gamma_L}{\quad} \right)^2 \right]^{1/3} \qquad (34)$$

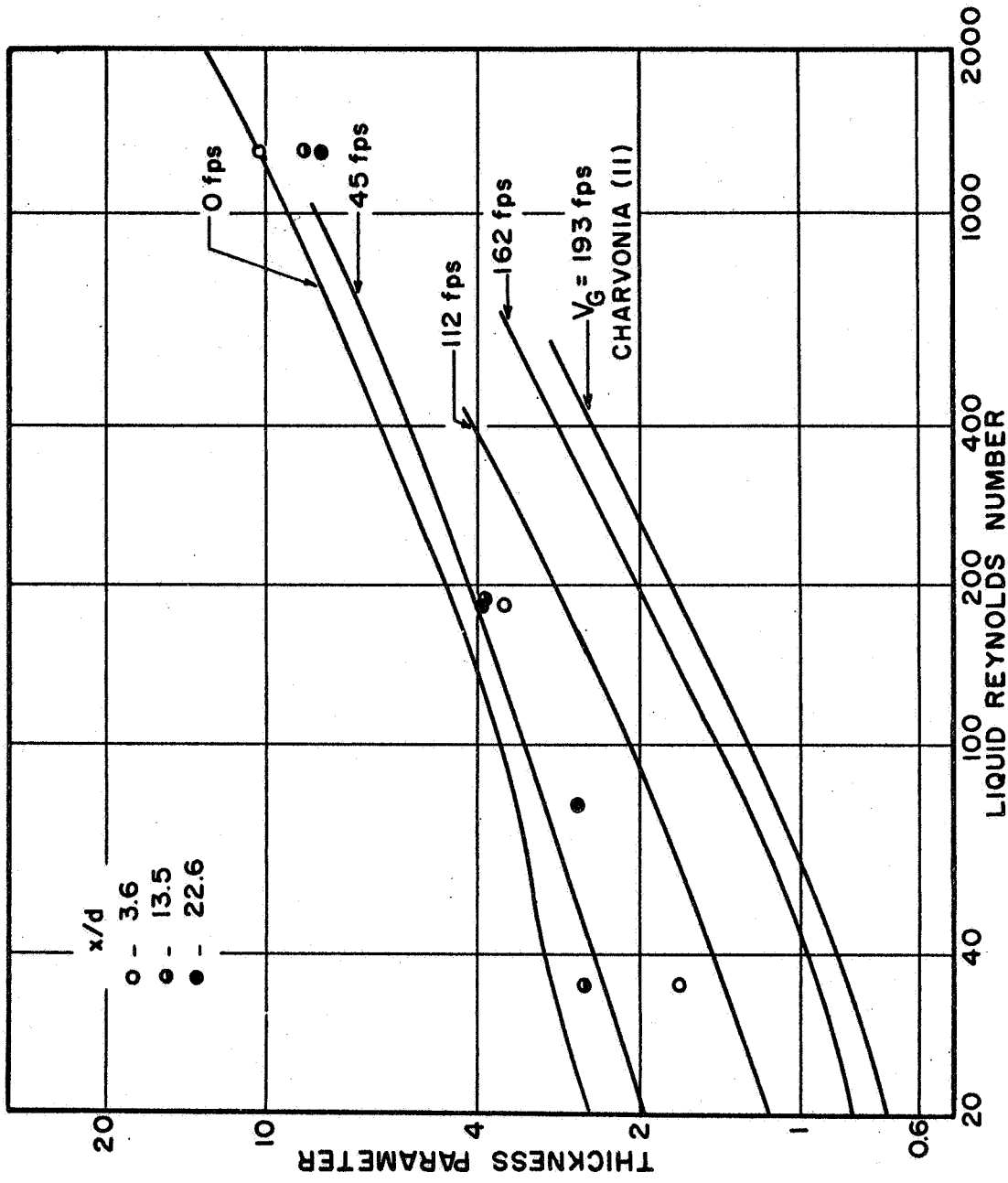

Fig. 19 Comparison of Present Film Thickness Results with Results of Charvonia (11)

where

δ = mean liquid film thickness, ft

g = gravitational constant, ft/sec^2

γ_L = specific weight of the liquid, lb/ft^3

μ_L = dynamic viscosity of the liquid, $lb\text{-}sec/ft^2$

Figure 19 presents the thickness parameter plotted as a function of the liquid Reynolds number. The results of the subject investigation are seen to be substantially parallel to the curves obtained by Charvonia for constant gas velocity. Furthermore, the datum points are near the line Charvonia's results indicate for a gas velocity of 45 fps. The gas velocity in the subject investigation was 48 fps. Thus, there is good agreement between the present film thickness values and those observed by Charvonia.

The data plotted in Fig. 16 do not indicate any significant variation in the mean film thickness with distance downstream from the point of injection of the liquid film. That result is in agreement with the data obtained by Chien and Ibele (12); their results show no significant variation in the mean film thickness with distance from the point of injection for liquid Reynolds numbers less than 1250.

As mentioned earlier, and also shown in Appendix E, it was necessary to know the wave velocity in order to calculate the surface area of the liquid film from the continuous measurements of film thickness as a function of time, It is of interest to compare the wave velocities measured in the subject investigation with

those determined by other investigators.

Figure 20 presents the wave velocity as a function of the flow parameter ($G'^2/\gamma_L \mu_L$) which was employed by Greenberg (27) in his correlation of wave velocity data, The parameter appeared originally in an analysis of the flow of a vertical, laminar film due to Nusselt. Nusselt's analysis, which is derived in reference 27, results in an expression for the maximum velocity in the film (velocity at the free surface). The Nusselt equation for the maximum film velocity is given by

$$V_{max} = \frac{1}{2} \left(\frac{9\, G'^2}{\gamma_L \mu_L}\right)^{1/3} \qquad (35)$$

where

V_{max} = maximum velocity in the film, fps

G' = peripheral liquid flow rate, lb/sec-ft

γ_L = specific weight of the liquid, lb/ft^3

μ_L = dynamic viscosity of the liquid, $lb\text{-}sec/ft^2$

Equation 35 is plotted in Fig, 20, along with the data obtained by Greenberg for the flow of water on the inside of a 2 1/2 in. I.D. vertical tube with no air flow, (It should be noted that in Fig. 21 of reference 27 the curve representing equation 35 is 'located incorrectly.) The bulk of the data due to Greenburg, which includes the results obtained with 8 different liquids, falls along Nusselt's curve. At the larger values of the flow parameter, however, they

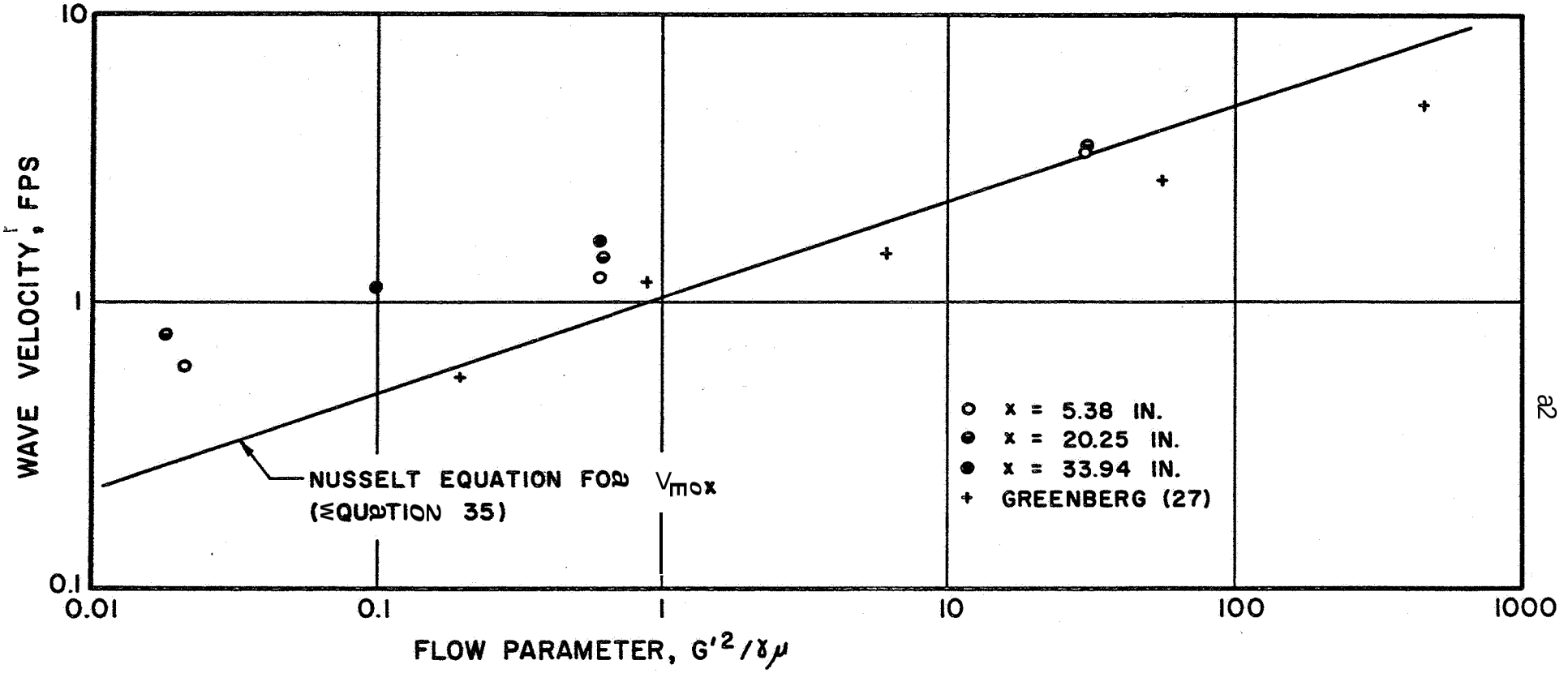

Fig. 20 Comparison of Present Wave Velocity Results with Results of Greenberg (27)

tend to fall below the Nusselt curve, as do the data for water (see Fig. 20) obtained in the subject investigation.

As one would expect, the data obtained in the subject investigation with concurrent air flow fall above those obtained by Greenberg with no air flow, because of the shearing action of the gas, which accelerates the liquid film, The wave velocity tends to increase somewhat with increasing distance from the plane of injection, but that effect is not very pronounced over the range of distances investigated. It appears that the waves approach their terminal velocity shortly (within a few diameters) after injection.

5. CONCLUSIONS AND RECOMMENDATIONS

5.1 Conclusions

The conclusions presented below are based upon the results of the research reported herein.

1. The experimental data obtained in the subject investigation were correlated by the following equations, for the local values of heat and mass transfer coefficients. Thus

$$Nu_x = 0.0205\ F_1\ Re_G^{0.8}\ Pr^{0.33} \tag{24}$$

$$Sh_x = 0.0138\ F_1\ Re_G^{0.83}\ Sc^{0.44} \tag{25}$$

where

$$F_1 = \begin{cases} 1 + \left(\dfrac{0.588}{x/d}\right)^{0.75} & \text{for } x/d > 0.166 \\ 5.51 - 11.6(x/d) & \text{for } x/d \leq 0.166 \end{cases} \tag{26}$$

All of the transfer properties were evaluated at the temperature which is the mean value for the average gas and liquid temperatures.

2. Correlation of the data by equations 24 and 25 indicates that for liquid Reynolds numbers in the range Re_L = 23 to 1350, there is no effect of Re_L upon the mass transfer.

3. In all cases, the measured increases in surface area of the liquid film, caused by waves on the surface of the film, were less than 0.1 per cent.

4. For a given gas stream velocity the mean film thicknesses were approximately the same as those measured by Charvonia (11) in a test section of larger diameter (1.67 times that employed in the subject research). The mean film thicknesses were essentially constant for values of x/d ranging from 3.6 to 22.6.

5. The velocities of the waves on the surface of the film increased with increasing liquid flow rate, and were larger than those measured by Greenberg (27) with no air flow, Over the range of liquid Reynolds numbers investigated, the wave velocities exceeded the values of maximum velocity calculated by Nusselt's analysis for laminar film flow.

5.2 Recommendations

The experiments reported herein show that there is neither an appreciable increase in the surface area of the film nor an effect due to the rate of flow of liquid on the mass transfer in downward, concurrent, annular, two-phase flow. According to the literature (39), however, there is a considerable increase in the rate of mass transfer with liquid flow rate for the case of countercurrent flow. No data are available concerning the increase in surface area of the film for countercurrent flow; the latter type of flow appears to be a fruitful area for further research,

It is recommended that a research program be initiated for investigating characteristics of the surface of the film and the rate of mass transfer in countercurrent, annular, two-phase flow.

Due to the apparent limitations of the light absorption technique for an investigation of that type of flow (32), it is further recommended that other methods of instantaneous film thickness measurement, including the fluorescence-spectrometer technique, be investigated to determine their feasibility as measurement techniques for countercurrent, annular, two-phase flow.

LIST OF REFERENCES

1. Ammann, H. H., "Viscosity effects in two phase annular flow," M.S.M.E. Thesis, Purdue University (August 1960).

2. Anderson, J. D., Bollinger, R. E., and Lamb, D. E., "Gas phase controlled mass transfer in two phase annular horizontal flow," A.I.Ch.E. J. 10, 640-645 (1964).

3. Barnet, W. I., and Kobe, K. A., "Heat and vapor transfer in a wetted-wall tower," Ind. Eng. Chem. 33, 436-442 (1941).

4. Belkin, H. H., MacLeod, A. A., Monrad, C. C., and Rothfus, R.R., "Turbulent liquid flow down turbulent walls," A.I.Ch.E. J. 5, 245-248 (1959).

5. Bennett, J. A. R., "Two phase flow in gas-liquid systems," A.E.R.E. CE/R 2497 (March 1958).

6. Boelter, L. M. K., Young, G., and Iversen, H. W., "An investigation of aircraft heaters. XXVII--Distribution of heat-transfer rate in the entrance section of a circular tube," NASA TN 1451 (1948).

7. Brauer, H., "Stromung und Warmeubergang bei Rieselfilmen," VDI-Forshungsh. 457 (1956).

8. Cairns, R. C., and Roper, G. H., "Heat and mass transfer at high humidities in a wetted wall column," Chem, Eng. Sci. 3, 97-109 (1954).

9. Cairns, R. C., and Roper, G. H., "Uni-directional heat and mass transfer at high humidities in a wetted wall column," Chem. Eng, Sci. 4, 221-228 (1955).

10. Charvonia, D. A., "A review of the published literature pertaining to the annular, two-phase flow of a liquid and a gaseous medium in a pipe," TM-58-1, Jet Propulsion Center, Purdue University (1958).

11. Charvonia, D. A., "A study of the mean thickness of the liquid film and the characteristics of the interfacial surface in annular, two-phase flow in a vertical pipe," 1-59-1, Jet Propulsion Center, Purdue University (1959).

12. Chien, S., and Ibele, W., "Pressure drop and liquid film thickness of two-phase annular and annular-mist flows," Trans. ASME, Ser. C: J. Heat Transfer 86, 89-96 (1964).

13. Chilton, T. H., and Colburn, A. P., "Mass transfer (absorption) coefficients," Ind. Eng. Chem, 26, 1183-1187 (1934).

14. Collier, J. G., and Hewitt, G. F., "Film-thickness measurements," ASME Paper 64-WA/HT-41 (1964).

15. Collins, D. E., "Co-current gas absorption," Ph.D. Thesis, Purdue University (August 1958).

16. Davey, T. B., "Entrance region heat transfer coefficients," Chem. Eng. Progr. Symp. Ser. 59, 47-51 (1963).

17. Deissler, R. G., "Analysis of turbulent heat transfer and flow in the entrance regions of smooth passages," NACA TN 3016 (1953).

18. Deissler, R. G., "Analysis of turbulent heat transfer, mass transfer, and friction in smooth tubes at high Prandtl and Schmidt numbers," NACA Rept. 1210 (1955).

19. Dhanak, A. M., "Momentum and mass transfer by eddy diffusion in a wetted-wall channel," A. I. Ch. E. J. 4, 190-196 (1958).

20. Emmons, D. L., "Effects of selected gas stream parameters and coolant physical properties on film cooling of rocket motors," TM-62-5, Jet Propulsion Center, Purdue University (1962).

21. Federov, B. I., "An experimental investigation of water evaporation in a non-isothermal turbulent boundary layer," Intern. Chem. Eng. 4, 408-412 (1964).

22. Fulford, G. D., "The flow of liquids in thin films," Advan, Chem. Eng. 5, 151-236 (1964).

23. Gilliland, E. R., and Sherwood, T. K., "Diffusion of vapors into air streams," Ind. Eng. Chem. 26, 515-523 (1934).

24. Gouse, S. W., Jr., "An index to the two-phase gas-liquid flow literature: part I," Mass Institute of Technology Eng. Projects Lab. Rept. DSR 8734-1 (1963).

25. Gouse, S. W., Jr., "An index to the two-phase gas-liquid flow literature: part II," Mass. Institute of Technology Eng. Projects Lab. Rept. DSR 8734-4 (1964).

26. Govier, G. W., "Developments in the understanding of the vertical flow of two fluid phases," Can, J. Chem. Eng. 43, 3-10 (1965).

27. Greenberg, A. B., "The mechanics of film flow on a vertical surface," I-56-2, Jet Propulsion Center, Purdue University (1956).

28. Hall Taylor, N., Hewitt, G. F., and Lacey, P. M. C., "The motion and frequency of large disturbance waves in annular two-phase flow of air-water mixtures," Chem, Eng. Sci. 18, 537-552 (1963).

29. Hardy, A. C., and Perrin, F. H., The Principles of Optics, (McGraw-Hill Book Co., Inc., New York, 1932), p. 23.

30. Hartnett, J. P., "Experimental determination of the thermal-entrance length for the flow of water and of oil in circular pipes," Trans, ASME 77, 1211-1220 (1955).

31. Hewitt, G. F., King, R. D., and Lovegrove, P. C., "Techniques for liquid film and pressure drop studies in annular two-phase flow," A.E.R.E. R 3921 (March 1962).

32. Hewitt, G. F., and Lovegrove, P. C., "The application of the light absorption technique to continuous film thickness recording in annular two-phase flow," A.E.R.E. R 3953 (July 1962).

33. Hewitt, G. H. Nicholls, B., and Lovegrove, P. C., "Film thickness measurements in annular two-phase flow using a fluorescence spectrometer technique. Part I--Description of method," A, E, R.E. R 4478 (1964).

34. Hilsenrath, J., et al., "Tables of thermal properties of gases," Nat. Bur. Std. Circ, 564 (November 1955).

35. Hodgman, C. D., editor, Handbook of Chemistry and Physics (Chemical Rubber Publishing Co., Cleveland, Ohio, 1955), 37th ed,

36. Jackson, M. L., and Ceaglske, N. H., "Distillation, vaporization, and gas absorption in a wetted-wall column," Ind. Eng. Chem. 42, 1188-1198 (1950).

37. Jacowitz, L. A., and Brodkey, R. S., "An analysis of geometry and pressure drop for the horizontal, annular, two-phase flow of water and air in the entrance region of a pipe," Chem. Eng. Sci. 19, 261-274 (1964).

38. Kafesjian, R., "Gas phase mass transfer in wetted-wall towers," Ph.D. Thesis, University of Louisville (June 1961).

39. Kafesjian, R., Plank, C. A., and Gerhard, E. R., "Liquid flow and gas phase mass transfer in wetted-wall towers," A.I.Ch.E. J. 7, 463-466 (1961).

40. Keenan, J. H., and Keyes, F. G., Thermodynamic Properties of Steam (John Wiley & Sons, Inc., New York, 1936).

41. Kinney, G. R., Abramson, A. E., and Sloop, J. L., "Internal-liquid-film-cooling experiments with airstream temperatures to 2000 F in 2- and 4-inch-diameter horizontal tubes," NACA Rept. 1087 (1952).

42. Knuth, E. L., "Evaporation from liquid wall films into a turbulent gas stream," Heat Transfer and Fluid Mechanics Institute, University of Southern California (July 1953).

43. Lilleleht, L. U., and Hanratty, T. J., "Measurement of interfacial structure for co-current air-water flow," J. Fluid Mech. 11, Part 1, 65-81 (1961).

44. Linton, W. H., and Sherwood, T. K., "Mass transfer from solid shapes to water in streamline and turbulent flow," Chem. Eng. Progr. 46, 258-264 (1950).

45. Luikov, A. V., "Heat and mass transfer in capillary-porous bodies," Advan. Heat Transfer 1, 123-184 (1964).

46. McCarter, R. J. and Stutzman, L. F., "Transfer resistance and fluid mechanics," A.I.Ch.E. J. 5, 502-505 (1959).

47. McManus, H. N., Jr., "Experimental methods in two-phase flow," Multi-Phase Flow Symposium, ASME Winter Annual Meeting, Philadelphia, November 17-22, 1963, pp. 75-78.

48. Mezey, R. S., "Measurements of mass transfer and pressure drop in annular, two-phase flow," TM-65-4, Jet Propulsion Center, Purdue University (March 1965).

49. Miller, W. S., "An experimental study of annular two-phase flow," M.S.M.E. Thesis, Purdue University (June 1962).

50. Nedderman, R. M., and Shearer, C. J., "The motion and frequency of large disturbance waves in annular two-phase flow of air-water mixtures," Chem. Eng. Sci. 18, 661-670 (1963).

51. Persson, S. L., "Method for determination of velocity distribution in a thin liquid film," AIAA J. 2, 372-373 (1964).

52. Portalski, S., "The mechanism of flow in wetted-wall columns," Ph.D. Thesis, University of London (1960).

53. Power Test Codes, Supplement on Instruments and Apparatus; Part 5. Measurement of Quantity of Materials: Ch. 4. Flow Measurement. Published by ASME, New York (February 1959).

54. Schwarz, W. H., and Hoelscher, H. E., "Mass transfer in a wetted-wall column: turbulent flow," A.I.Ch.E. J. 2, 101-106 (1956).

55. Shenker, H., Lauritzen, J. I., Jr., Corruccini, R. J., and Lonberger, S. T., "Reference tables for thermocouples," Nat. Bur. Std. Circ. 561 (April 1955).

56. Sherwood, T. K., and Pigford, R. L., Absorption and Extraction (McGraw-Hill Book Co., Inc., New York, 1952), 2nd ed., Chap. III.

57. Silvestri, M., "Fluid mechanics and heat transfer of two-phase annular-dispersed flow," Advan, Heat Transfer 1, 355-446 (1964).

58. Stirba, C., and Hurt, D. M., "Turbulence in falling liquid films," A.I.Ch.E. J. 1, 178-184 (1955).

59. Tailby, S. R., and Portalski, S., "Hydrodynamics of liquid films flowing on a vertical surface," Trans. Inst. Chem, Engrs. (London) 38, 324-330, Discussion 343-346 (1960).

60. Tailby, S. R., and Portalski, S., "Wave inception on a liquid film flowing down a hydrodynamically smooth plate," Chem. Eng. Sci. 17, 283-290 (1962).

61. Wexler, A,, and Brombacher, W. G., "Methods of measuring humidity and testing hygrometers," Nat. Bur, Std. Circ. 512 (September 1951).

62. Wolf, H., "The experimental and analytical determination of the heat transfer characteristics of air and carbon dioxide in the thermal entrance region of a smooth tube with large temperature differences between the gas and the tube wall," Ph.D. Thesis, Purdue University (March 1958).

63. Jones, J. B., and Hawkins, G. A., Engineering Thermodynamics (John Wiley & Sons, Inc., New York, 1960) Art, 12.11.

APPENDICES

APPENDIX A

NOMENCLATURE

Symbol	
A	surface area of the gas-liquid interface, ft2.
ΔA	fractional increase in the interfacial surface area.
b	absorption coefficient of the dyed water, ft^{-1}.
C	concentration of dye in the dyed liquid, at the point of measurement, lb/lb.
c_i	concentration of dye in the dyed liquid at the plane of injection, lb/lb.
c_L	specific heat of the liquid, B/lb-R.
c_p	constant pressure specific heat of the gas, B/lb-R.
C	constant.
C_i	concentration of the diffusing vapor at the gas-liquid interface, lb/ft^3.
ΔC_m	log mean concentration of the diffusing vapor, lb/ft3.
d	inside diameter of the test section, ft.
5	molecular diffusivity of the diffusing vapor in the gas, ft2/sec.
f	friction factor.
F	function of x/d.
g	gravitational constant, ft/sec2.

G	mass velocity, lb/hr-ft^2.
G'	peripheral liquid flow rate, lb/sec-ft.
Gu	Gukhman number, $(T_a - T_b)/T_a$.
h	specific enthalpy, B/lb.
h_H	heat transfer coefficient, B/sec-ft2-R.
h_M	mass transfer coefficient, ft/sec.
i	reading of the galvanometer or oscillograph.
I	constant.
I	intensity of transmitted light.
I_o	intensity of incident light.
j_D	mass transfer j-factor.
k_G	thermal conductivity of the gas, B/sec-ft-R.
K	molar mass transfer coefficient, lb moles/hr-ft2-atm.
L	length of the test section, ft.
M_m	mean molecular weight.
Nu	over-all Nusselt number, $h_H d/k_G$.
Nu_x	local Nusselt number, $h_{Hx} d/k_G$.
Nu_{fd}	Nusselt number for fully-developed flow.
p_{BM}	log mean partial pressure of the diffusing vapor, $(p_{Bi} - p_{Bo})/\ln (p_{Bi}/p_{Bo})$, psia.
p_v	vapor pressure of the liquid, psia.
P	pressure, psia.
ΔP	pressure drop across the test section, psi.
Pr	Prandtl number, $\mu_G c_P/k_G$.
Q	rate of heat transfer, B/sec.

R_{Sh}	Sherwood number ratio, Sh/Sh_{calc}.
R_v	gas constant of the diffusing vapor, ft/R.
Re_G	Reynolds number of the gas phase, based upon the gas velocity relative to the test section, $\rho Vd/\mu_G$.
Re_G'	Reynolds number of the gas phase, based upon the gas velocity relative to the velocity of the surface of the liquid, $\rho V'd/\mu_G$.
Re_L	Reynolds number of the liquid phase, $4G'/g\mu_L$.
S	cross-sectional area of the test section, ft.
sc	Schmidt number, $\mu_G/\rho D$.
Sh	measured over-all Sherwood number, $h_M d/D$.
Sh_{calc}	calculated over-a11 Sherwood number, $h_M d/D$.
Sh_x	local Sherwood number, $h_{Mx} d/D$.
t	thickness of the dyed liquid through which the beam of light passes, ft.
T	temperature, R.
T_a	free stream temperature, R.
T_b	adiabatic saturation temperature, R.
T_L	temperature of the liquid, R.
T_W	temperature of the wall, R.
TP	thickness parameter, $\delta[(\gamma_L/\mu_L)2/g]\ 1/3$.
V	mean gas velocity, fps.
V_{max}	maximum velocity in the liquid film, fps.
V_W	wave velocity, fps.
W	weight rate of flow, lb/sec.
x	distance from the inlet of the test section, ft.

x_D effective film thickness for mass transfer, ft.

Greek Symbols

γ specific weight, lb/ft3.

δ displacement of a wave on the oscillograph, ft.

δ mean thickness of the liquid film, ft.

μ dynamic viscosity, lb-sec/ft2,

ν kinematic viscosity, ft2/sec.

ρ density of the gas, slug/ft^3.

σ dynamic surface tension, lb/ft.

τ time, sec.

ω specific humidity, lb water/lb dry air.

Subscripts

1 plane 1.

2 plane 2.

a air.

ev evaporating liquid.

G gas.

i inlet of the test section.

L liquid.

m mean.

o outlet of the test section.

v diffusing vapor.

APPENDIX B

DESCRIPTION OF THE EXPERIMENTAL APPARATUS

The experimental apparatus employed in the subject investigation was quite similar to that employed by Charvonia (11). Most of the changes in the apparatus were to enable measuring the rate of mass transfer; many of the changes are described by Mezey (48).

B.1 Air Flow System

The air used in the experimental investigation was drawn from the high pressure supply tanks which comprise the blow-down air supply for the Jet Propulsion Center. (Figure 21 presents a schematic diagram of the air flow system.) The tanks have a volume of 900 cu ft and were charged to a maximum pressure of 2400 psig by a Worthington 4-stage compressor. By operating a 4 in. gate valve (valve 1 in Fig. 21) the tanks could be isolated from the apparatus when the apparatus was not in use. The absolute humidity of the air drawn from the supply tanks was always less than 0.0006 lb moisture per lb dry air, as determined by psychrometric measurements.

The air pressure was reduced from the tank pressure to approximately 140 psig by means of a Grove Powereactor Dome Regulator; the latter was loaded by an Atlas hand-loaded pressure regulator. The flow regulating valve was a Hammel-Dahl Pressure Loaded Balanced

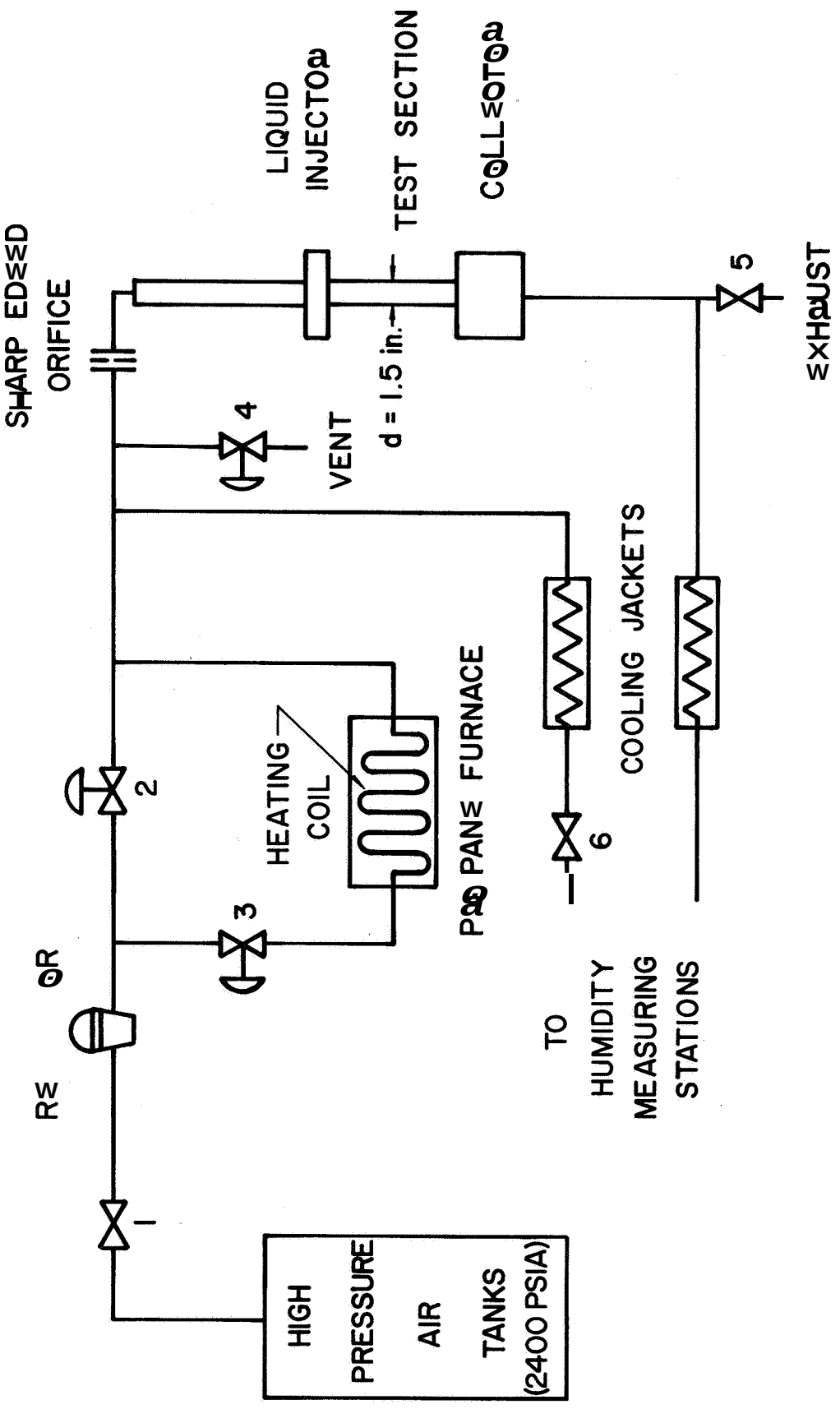

Fig. 21 Schematic Diagram of the Air Flow System

Diaphragm Control Valve (valve 2, Fig. 21), and it was loaded by a Moore Nullmatic hand-loaded pressure regulator.

The control of the temperature of the air entering the test section was achieved by causing a part of the air to bypass valve 2 and flow through a heat exchanger comprising a helical coil located inside a propane-air furnace. In the heat exchanger the bypassed air was heated to approximately 1600 F before it rejoined and mixed with the main air stream, The proportion of the air passing through the heating coil was regulated by a Honeywell Diaphragm Control Valve (valve 3), which was controlled by a Honeywell Electronik strip chart pneumatic controller. The pneumatic output of the controller was proportional to the difference between the desired air temperature, as set on the controller, and the temperature of the air measured at the entrance to the test section, At the highest temperature investigated, 350 F, it was necessary to vent some air to the atmosphere, through valve 4, in order to maintain the aforementioned air temperature at the entrance to the test section.

The air flow rate was measured by means of a thin plate orifice constructed according to A.S.M.E. specifications (53). The 1 1/8 in. diameter orifice plate was constructed from 1/8 in. stainless steel plate and was located in a section of 2.930 in. I.D. stainless steel tubing. The approach section of 20 diameters was preceded by a flow straightener. The exit section was 12 diameters. Because of its large sire it was not possible to calibrate the orifice meter, and the discharge coefficient presented in reference 53 was employed in making flow calculations.

The test section was preceded by a 6 ft length of 1.495 in, I.D. stainless steel tubing, which was carefully aligned to within 1/32 in. of the vertical. Total pressure traversing measurements (48) established that the velocity profile of the air entering the test section was that of a fully developed turbulent flow. After leaving the test section, the air was exhausted through ducting to the outside atmosphere.

All of the air flow system downstream from the propane furnace was insulated with Johns-Manville Superex Insulation, 85% Magnesia Insulation, or insulating cement, depending upon the air temperature and piping geometry.

Continuous samples of the air entering and leaving the test section were run to the two humidity measuring stations (described in Section 6.6) employed for measuring the inlet and outlet humidities. The rate of flow of the air to the inlet humidity measuring station was controlled by valve 6. A butterfly valve in the air exhaust ducting, valve 5, controlled the flow to the outlet humidity measuring station and also the static pressure in the test section. Cooling jackets, using tap water as the coolant, served to cool the air samples to approximately room temperature before they flowed into the humidity measuring stations.

6.2 Water Supply System

Figure 22 is a schematic diagram of the water supply system. Deionized water at approximately room temperature was supplied to the liquid injector from one of two pressurized supply tanks, termed the

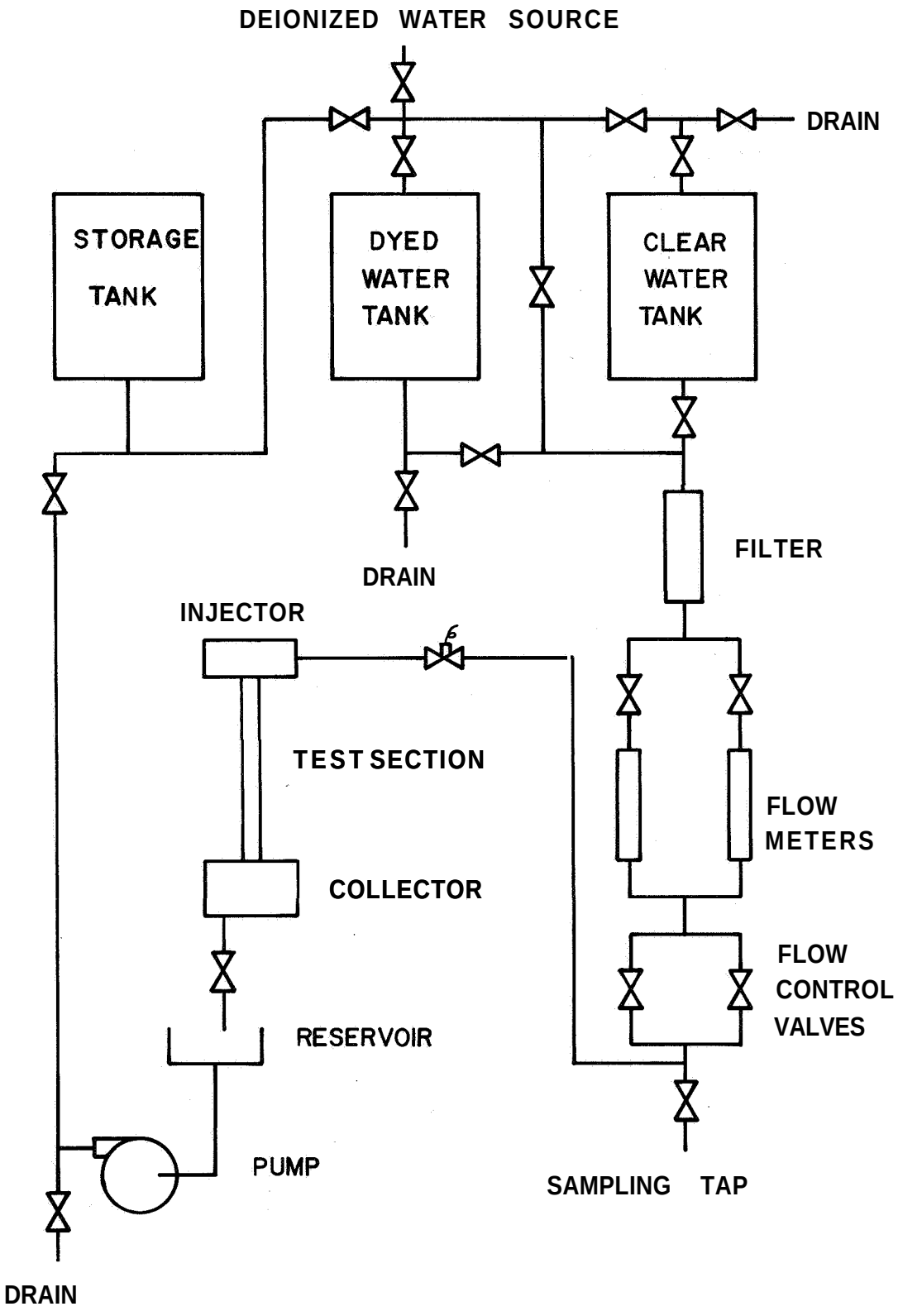

Fig. 22 Schematic Diagram of the Water Flow System

dyed water tank and the clear water tank (see Fig. 22). The tanks were pressurized by shop air which entered the tanks through Grove Powereactor Dome Regulators. The dome regulators were loaded to the desired pressure with a Moore Nullmatic hand-loaded pressure regulator and an Atlas hand-loaded pressure regulator, respectively.

Water flow rates were measured employing two Fischer & Porter Flow-rators, which were calibrated in place by the weight-time technique and were capable of measuring water flows from 0.0015 to 0.1 lb per sec. Flow rates were controlled by two parallel globe valves, one providing course and the other fine regulation. A sampling tap provided a means for extracting a small quantity of dyed water from the system for use in calibrating the optical system employed in the film thickness studies.

After leaving the test section the water flowed into a reservoir, from which it was pumped to a drain. It was also possible to return the water from the reservoir into any of the three tanks shown in Fig. 22. This capability was utilized when introducing dyed water into the system, the dye being mixed with water in the reservoir and then pumped into the dyed water tank.

Any of the tanks could be filled with deionized water from the bui1ding's tap water system. Deionization was accomplished employing a Culligan Duo-Bed Deionizing Unit. Water could be transferred from one tank to another, as during the mixing of the dyed water solution prior to conducting the experiments concerned with the film surface characteristics.

B.3 Test Section Assembly

Figure 23 presents an assembly drawing of the test section assembly, shown with an 8 in. glass tube in place. This drawing will be referred to in the subsequent description. Figure 24 is a photograph of the test section assembly, including the optical system described in Section 8.7. The test section assembly comprised three components--the injector assembly, the test section (glass tube), and the collector assembly--and will be described accordingly. The test section assembly was located in a light-tight room which could be completely darkened, as was necessary during the experiments employing the optical system.

B.3.1 Injector Assembly

The injector assembly, (e) in Fig. 23, was similar to that employed by Greenberg (27) and other investigators at the Jet Propulsion Center. Water from the supply system entered the injector through nine equally-spaced holes along the outside of the injector (f) and flowed past a baffle and into a circular manifold. The manifold was connected with the inside wall of the test section by a thin slot. The slot, formed by two conical surfaces, made a 45^{0} angle with the axis of the test section. With the two large plates of the injector bolted together, the two conical surfaces forming the slot touched. By inserting shims between the two large plates at the points where the bolts were located, the plates could be held a known distance apart, resulting in a slot of known width. Due to the angle made by the slot with the test section axis, the slot width was equal to the shim thickness divided by $\sqrt{2}$. Preliminary experiments established that a slot width of 0.018 in. (0.025 in. shims) was optimum for the range of flow rates investigated.

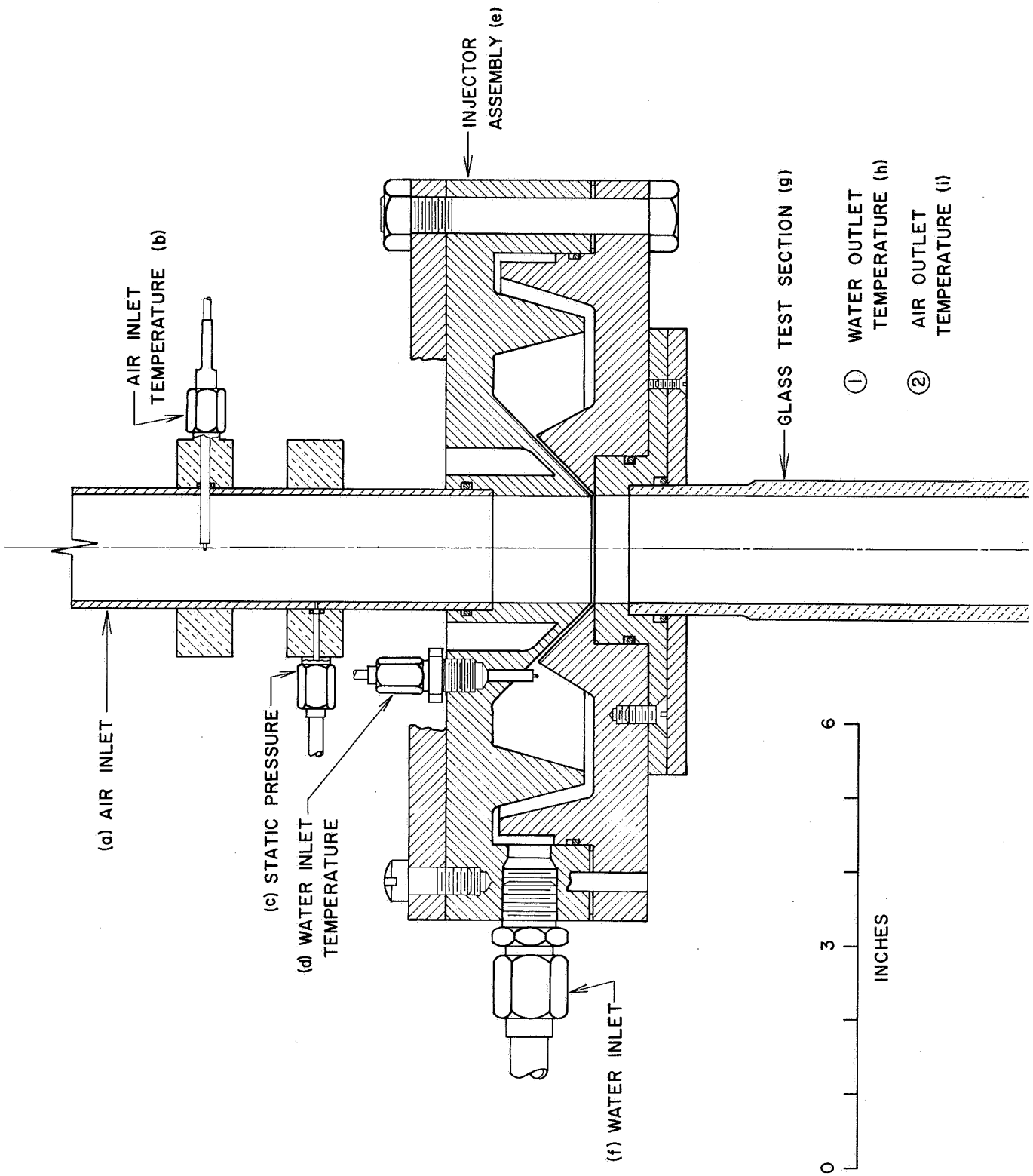
INJECTOR ASSEMBLY (e)
AIR INLET TEMPERATURE (b)
GLASS TEST SECTION (g)
① WATER OUTLET TEMPERATURE (h)
② AIR OUTLET TEMPERATURE (i)
(a) AIR INLET
(c) STATIC PRESSURE
(d) WATER INLET TEMPERATURE
(f) WATER INLET
0
3
6
INCHES

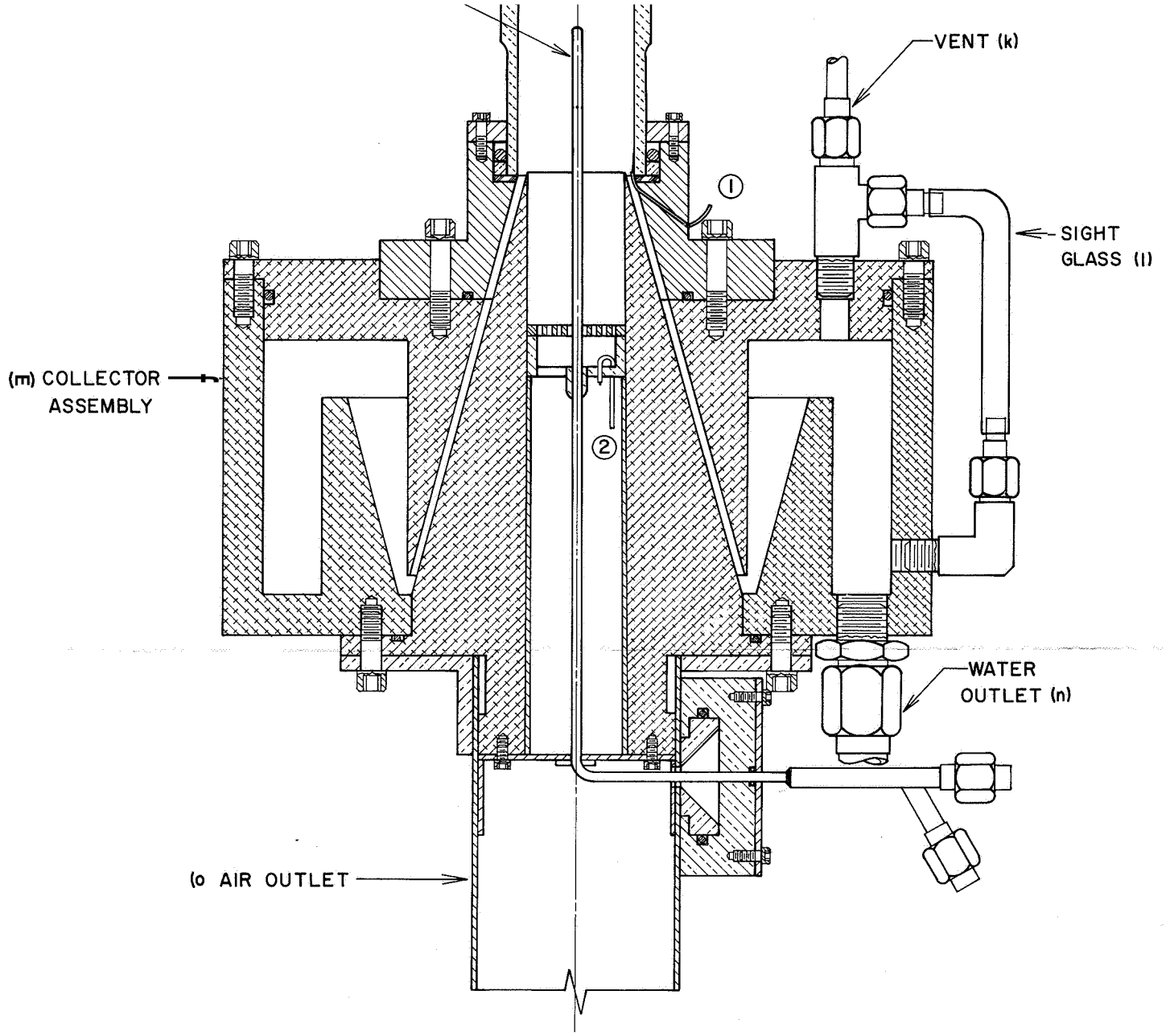

Fig. 23 Diagram of the Test Section Assembly

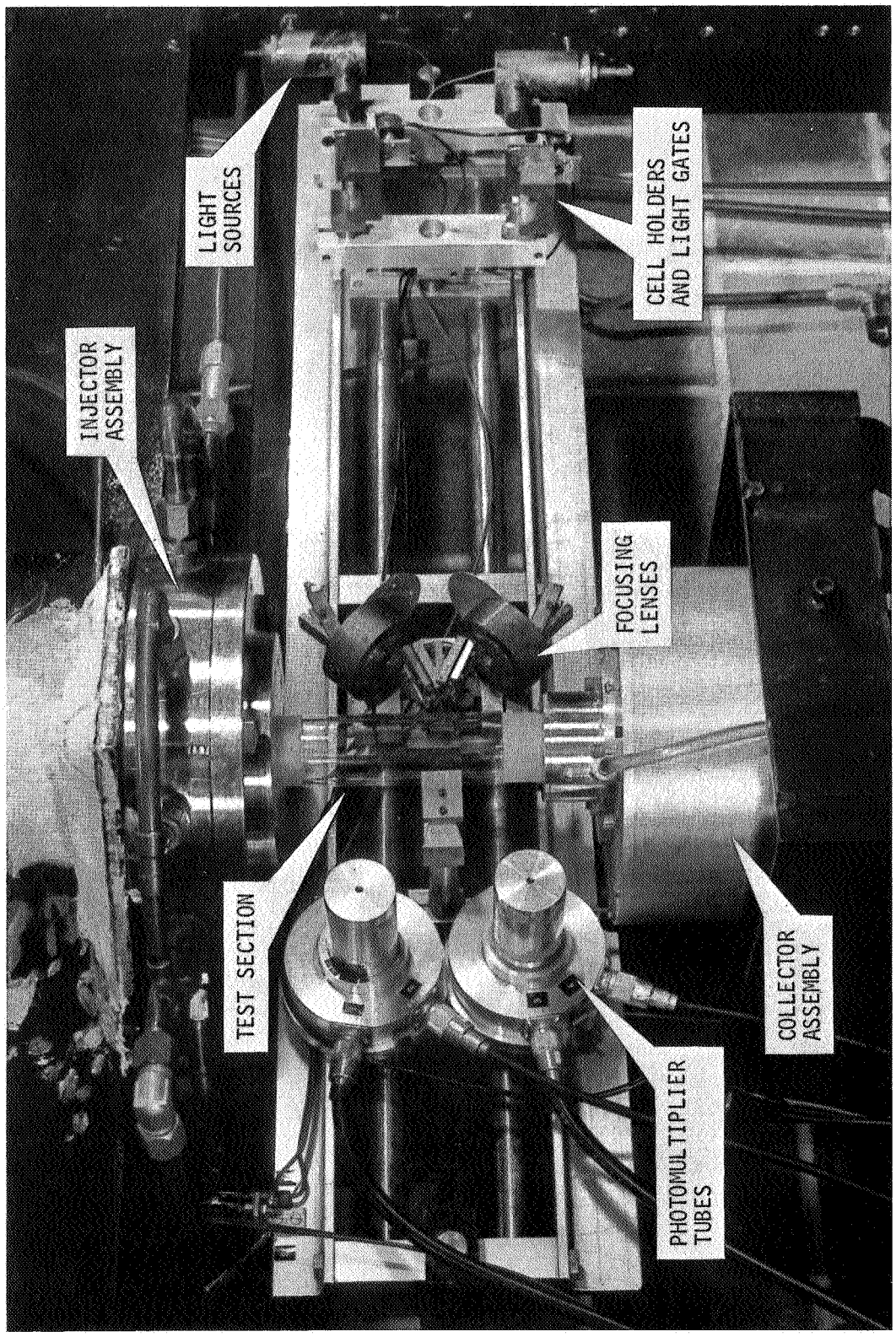

Fig. 24 Photograph of the Test Section Assembly and the Optical System

The upper injector plate was bolted to a rigid frame constructed of welded steel I-beams and aligned with the air approach-section (a), which fitted into the top of the upper injector plate. The inside diameter of the upper injector plate was 1.495 in., matching that of the air approach section. Since it was necessary to disassemble the injector assembly periodically for cleaning, dowel pins were employed to insure proper alignment of the upper and lower plates.

The transition between the injector plates and the glass tube (g) was made with the stainless steel transition plate, which was screwed to the lower injector plate, The inside diameter of the transition plate formed the first 0.5 in. of the test section, and it was of 1.502 in. I.D. to match the size of the glass tubes. O-ring seals were located between the various mating parts wherever pressure seals were required.

Figure 23 indicates where the chromel-alumel thermocouples (b,d) for measuring the air and water inlet temperatures were located. Also shown is the upstream pressure tap (c) employed for measuring the static pressure at the entrance of the test section, A correction to the measured pressure to account for the distance between the location of the pressure tap and the point of water injection (test section Inlet) was made assuming a friction factor corresponding to a smooth pipe and the prevailing air Reynolds number and properties.

As mentioned above, the actual test section length was 0.5 in. longer than the glass tube length due to the portion of the transition plate over which the film flowed before it reached the glass tube itself.

B.3.2 Glass Tube

The primary component of the test section assembly was the glass tube (g). As noted previously, glass tubes of different lengths (nominally 8, 16, 24, 32, and 40 in.) were employed, The tubes were all precision bore borosilicate glass tubes having measured inside diameters of 1,502 ± 0.001 in. and outside diameters of 1 27/32 in. To facilitate mounting and aligning a tube in the test section assembly, the outside diameters of the upper and lower portions of each tube were ground to a diameter of 1.785 ± 0.001 in., concentric with the inside diameter, far a distance of 1 1/2 in. from each end of the tube, During the course of the investigation some inadvertent chipping and cracking of the ends of the tubes occurred, necessitating cutting off a small amount from the faulty end, Such modification resulted in the shortening of some of the tubes. In all of the calculations, the actual tube dimensions were employed,

'As indicated in Fig, 23, the glass tube was mounted between the injector and collector assemblies in a manner that resulted in a smooth transition between the transition plate and the top of the tube, The method of mounting also, allowed for small changes in the position of the various components, such as occurred during installation, without danger, of excessively stressing the tube, Accordingly, there was a metal to glass junction at the top of the tube, and the O-ring which served as a seal also was used for obtaining axial alignment. A cork or rubber gasket was fitted between the lower end of the tube and the top piece of the collector assembly, allowing for some relative

shifting of the components. Axial alignment was again established by the sealing O-ring.

B.3.3 Collector Assembly

The purpose of the collector assembly (m) was to separate the water which had not evaporated into the air stream from the air stream, without letting air escape from the apparatus, an essential requirement for insuring that the air sample removed for determiningthe outlet air humidity was a valid sample for the entire air stream.

The design of the collector assembly (m) was similar to that of Collins (15). A circular knife-edge formed the entrance of a slot 0.1 in. wide into which the liquid film flowed. The liquid then flowed over a baffle into the outer section of the collector, from which it drained into the reservoir through three holes in the bottom of the outer section (n). The level of the liquid in the collector could be observed by means of a sight glass (l). By holding the liquid at the proper level in the collector, as could be done by regulating the flow out of the collector, a liquid seal was kept in the slot, prohibiting all but a minute amount of air from escaping,

During the experiments concerned with the surface characteristics of the liquid film the room in which the test section was located was darkened, making it impossible to visually dectect the level of the liquid in the collector. For those experiments a supplementary collector reservoir (not shown in Fig. 23) of volume several times that of the collector was mounted at the same approximate height as the collector and connected to the collector by tubing. A sight

glass outside the darkened room was connected to the supplementary reservoir, and a solenoid valve connected the supplementary reservoir to the drain, Due to the large additional volume of the supplementary reservoir, the level of the liquid in the collector fluctuated less, and as a result the level could be held satisfactorfly by occasionally draining water from the supplementary reservoir through the solenoid valve.

A Pitot-static tube (j) was employed for measuring the center-line velocity and the static pressure of the air leaving the test section. A chromel-alumel thermocouple (i) for measuring the outlet temperature of the air was located in the air exhaust line just below the knife-edge, It was preceded by a perforated plate which mixed the air stream prior to measurement of its temperature,

The temperature of the water leaving the test section was measured employing a chromel-alumel thermocouple (h) cemented to the inside of the glass tube about 1/2 in. above the lower end of the tube, The thermocouple was constructed from 0.003 in. diameter chromel and alumel wires welded together, with the resulting bead flattened to a thickness of about 0.002 in. The bead was then cemented to the tube with epoxy glue, being held in place during hardening of the glue by a piece of teflon with a 0.75 in. radius on one side. The teflon served both to support the bead until hardening of the glue and also to insure that no excess glue extended out from the wall causing a flow disturbance, The resulting installation was sufficiently smooth that the film failed to completely wet the thermocouple bead only in a few instances.

The collector assembly was mounted on a platform which provided for adjustment of the position of the collector assembly for proper alignment with the glass tube. The platform could be raised and lowered to accommodate the various lengths of test sections investigated.

The main body of the collector assembly (m) was constructed from a 9 in. billet of aluminum (donated by the Aluminum Company of America) and was anodized following machining. O-ring seals were employed wherever pressure seals were required.

B.4 Temperature Measurement

During each experimental run, five temperatures were measured and recorded: the air inlet temperature, the water inlet temperature, the air outlet temperature, the water outlet temperature, and the air temperature measured 15 in. downstream from the orifice. Chromel-alumel thermocouples were employed for the temperature measurements; all of the cold junctions were located in a common ice-water bath (32 F). The thermocouples were connected to a manually operated stepping switch, with which each could in turn be connected with a Honeywell Electronik strip recorder. All of the leads connecting the thermocouples to the ice bath and to the stepping switch leads were made from chromel and alumel wire, Copper wire was used for all other connections, All of the junctions between the thermocouple wire and the copper wire were located within a thermally insulated box, so that all of those junctions would be at the same temperature. A beeds & Northrup potentiometer was connected to the recorder through the stepping switch; the potentiometer was employed for calibrating the recorder.

The thermocouples were all calibrated against a precision thermometer in a constant temperature water bath over a range of temperatures from 60 to 180 F. The resulting calibration curves were fitted with straight lines which were employed in the data reduction computer program.

B.5 Pressure Measurement

All pressure measurements were made with U-tube manometers, using either mercury or Meriam Indicating Fluid (Sp. Gr. 1.00). The static pressure drop across the test section was measured employing a National Laboratories precision manometer,

B.6 Humidity Measuring Stations

Figure 25 is a photograph of the two humidity measuring stations employed for measuring the humidity of the air entering and leaving the test section.

Each station contained a dry-bulb and a wet-bulb thermometer over which the sample of air flowed continuously. Total and static pressure taps in each station allowed the velocity of the air flowing across the thermometer bulbs to be measured employing an inclined tube manometer. A minimum air velocity of 15 fps across the bulbs was set for all measurements. Thermometer Corporation of America precision thermometers with 0.1 C graduations were employed in the stations. The wicks of the wet-bulb thermometers were moistened with distilled water, and new wicks were used each day to avoid errors due to possible contamination of the wicks.

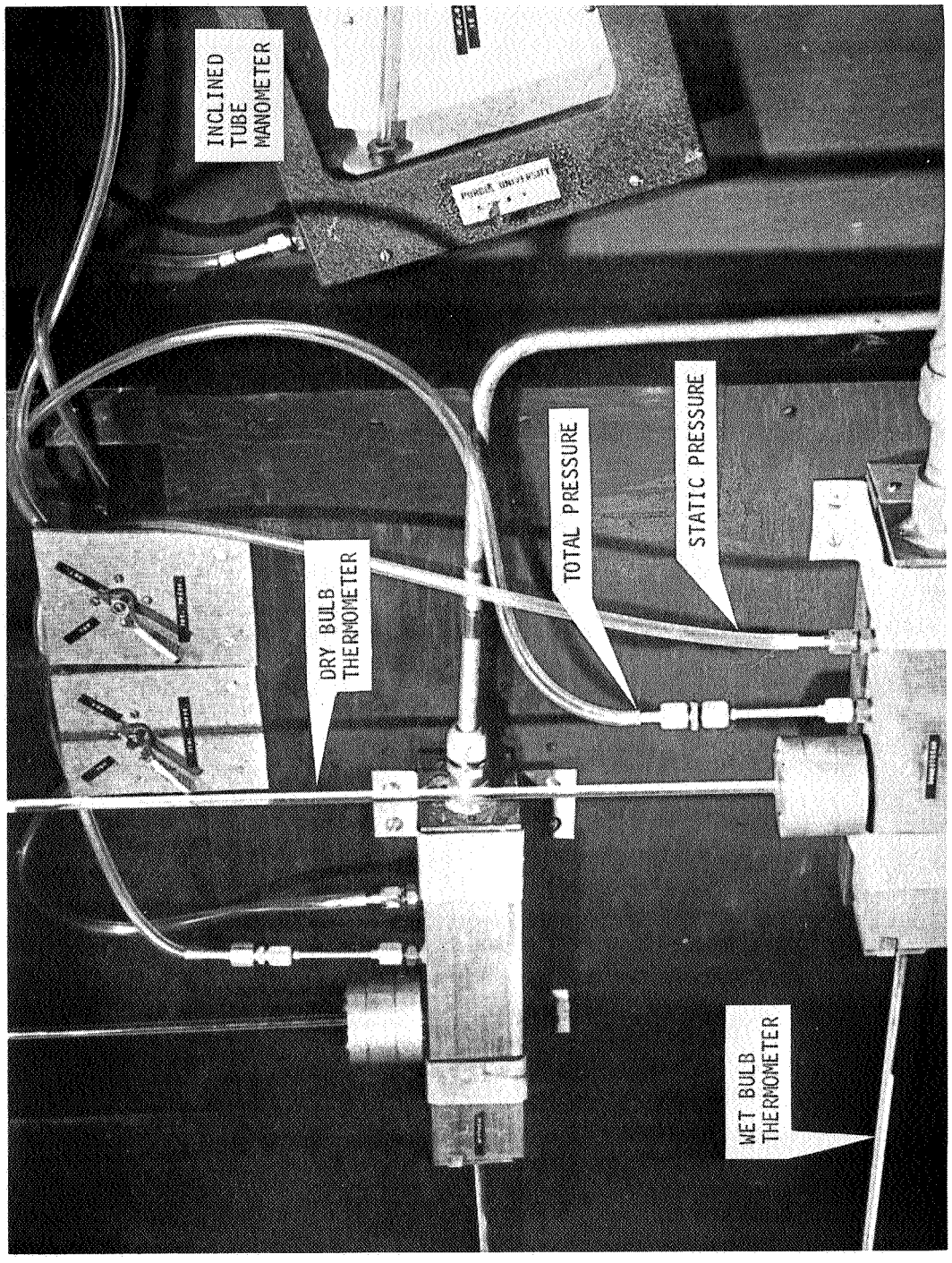

Fig. 25 Photograph of the Humidity Measuring Stations

B.7 Optical System and Associated Equipment

Figures 26 and 27 present schematic diagrams of the optical system and the associated electronic equipment employed in the measurement of the surface characteristics of the liquid film.

The light sources were General Electric No, 605 light bulbs rated at 6.1 v. The bulbs were connected in parallel across the output of a Sorensen Nobatron D.C. power supply, (see Fig. 27), which was operated at 12 v. A 0-5 ohm variable resistor was placed in series with each bulb to allow the relative brightness of the bulbs to be varied.

The bulbs were mounted in opaque light holders each with a 0.0135. in. diameter aperture through which the beam of light emerged (see Fig. 26). The focusing lenses were approximately 21 1/2 in. from the light holder apertures; each focusing lens consisted of two double convex lenses of 7 in. focal length mounted adjacent to each other on the same axis, resulting in an effective focal length of 3.5 in. Apertures of 0.125 in. diameter preceded the focusing lenses, First-surface plane mirrors were employed to bring the axes of the two light beams to within 0.25 in, of each other, Light gates operated by 24 v. D.C. solenoids provided a means of blocking the light beams without disturbing the voltage applied to the bulbs.

Figure 28 is a photograph of the test section showing the location and configuration of the film divider. The film divider was cut from 1 1/2 in. O.D. by 1/16 in. wall bakelite, and was cemented to the

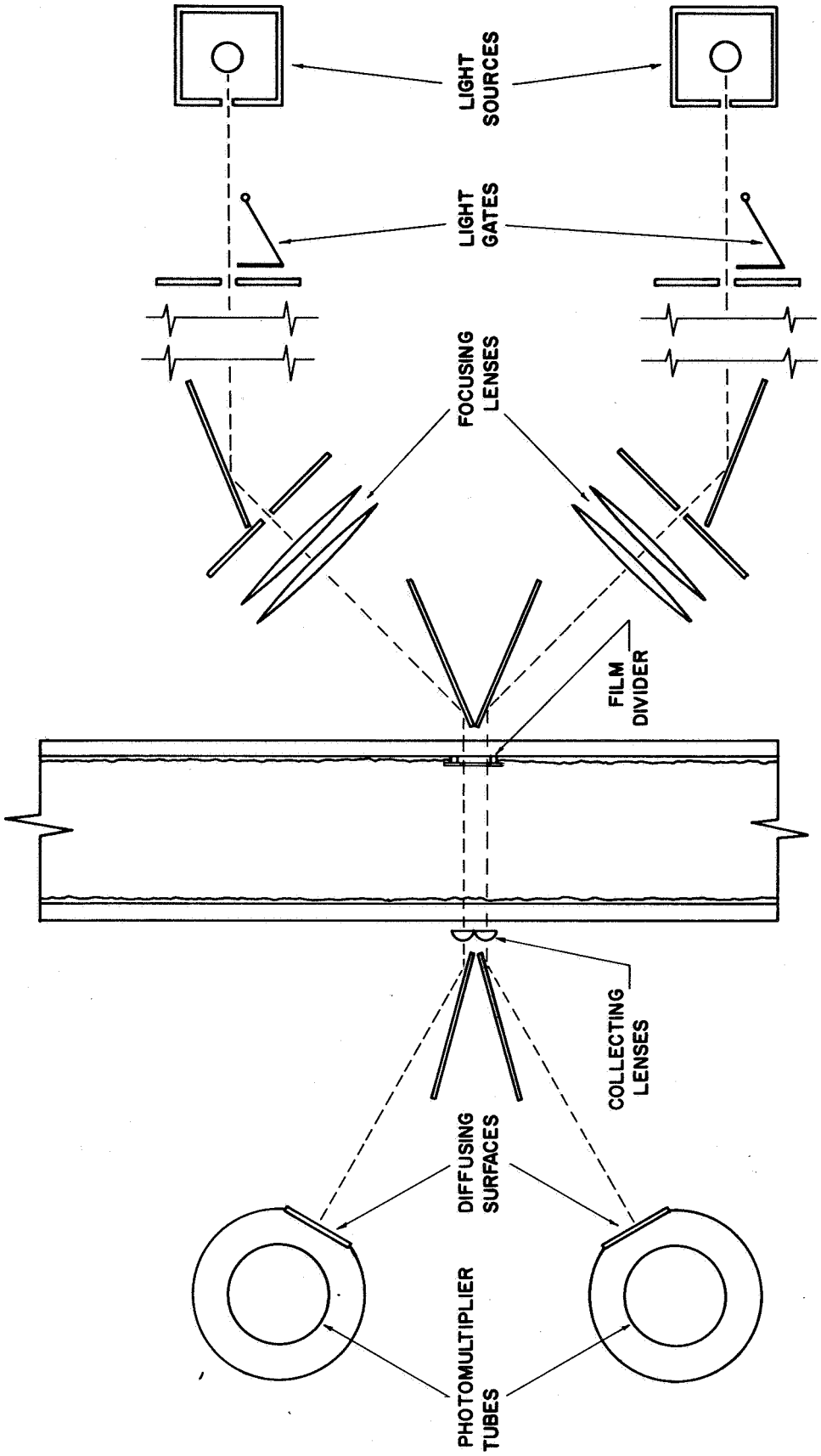

Fig. 26 Schematic Diagram of the Optical System

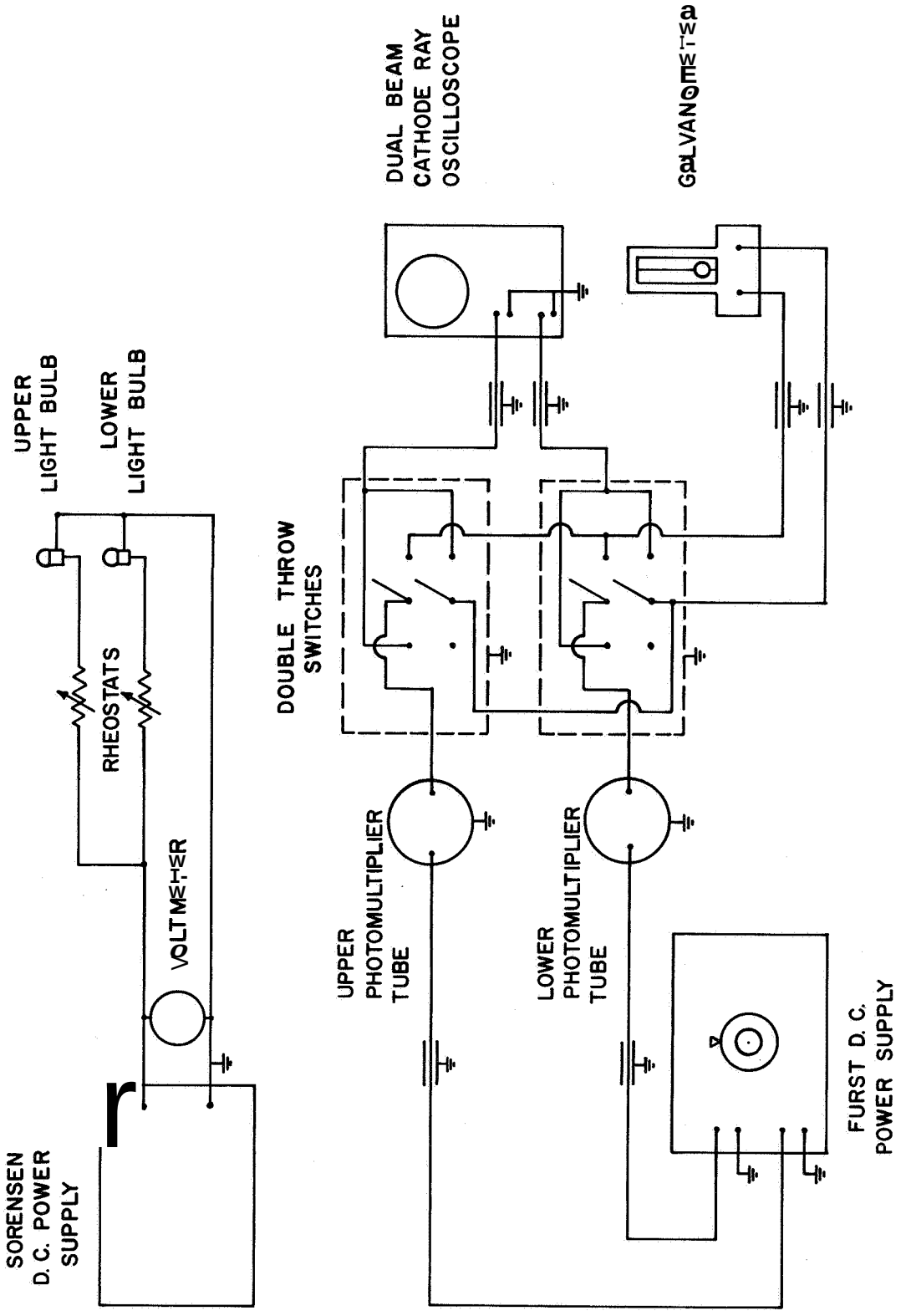

Fig. 27 Schematic Diagram of the Electronic Apparatus

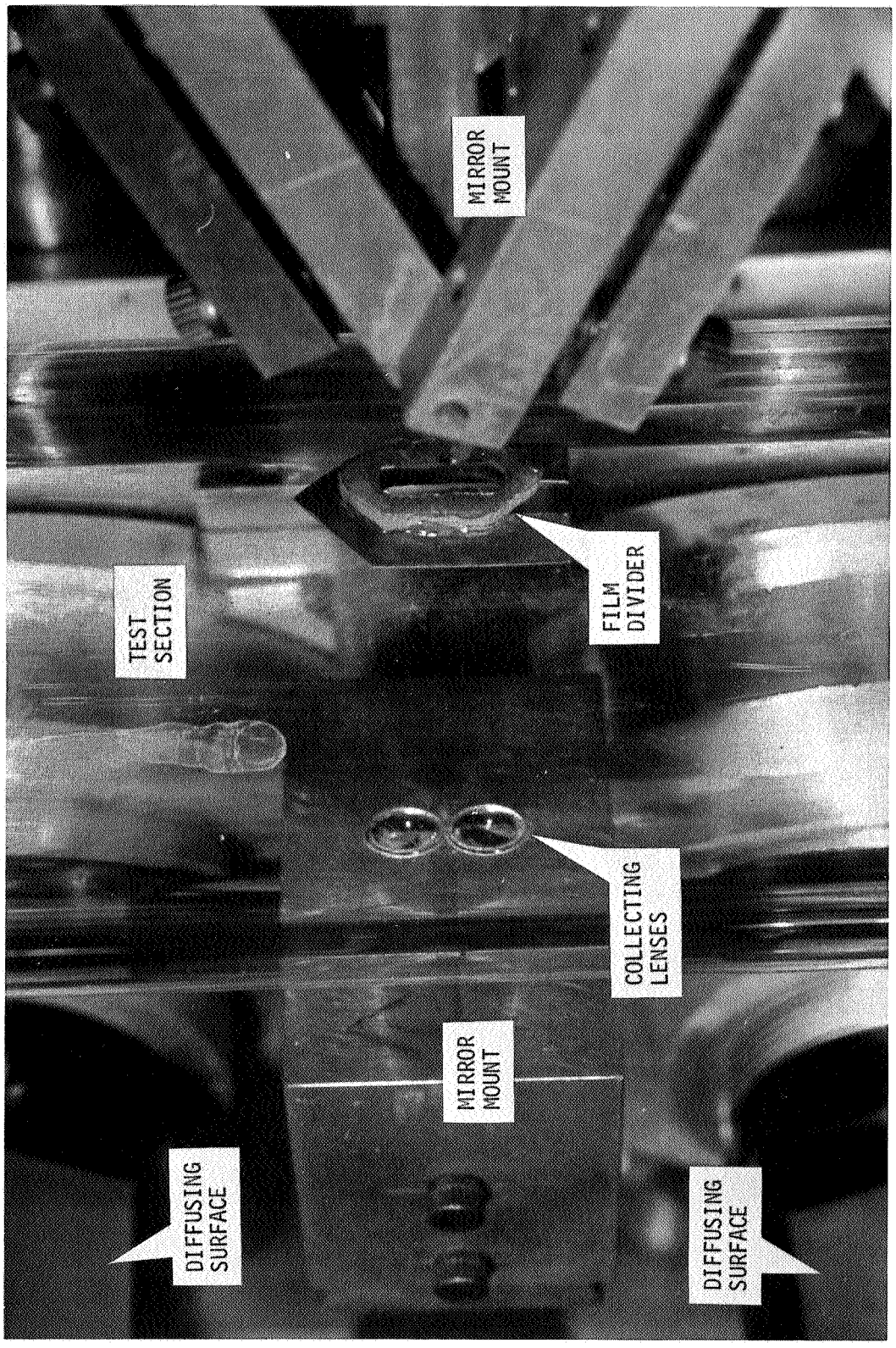

Fig. 28 Photograph of the Film Divider

inside wall of the tube at the location where the light beams entered the glass tube. The film divider, which was 0.53 in. long and 0.20 in. wide, had streamlined front and back edges to minimize disturbance of the flow of the film. A hole in the center of the film divider allowed the beams of light to pass through. To minimize the tendency of droplets of water to deposit in this hole under some flow conditions, a shield 0.73 in. long and 0.40 in. wide was cut from 0.012 in. brass sheet and cemented on the inward side of the flow divider.

The optical system and the tube were aligned so that the light beams came to a focus 0.01 in. before they reached the inside wall of the glass tube, on the side opposite where they entered the tube. The focal points corresponded to the approximate position of the surface of the film; the diameters of the beams at the focal points were theoretically 0.0025 in. The diameter of each beam increased at the rate of 0.036 in. per inch distance from the focal point in either direction along the optical axis. Actually the curvature of the glass tube where the beams entered it caused some distortion of the image. Calculations indicated that horizontal rays of light would focus 0.037 in. beyond the focal point for the vertical rays, At a point halfway between the two focal points calculations indicated that the diameter of the beam was approximately 0.0034 in. In the investigation the latter, diameter is quite satisfactory for describing the geometries of the waves, because the wave lengths were much larger than 0.0034 in.

Refraction phenomena at the surface of the film caused the light beam to be deflected from the optical axes. It was necessary, therefore,

to redirect the refracted rays so that they fell on the sensing elements of the photomultiplier tubes. The redirection was accomplished by means of two collecting lenses, plano-convex lenses of 6 mm diameter and 7 mm focal length, which were positioned with their plane surfaces located 5/32 in. from the outer surface of the glass tube (see Fig. 26). Preliminary experiments indicated that the selected location for the collecting lenses resulted in the least signal distortion due to refraction.

RCA type 931A photomultiplier tubes were employed for detecting the intensity of the transmitted light beams (see Fig. 26). Since the output of that type of photomultiplier tube is strongly dependent upon the position where the light beam strikes the sensing element of the tube, and that position varied somewhat due to the aforementioned refraction phenomena, the transmitted light beams were directed onto a double thickness of ground glass placed in front of the sensing element. The sensing element then detected the light impinging on the ground glass, and was much less sensitive to slight variations in beam position.

Power was furnished to the photomultiplier tubes from a Furst D.C. power supply at 750 v (see Fig. 27). Further details regarding the tube circuitry for the photomultiplier tubes are presented in reference 11.

The output of the photomultiplier tubes was displayed on a Tektronix Type 502 dual-beam oscilloscope. The 1 megohm input impedance of the oscilloscope served as the load impedance for the

photomultiplier tubes. Records of the outputs from the photomultiplier tubes were obtained by photographing the screen of tbe oscilloscope with a Dumont Type **321-A** Oscillograph-Record Camera; **35** mm Kodak Tri-X film was used and was developed in Baumann Diafine developer, resulting in an effective **A.S.A.** film speed rating of **2400.**

Two double throw switches were connected in the output circuits of the photomultiplier tubes so that a Leeds & Northrup mirror galvanometer could be placed in series with either circuit.

All of the electrical leads were shielded, and the photomultiplier tubes and switches were encased in grounded aluminum shields to minimize the effects due to extraneous signals.

APPENDIX C

EXPERIMENTAL PROCEDURE

The present appendix describes the procedures followed during the course of the experimental investigation. Subsequent appendices explain how the experimental data were reduced and converted into experimental results. All of the experiments were conducted in the Gas Dynamics Laboratory, Jet Propulsion Center,

C.1 Mass Transfer Experiments

Prior to starting a series of experimental runs (a series of runs includes all runs made with a test section of given length) the supply of propane and also the deionizer were checked to insure they were adequate for conducting the experiments of that series. The test section was thoroughly cleaned with a solution of concentrated sulphuric acid and sodium dichromate and then washed with a solution of Alconox detergent and water, Prior to installation of the test section, the injector assembly was disassembled and also washed with the detergent solution. The test section was then installed between the injector and collector assemblies, being carefully aligned with the vertical employing a plumb line.

The Honeywell Electronik controller and the recorder were energized at least 12 hours prior to the time of running.

Due to its larger capacity, the dyed water tank was employed during the mass transfer experiments; it was filled with deionized water and pressurized to 35 psig,

When the outside temperature was slightly above freezing, a significant amount of condensed moisture accumulated inside the high pressure air storage tanks and the lines that connected them to the laboratory. If the flow rate of air through the experimental apparatus was sufficiently high, some of that moisture was picked up by the air stream, was carried through the apparatus, and contaminated it. Since relatively high air flow rates were required for heating the lines between the heating coil and the apparatus before conducting a run at the higher temperatures, it was necessary to purge the tanks and the air lines of all accumulated mosture. Consequently, before each series of runs, air was blown through one of the supersonic wind tunnels located in the Gas Dynamics Laboratory at a flow rate of approximately 10 lb per sec until the air pressure in the storage tanks had been reduced approximately 100 psi. Any moisture condensed in the tanks and lines was thus exhausted through the wind tunnel, and subsequent operation of the experimental apparatus could be conducted without the danger of moisture contaminating the apparatus.

A flow rate corresponding to an air velocity of about 100 fps was established, and the propane furnace was ignited. The bath of ice water which served as the cold junction for the thermocouples was prepared and the Honeywell Electronik controller was set at the desired

air inlet temperature. When that temperature had been reached, the flow rate was reduced to that corresponding to an air inlet velocity of 48 fps, and the system was allowed to stabilize at that temperature and flow rate.

The Honeywell Electronik recorder was calibrated against the Leeds & Northrup potentiometer for the range of temperatures to be measured (usually 32 to 600 F). The emf values tabulated in reference 55 were employed in the calibration. Following the runs made each day, the recorder again was calibrated against the potentiometer. It was unnecessary to calibrate %he Honeywell Electronik controller each day, since its calibration remained approximately constant. After the air inlet temperature was approximately stabilized, the temperature setting for the controller was adjusted until the recorder indicated the desired air inlet temperature,

During the aforementioned heating operation, a film of water was always maintained in the test section to prevent the impurities in the air stream from contaminating it. Deionized tap water was employed for maintaining that film during the warm-up period; the water in the dyed water tank was used only when data were being recorded. Care was taken at the highest air temperature to insure that there were no pressure surges in the tap water system, Such surges caused a momentary cessation of the water flow to the test section, usually resulting in cracking of the test section, due to the sudden heating and chilling experienced by the inside wall of the test section.

Fresh wicks were fitted to the wet-bulb thermometers employed in the humidity measuring stations. The rates of air flow through the humidity measuring stations were adjusted so that the air velocities at the thermometer bulbs were approximately 20 fps. The flow of tap water was initiated in the heat exchangers located in the air sampling lines.

The flow of water: from the collector assembly was adjusted to create and maintain the water seal in the collector assembly (see Section B.3.3 for a discussion of the seal). The outside of the test section was covered with thermal insulation.

The zero reading of the precision manometer was taken, and the atmospheric pressure was read from a mercury barometer.

When the air inlet temperature had stabilized at the desired value, the flow of tap water to the test section was stopped, and simultaneously the flow of water from the pressurized dyed water tank (containing clear water in this case) was begun. The water flow rate was set at the desired value. The wicks of the wet-bulb thermometers were wet with distilled water, and the thermometers were inserted into the humidity measuring stations. Preliminary experiments indicated that a five minute wait was sufficient for the different temperatures and pressures which were to be measured to attain their equilibrium values. During that period the air and water flow rates and the air temperature were monitored to insure that they remained at the desired values. If any variation occurred, the conditions were corrected, the wicks were again wet, and the five-minute waiting period was begun

again. In addition, the readings of the wet-bulb thermometers were carefully monitored. After its wick was wet and a thermometer was inserted into the humidity. measuring station, its temperature decreased until it reached the wet-bulb temperature. It remained at that temperature until the wick began to dry. If at the end of the waiting period the wick had not yet reached its equilibrium (wet-bulb) temperature, the waiting period was extended until the equilibrium condition was reached, If, on the other hand, the wick reached' its equilibrium temperature and then began to dry before the end of the waiting period, it was again wet with distilled water, and the waiting period was concluded when the equilibrium temperature was reached.

At the conclusion of the waiting period, the following parameters were recorded: the orifice pressure drop, the test section pressure drop, the orifice upstream pressure, the static pressure at the exit of the test section, the centerline velocity head at the exit of the test section, the reading of the water flowrater, the wet-bulb and dry-bulb temperatures at both humidity measuring stations, the air temperature downstream from the orifice plate, the inlet air and water temperatures, and the outlet air and water temperatures.

The foregoing procedure was repeated for each water flow rate to be investigated. When the experiments had been conducted over the entire range of water flow rates, the temperature of the air was increased to the next air inlet temperature. The runs at that temperature were then conducted, and the entire procedure was repeated until all of the runs for the test section being investigated had been

completed. At that time the air and water flows were stopped, and the recorder was post-calibrated. The data-taken were transcribed onto punched IBM cards, and the desired calculations were made employing an IBM 7094 digital computer.

C.2 Experiments Concerned with the Film Surface Characteristics

The operation of the part of the experimental apparatus concerned with the flow of air and water was essentially the same for the mass transfer and the surface characteristics experiments. Consequently, that aspect of the operation of the apparatus is not repeated here. The primary differences between the two sets of experiments were the measurements which were made.

The power supplies for the photomultiplier tubes and the light bulbs were turned on, and the covered photomultiplier tubes were energized at least 12 hours before the start of the experiments. The oscilloscope and the light bulbs were energized several hours before the experiments were initiated.

The dyed water solution was prepared in the following manner (see Fig. 22). The reservoir was half filled with deionized water, and approximately 100 g of finely ground Nigrosine dye were slowly dissolved in the water, which was continuously stirred. After all of the dye had been dissolved, the solution was pumped into the empty dyed water tank, The reservoir was then rinsed several times with deionized water; each time the water was pumped into the dyed

water tank. Finally the dyed water tank was filled with deionized water, resulting in a solution of approximately 0.0005 lb dye per lb water. The dyed water solution was circulated to the storage tank (see Fig. 22) and back to the dyed water tank several times to insure complete mixing of the dyed water solution.

Both the clear water tank, which was filled with clear deionized water, and the dyed water tank were pressurized to **35** psig.

The injector assembly and the test section (with the film divider installed) were cleaned (see Section C.1 for the method of cleaning), and the injector assembly was installed. The optical system was mounted and aligned with respect to the injector assembly. The glass test section was then installed between the injector and collector assemblies, with the film divider positioned so that the light beams entered the test section through the hole in the film divider, The room housing the apparatus was then darkened, and the covers removed from the photomultiplier tubes.

After the air temperature and flow rate had stabilized at the first operating point, the flow of tap water was cut off, and the water was taken from the supply in the clear water tank. The variable resistors in the light bulb circuits were adjusted so that the outputs from the photomultiplier tubes, as viewed on the oscilloscope, were approximately equal. The apparatus was then allowed to run for another ten minutes after which the initial readings were made with the optical system.

Three different types of photomultiplier current readings were of interest. They will be referred to as the zero, the infinity, and the run readings. The zero readings corresponded to zero liquid film thickness. Experiments demonstrated that the output of the photomultiplier was essentially the same for either no flows of water and air, or when the rate of flow of clear water was approximately 0.025 lb per sec and the air velocity was approximately 48 fps. Due to the inconvenience of shutting off the flows of air and water, and the risk of breaking the test section during such a shutdown, the latter mode of operation (clear water and air flows) was chosen for taking the zero readings. The infinity readings corresponded to a liquid film of infinite thickness; i.e., with no light reaching the photomultiplier tubes. The infinity readings were, therefore, accomplished by activating the light gates to that the beam of light was blocked off immediately after it left the source. The run readings were taken with dyed water and air flowing through the test section. The light gates were not used when taking zero or run readings.

All of the measurements of film thickness were based upon readings obtained with the lower optical system; that system had the lower noise level and showed the least signal distortion because of losses due to reflection and refraction. Both optical systems were employed for determining the wave velocities. When zero and infinity readings were made, the current of the lower photomultiplier tube was read on

the galvanometer and a photographic record of approximately two in. was taken with the oscillograph record camera., When the run readings were made, the readings of the lower galvanometer were recorded, and photographic records were taken; the latter varied from about 12 to 24 in.

Infinity and zero readings were taken after a 10 minute stabilization period. The water flow was then changed from clear to dyed water, and its flow rate adjusted to its maximum value (0,07182 lb per sec). The output of the photomultiplier tubes decreased when the dyed water reached the test section. When the output had reached an equilibrium mean value, as noted by the galvanometer reading, indicating that all of the clear water had been purged from the system, the run and infinity readings of the galvanometer and oscilloscope were taken. The following parameters were recorded: the orifice pressure drop, the test section pressure drop, the orifice upstream pressure, the static pressure at the exit of the test section, the reading of the water flowrater, the air temperature downstream from the orifice plate, the inlet air and water temperatures, and the outlet air and water temperatures, A sample of the dyed water was collected through the sampling tap, and the liquid flow rate was reduced to the next value. After all of the flow parameters had attained their steady values, another set of readings was taken. The water flow rate was again reduced, and the entire procedure repeated until the investigation had been conducted over the complete range of water flow rates for the desired air temperature, The water flow was changed from dyed

to clear water, and after the output of the photomultiplier indicated that clear water was again flowing in the test section,. the zero and infinity readings were taken. The above procedure was then repeated for the next air temperature. After all of the desired constant air temperatures has been investigated, the air and water flows were shut off, and the optical system was calibrated.

Calibration of the optical system was necessary since the exact concentration of the dyed water solution was not known. It was calibrated by observing the decrease in the intensity of the transmitted light beam when a sample of dyed water of known thickness was inserted in the path of the light beam, and the result was compared with the corresponding decrease in intensity caused by a geometrically identical sample of clear water; the first and last samples of dyed water taken for the series of runs were employed, and in all cases gave practically identical results. The results of the calibrations indicated the concentration of the dyed water entering the test section was constant throughout all of the runs made during a given day.

In all the experiments reported herein, a calibration cell with a 0.00984 in, space between two optical flats was employed in the calibration of the optical system. The cell was filled with dyed water from the first sample. Infinity, zero, and "run" readings were taken employing the galvanometer; the run readings here refer to the readings with the calibration cell in the path of the light

beam (a specially constructed mount held the calibration cell in the same position each time it was .inserted in the path of the light beam). The cell was thoroughly cleaned with distilled water and then filled with distilled water. Infinity, zero, and run readings were taken. The cell was then rinsed with dyed water taken from the final sample, and filled with dyed water from that sample. Readings were again taken, completing the optical system calibration.

APPENDIX D

ANALYSIS OF THE MASS TRANSFER DATA

The mass transfer data were correlated by means of relations for the local values of heat and mass transfer. The empirical constants in those relations were selected so that, for a given set of inlet conditions for the flow of the gas and the liquid, the calculated value of the dimensionless mass transfer coefficient, the Sherwood number Sh, was the same as that measured experimentally. The present appendix presents the methods employed for calculating the Sherwood number (a) from the experimental data and (b) by analysis based on the inlet conditions for the flow.

D.1 Calculation of the Measured Value of Sh

The over-all Sherwood number Sh is defined by

$$Sh = \frac{h_M d}{D} \qquad (D\text{-}1)$$

where h_M = over-all mass transfer coefficient, ft/sec

d = test section inside diameter, ft

D = molecular diffusivity of water vapor in air, evaluated at the average of the average bulk temperatures of the gas and liquid, ft^2/sec

The over-all mass transfer coefficient appearing in equation D-1 is defined by

$$h_M = \frac{W_{ev}}{\pi dL\ (\Delta C_m)} \qquad \text{(D-2)}$$

where W_{ev} = weight rate of evaporation of the liquid in the test section, lb/sec

L = length of the test section, ft

ΔC_m = log mean vapor concentration difference between the gas and the gas-liquid interface, lb/ft^3

The weight rate of evaporation of the liquid is calculated by taking the difference between the weight rate of flow of vapor in the gas stream crossing the outlet section of the test section and that crossing its inlet. The weight rate of flow of vapor in the gas stream is given by

$$W_v = \omega W_A \qquad \text{(D-3)}$$

where W_v = weight rate of flow of the vapor in the gas stream, lb/sec

ω = specific humidity of the vapor in the gas stream, lb vapor/lb dry air

W_A = weight rate of flow of dry air in the gas stream, lb/sec

The specific humidity is determined by psychrometric means from the wet-bulb and dry-bulb temperatures of the samples of the air entering and leaving the test section, (For details of the calculation procedure, including the equations employed, see Appendix F.)

The concentration difference employed in equation D-2 is the difference between (a) the concentration of the vapor in the gas stream, and (b) the concentration of the vapor at the gas-liquid interface. The latter is calculated by means of the perfect gas law. Thus

$$C_i = \frac{p_v}{R_v T_L} \qquad (D\text{-}4)$$

where C_i = concentration of the vapor at the gas-liquid interface, lb/ft^3

p_v = vapor pressure of the liquid, corresponding to the temperature of the liquid film, lb/ft^2

R_v = gas constant for the vapor, ft/R

T_L = temperature of the liquid film

The concentration of the vapor in the gas stream is obtained by multiplying the specific humidity of the air by its specifice weight. Bulk (mixing-cup) values of temperature are employed for calculating properties of the gas stream.

D.2 Calculation of the Analytical Value of Sh

D.2.1 Introduction

An analysis was developed employing the equations of conservation of mass and energy, and the expressions for the local dimensionless heat and mass transfer coefficients Nu_x and Sh_x. That procedure enabled calculating the heat and mass transfer that occurred in concurrent annular, two-phase flow in a vertical pipe. The starting point for the analysis comprised the inlet conditions of the gas and liquid flows; i.e., the flow rates and temperatures of the air, the vapor, and the liquid, From

the analysis the corresponding conditions at the outlet of the pipe could be computed. Employing the aforementioned inlet and outlet conditions, the over-all dimensionless mass transfer coefficient Sh was calculated by the method described in Section D.1.

D.2.2 Assumptions

The following assumptions were made in calculating the analytical values for the heat and mass transfer in concurrent, annular, two-phase flow in a vertical pipe:

1. The test section is a vertical, right circular hollow cylinder having an inside diameter of 1.502 in.

2. There is no heat transfer through the test section wall.

3. All properties of the gas and liquid phases are axisymmetrical, with no gradients in the tangential direction.

4. The perfect gas law applies to both the air and the vapor, in the gas phase.

5. There is perfect mixing of the liquid film so that the liquid temperature is independent of its distance from the inside wall of the hollow cylinder, so that the surface and bulk temperatures of the liquid are identical.

6. 'Equilibrium exists at the gas-liquid interface, Consequently, (a) the gas temperature at the interface equals the liquid temperature, and (b) the partial pressure of the vapor in the gas phase at the interface is equal to the vapor pressure of the liquid.

7. The flow is steady and frictionless.

8. No external work is performed by the two fluid media.

9. The potential and kinetic energy terms in the energy equation are negligible.

10. The static pressure is constant through the test section.

D.2.3 Model

Figure 29 presents a schematic diagram of the physical model employed in the analysis. Liquid is injected onto the inside wall of a test section of diameter d, at section i. The liquid flows down the inside of the test section, partially evaporating into the gas stream flowing through the test section. At the outlet from the test section, which is denoted as section o and located at a distance L below the inlet, the liquid is separated from the gas.

Consider the increment AX of the test section bounded by planes 1 and 2. Plane 1 is located at distance x below the inlet plane i; plane 2 is located AX below plane 1. Figure 30 presents, a schematic diagram of the fluids crossing plane 1 and crossing plane' 2. The gas temperatures indicated are the bulk (mixing-cup) temperatures. Due to the axisymmetric nature of the flow, the diagram in Fig. 30 represents the assumed model. The rate at which heat is transferred from the gas to the liquid is Q B per sec, and the liquid evaporates into the gas stream at the rate W_{ev} lb per sec.

D.2.4 Equations

Based upon the assumptions and the model presented in Fig. **30,** the following equations may be written. Thus

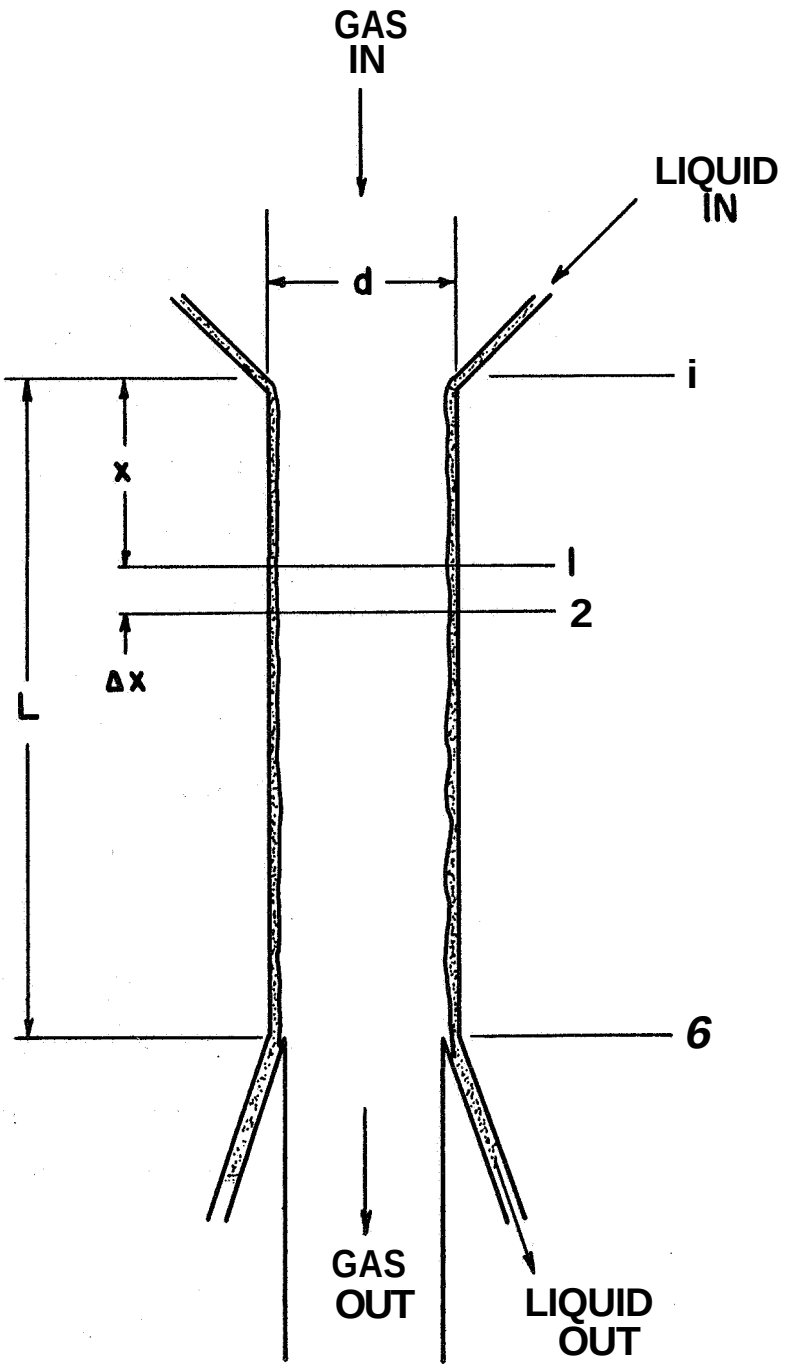

Fig. 29 Schematic Diagram of the Model Employed in the Annalysis

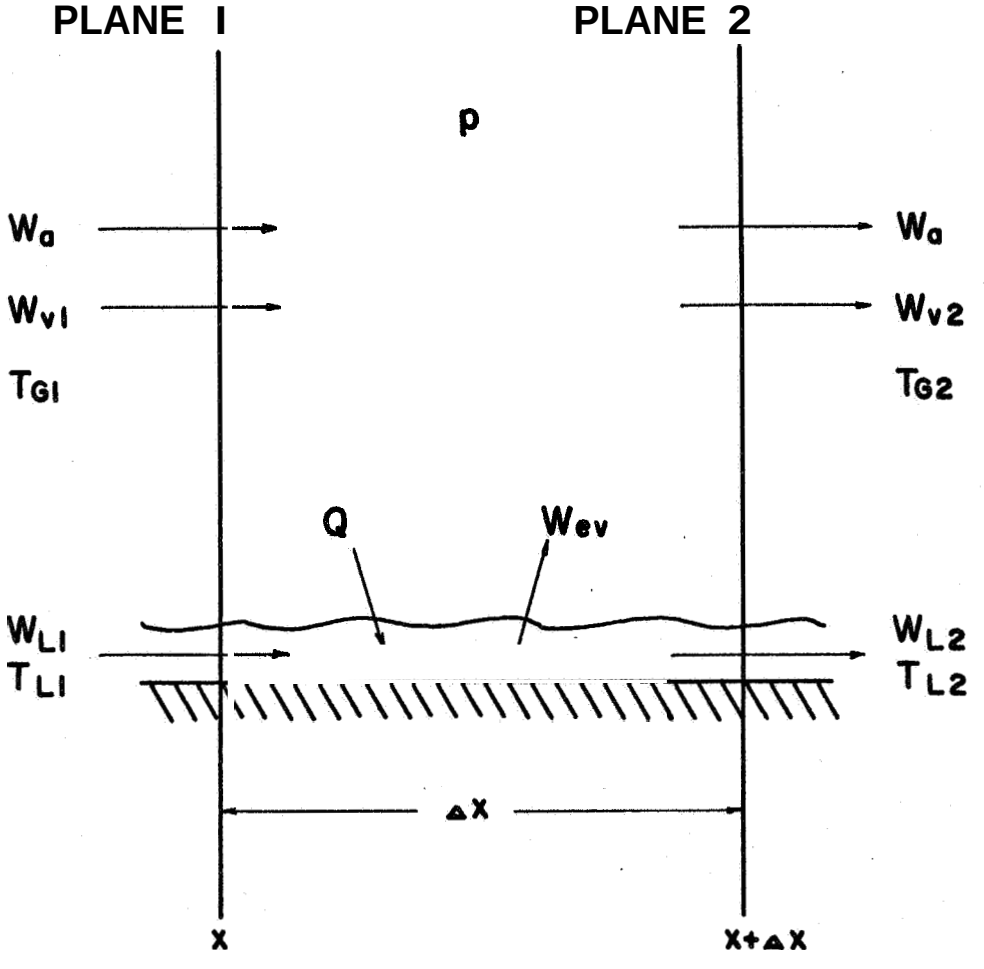

Fig. 30 Schematic Diagram of an Increment of the Model Employed in the Analysis

Gas Phase:

Conservation of mass

$$W_{a2} = W_{a1} \tag{D-5}$$

$$W_{v2} = W_{v1} + W_{ev} \tag{D-6}$$

Conservation of Energy

$$W_{a1}\, c_p\, (T_{G2} - T_{G1}) + W_{v2}h_{v2} - W_{v1}h_{v1} = W_{ev}h_{ev} - Q \tag{D-7}$$

Liquid Phase:

Conservation of Mass

$$W_{L2} = W_{L1} - W_{ev} \tag{D-8}$$

Conservation of Energy

$$W_{L2}c_L\, (T_{L2} - T_{L1}) = - W_{ev}h_{ev} + Q \tag{D-9}$$

Rate Equations:

Heat Transfer

$$Q = h_H\, \pi\, d\, (\Delta x)\, (T_{Gm} - T_{Lm}) \tag{D-10}$$

Mass Transfer

$$W_{ev} = h_M \pi d (AX) (\Delta C_m) \quad \text{(D-11)}$$

Where W = weight rate of flow, lb/sec

c_p = constant pressure specific heat of the air, B/lb-R

T = temperature, R

h = enthalpy, B/lb

Q = rate of heat transfer, B/sec

c_L = specific heat of the liquid, B/lb-R

h_H = heat transfer coefficient, B/sec-ft2-R

h_M = mass transfer coefficient, ft/sec

ΔC_m = average concentration difference between vapor in gas stream and at interface, lb/ft^3

d = test section diameter, ft

Subscripts:

1 = plane 1

2 = plane 2

a = air

v = vapor

G = gas

L = liquid

ev = liquid evaporating into the gas stream

m = average of values at stations 1 and 2.

Two equations relate the local values of the heat and mass transfer coefficients to the flow conditions; the latter are represented by the dimensionless groups x/d, Re_G, Pr, and Sc. The two equations are as follows. Thus

$$Nu_x = C_1 F_1(x/d) Re_G^{C_2} Pr^{C_3} \quad \text{(D-12)}$$

$$Sh_x = C_4 F_2(x/d) Re_G^{C_5} Sc^{C_6} \quad \text{(D-13)}$$

where C_1 through C_6 are constants and $F_1(x/d)$ and $F_2(x/d)$ are functions of the ratio x/d.

The dimensionless groups in equations (D-72) and (D-13) are defined by the following equations. Thus

$$Nu_x = \frac{h_{Hx}\, d}{k_G} \quad \text{(D-14)}$$

$$Sh_x = \frac{h_{Mx}\, d}{D} \quad \text{(D-15)}$$

$$Re_G = \frac{\rho V d}{\mu_{GG}} = \frac{4W_G}{\pi\, dg\, \mu_{GG}} \quad \text{(D-16)}$$

$$Pr = \frac{\mu_G c_p}{k_G} \quad \text{(D-17)}$$

$$Sc = \frac{\mu_G}{\rho D} \quad \text{(D-18)}$$

where k_G = thermal conductivity of the gas, B/sec-ft-R

μ_G = dynamic viscosity of the gas, evaluated at the average between the average gas temperature and the average liquid temperature, lb-sec/ft^2

μ_{GG} = dynamic viscosity of the gas, evaluated at the average gas temperature, lb-sec/ft^2

W_G = weight rate of flow of the gas, lb/sec

As was pointed out in section 3.1.2, no attempt was made in the subject research to evaluate the constants C_2, C_3, C_5 and C_6. Instead, published values for those constants were employed (3). Furthermore, based upon the analysis of Deissler (18), the functions F_1 and F_2 were assumed to be identical and of the form

$$F_1 = F_2 = 1 + \left(\frac{1}{x/d}\right)^{0.75} \qquad \text{(D-19)}$$

Substituting from equation D-19 into equations D-12 and D-13 one obtains

$$Nu_x = C_1 \left[1 + \left(\frac{I}{x/d}\right)^{0.75}\right] Re_G^{0.80}\, Pr^{0.33} \qquad \text{(D-20)}$$

$$Sh_x = C_4 \left[1 + \left(\frac{I}{x/d}\right)^{0.75} 1\right] Re_G^{0.83}\, Sc^{0.44} \qquad \text{(D-21)}$$

D.2.5 Application of the Equations to the Calculation of the Heat and Mass Transfer in One Increment of the Test Section

The equations listed in the previous section were employed for calculating the heat and mass transfer in a given increment of the test section, according to the method outlined below.

1. Values were chosen for the constants C_1, C_4 and I in equations D-20 and D-21, initially based upon the work of other investigators. Those constants subsequently were adjusted until the chosen values yielded satisfactory correlation of the experimental data.

2. The inlet conditions of flow for the increment were established. The inlet conditions required were air, vapor, and liquid flow rates, and the bulk temperatures of the gas stream and the liquid film. For the first increment, those conditions were the measured inlet conditions for the test section. For all other increments, those conditions were the calculated outlet conditions for the increment immediately preceding the increment being considered.

3. Based upon the inlet conditions, the dimensionless parameters Re_G, Pr, and Sc were calculated, and equations D-20 and D-21 were employed for obtaining values of Nu_x and Sh_x. Equations D-14 and D-15 were then employed for evaluating h_{Hx} and h_{Mx}; the latter were used for calculating Q and W_{ev} employing equations D-10 and D-11.

4. The outlet conditions for the increment were calculated, based upon the inlet conditions and the calculated values of Q and W_{ev}, employing equations D-6 through D-9.

5. The parameters Re_G, Pr, and Sc were again evaluated, this time at the average of the inlet and the outlet conditions, and the dimensionless heat and mass transfer coefficients Nu_x and Sh_x were computed. Employing the new values of Nu and Sh_x, the heat and mass transfer coefficients h_{Hx} and h_{Mx} were calculated. They in turn were employed for calculating Q and W_{ev}, again using the average of the inlet and outlet conditions for

evaluating the properties and the temperature and concentration differences appearing in the rate equations, equations D-10 and D-11.

6. The values of Q and W_{ev} calculated in part 5 were employed for computing the outlet conditions, which were compared with the outlet conditions calculated previously. If there was a negligible difference between those two sets of outlet conditions, the calculation of the heat and mass transfer for that increment was considered correct. If however, there was a significant difference between the two sets of outlet conditions, the calculation of part 5 was repeated, employing the most recently determined outlet conditions. This procedure was repeated until the outlet conditions employed for the calculations matched those resulting from the calculations. The calculation was considered correct when the values of Q and W_{ev} for two successive computations each changed less than 0.1 per cent. A more precise agreement between successive calculations had no significant effect up on the results.

D.2.6 Calculation of Sh

Section D.2.5 outlines the procedure for calculating the heat and mass transfer in one increment of the test section. The heat and mass transfer for the entire test section were determined by applying that procedure to all of the increments into which the test section was divided, beginning at the inlet and proceeding to the outlet. The outlet conditions for the final increment were the outlet conditions for the test section. The total rate of evaporation of the liquid into the gas stream for the test section was the sum of the rates of evaporation of the increments.

The method of Section D.1 was finally employed for calculating the analytical value of Sh.

Several additional comments regarding the analytical determination of Sh are pertinent.

For small values of x (near the inlet to the test section) the function $F_1(x/d)$ was very large, approaching infinity as x approached zero. It must, in fact, behave in that manner, as was pointed out in Section 2.4. That behavior, however, made the calculations extremely sensitive to increment size, Therefore, particularly since no experimental data exist for small values of x/d, it was decided to employ a straight line for the function F_1 for values of x smaller than 0.25 in. The straight line was defined to be tangent to the function F_1 at x = 0.25 in, It can be shown that the equation for such a line is given by

$$F_1' = 1 + 4.95\ I^{0.75} - 12.75\ I^{0.75}\ (\frac{x}{d}) \qquad \textbf{(D-22)}$$

Equation D-22 was employed for calculating F_1 for values of x smaller than 0.25 in.

Several considerations influenced the choice of the size of the increments employed in the calculations. The increment size should be small, because in the .calculations the conditions controlling the heat and mass transfer in each increment were approximated by the conditions at the two ends of the increment. The smaller the increment, the better

such an approximation would be, since there were nonlinearities involved in the calculations. A lower limitation was imposed on the increment size by the amount of time required for the calculations on the digital computer; the time required was approximately inversely proportional to the increment size. Accordingly, since the calculations were repeated several times for all of the data, the increments should be no smaller than necessary.

The use of increments 1/8 in. in length yielded calculated results essentially the same as those obtained with 1/4 in. increments. There was a significant (nearly 1 per cent) difference between the calculations with 1/4 and 1/2 in, increments, however. Consequently, 1/4 in. increments were employed for the final calculations.

D.3 Determination of the Correlation Coefficients

The object of the analysis was the determination of values of the constants C_1, C_4, and I such that the calculated values of Sh agreed with those measured experimentally. The coefficients were determined by a trial and error procedure, Values of the coefficients were assumed, and the calculations of Section D.2 were performed. The results of the calculations were compared with the experimental values, Based upon that comparison, the values of the coefficients were adjusted, and the procedure repeated, The effects of varying the constants were as follows:

Varying C_1 primarily influenced the outlet temperatures of the gas and the liquid. It had some effect upon the total amount of evaporation, although it changed the value of Sh only slightly,

Varying C_4 primarily influenced the amount of mass transfer; it had a pronounced effect upon the value of Sh.

Varying I primarily influenced the relative values of Sh calculated for test sections of different lengths.

The Sherwood number ratio R_{Sh} was defined for comparing the calculated and experimental values of Sh. Thus

$$R_{Sh} = Sh/Sh_{calc} \qquad (D\text{-}23)$$

where Sh = experimentally determined value of Sh

Sh_{calc} = analytically determined value of Sh

The constants C_4 and I were chosen to yield an average value of R_{Sh} as near unity as possible for all of the experimental data for each test section length. C_1 was chosen to yield the best agreement between the analytical and experimental values of the total mass transfer.

D.4 Illustration of the Effect of the Water Inlet Temperature on the Over-All Sherwood Number

It was noted in Section 3.1 that correlation of the experimental data by plotting $Sh/Re_G^{0.83} Sc^{0.44}$ as a function of Re_L, as was done in Fig. 3 through 7, was unsatisfactory. It was stated that the log mean concentration difference was inadequate for representing the driving force for mass transfer, because of the varying temperature of the liquid, That effect is illustrated by employing the analysis described in this appendix for calculating the parameter $Sh/Re_G^{0.83}Sc^{0.44}$

for sets of inlet conditions which are identical, except for differing liquid inlet temperatures.

The calculations were performed for a test section of 1.5 in. I.D. and 40 in, long. The static pressure of the gas was 15 psia, and initially dry air and water were the two fluid media.

Air inlet temperatures of 110, 230, and 350 F were considered. The flow rates were 0.045, 0.037, and 0.032 lb per sec, respectively, corresponding to a velocity of approximately 48 fps in all cases. Water flow rates were 0.0015, 0.0019, 0.0042, 0.0100, 0.0265, and 0.0718 lb per sec, and water inlet temperatures were 60 and 80 F. Equations 24 through 26 were employed for calculating the local heat and mass transfer.

Figure 31 presents the mass transfer group $Sh/Re_G^{0.83}\ Sc^{0.44}$ as a function of liquid flow rate, (The liquid flow rate was employed rather than the liquid Reynolds number to simplify the calculations. The range of the liquid Reynolds numbers shown is approximately 25 to 1300.) Figure 31 indicates a large variation in the mass transfer group with liquid flow rate, even though all of the calculations used the same expressions for the local heat and mass transfer, The conclusion that this variation is caused by the different liquid inlet temperatures is supported by the different values of the mass transfer group corresponding to the different liquid inlet temperatures.

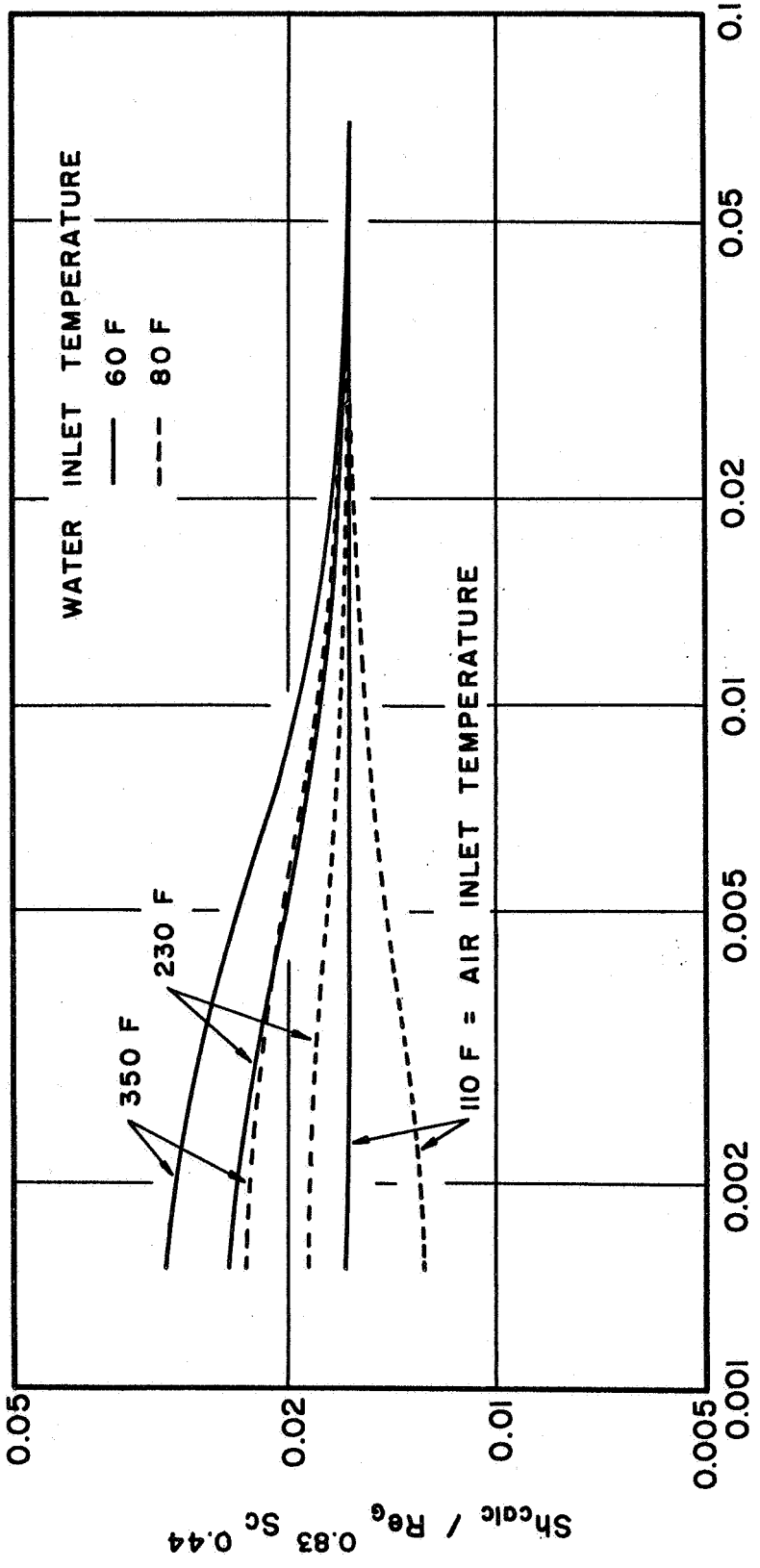

Fig. 31 Effect of the Liquid Reynolds Number on the Mass Transfer Group as Determined by the Analysis

APPENDIX E

METHOD OF MEASUREMENT OF THE SURFACE CHARACTERISTICS

Three characteristics of the surface of the liquid film were measured, employing the light absorption technique of film thickness measurement. Those characteristics were the mean film thickness, the wave velocity, and the surface area, The apparatus employed for measuring those characteristics is described in Appendix B, and the experimental procedure is outlined in Appendix C. The present appendix describes the measurements which were made and the calculations necessary for determining the aforementioned characteristics of the surface of the liquid film.

E.1 Film Thickness

Measurement of the film thickness was based upon Beer's law (29), which may be written

$$I = I_o e^{-bct} \qquad \text{(E-1)}$$

where

I_o = intensity of the incident light

I = intensity of the tramsitted light

b = absorption coefficient for unit concentration of the solute

c = concentration of the solute

t = distance the light passes through the solution

It was pointed out in the description of the apparatus (Section B.7), that a beam of light reflects from a mirror, passes in through the wall of the glass test section, passes through the liquid film, passes out through the test section wall, passes through the collecting lens, and reflects from a mirror before it impinges upon the diffusing surface of the photomultiplier. A small portion of the Incident light is lost due to reflection losses at the glass-air interfaces, and some of the light is absorbed and reflected by the foreign matter on the surfaces of the mirrors, lenses, and the walls of the test section. Those losses are assumed to remain constant during any set of experimental runs. The intensity of the incident light I_0 is defined as the intensity of the light detected by the photomultiplier tube when there is no film flowing in the test section, and there are no other obstructions to the light beam.

The method for calculating the film thickness t will now be illustrated. It is assumed initially that the factor bc in equation E-1 is known. It will be shown subsequently how the factor bc is evaluated by calibrating the optical system, and from the calculation of the fraction of the injected liquid which has been evaporated upstream from the station where the film thickness measurement is made.

Two different types of film thickness measurements were made, average and instantaneous, The average film thickness was obtained from the average ouput current of the photomultiplier tube, employing a galvanometer, The instantaneous film thickness was determined from

the photographic record of the output of the photomultiplier tube which was displayed on a cathode ray oscilloscope. Regardless of the type of film thickness measurement, the following types of readings were of interest; (a) the zero reading, (b) the infinity reading, and (c) the run reading. Those readings correspond to (a) no obstruction to the light beam with no liquid flowing, (b) complete obstruction of the light beam with no liquid flowing, and (c) the only obstruction to the light beam being the film of dyed water flowing in the test section. A more detailed explanation of the aforementioned three readings is presented in Section C.2. For convenience the three readings are denoted by the following symbols: zero, i_0; infinity, i_i; and run, i_r. Again, the latter readings may correspond to either galvanometer readings or oscilloscope scale readings, depending on whether the average or the instantaneous film thickness is being measured.

The values of the two light intensities appearing in equation E-1 are given by

$$I = i_r - i_i \tag{E-2}$$

and

$$I_o = i_o - i_i \tag{E-3}$$

Substituting equations E-2 and E-3 into equation E-1 and solving for the film thickness t, the following expression is obtained. Thus

$$t = - \frac{\ln \left(\frac{i_r - i_i}{i_o - i_i} \right)}{bc} \tag{E-4}$$

The unit of t is the inch, the inverse of that for bc.

The magnitude of bc for the liquid entering the test section, denoted bc_i, was obtained by calibrating the optical system with no air or liquid flowing through the test section. A sample of the dyed liquid, taken from the liquid supply system during the experimental runs, was placed in a calibration cell, which consisted of two optical flats 0.00984 in. apart. The construction of the cell was such that the space between the flats was filled with the liquid. Be measuring the fraction of the light absorbed by the thickness of liquid in the cell, bc was calculated by applying equation E-1. One additional complication was introduced, however, due to the presence of two more pieces of glass through which the light beam passed, namely the two optical flats, To account for the light losses occuring at the surfaces of the optical flats, it was also necessary to measure the fraction of the light absorbed by the calibration cell when it was filled with clear water. The nomenclature employed for the pertinent readings of the galvanometer or the oscilloscope is as follows:

i_r = reading with dyed water in the cell, units on the galvanometer scale or the oscilloscope scale

= reading without the cell

i_i = reading with the light beam blocked

i_{rc} = reading with clear water in the cell

i_{oc} = reading without the cell during the series of readings with clear water

i_{ic} = reading with the light beam blocked during the series of readings with clear water

In the calculations for the calibration of the optical system the light intensities I and I_o, in equation E-1, are given by

$$I = (i_r - i_i) \tag{E-5}$$

and

$$I_o = (i_o - i_i)\left(\frac{i_{rc} - i_{ic}}{i_{oc} - i_{ic}}\right) \tag{E-6}$$

Substituting equations E-5 and E-6 into equation E-1 and solving for the factor bc_i yields

$$bc_i = -\frac{\ln \dfrac{(i_r - i_i)(i_{oc} - i_{ic})}{(i_o - i_i)(i_{rc} - i_{ic})}}{t} \tag{E-7}$$

The calculation of the factor bc, which applies at the point of measurement, requires introducing an adjustment to account for the increase in the dye concentration c caused by evaporation of water from the liquid film. Hence

$$bc = bc_i\left(\frac{W_{Li}}{W_L}\right) \tag{E-8}$$

where

W_{Li} = weight rate of flow of liquid entering the test section, lb/sec

W_L = weight rate of flow of liquid at the point of film thickness measurement, lb/sec

W_{Li} was measured during the experiments, and W_L was calculated by applying the correlation equations for heat and mass transfer as discussed in Section D.2.6.

E.2 Wave Velocity

The velocity of a wave appearing on the surface of the liquid film was measured by measuring the time required for that wave to travel the distance (0.25 in.) between the two light beams of the optical system. Assuming that the wave velocity remained sensibly constant, between the two beams of light, the velocity of the wave is given by

$$V_W = 0.0208/\Delta\tau$$

where

V_W = velocity of the wave, fps

$\Delta\tau$ = time required for the wave to travel 0.25 in,, sec

Figure 32 presents a sketch of a typical oscillograph-record camera negative. The upper trace in Fig. 32 corresponds to the output of the upper optical system photomultiplier; the direction of the motion of the photographic film is indicated in the figure, The time for a wave to travel the distance between the two light beams was determined by measuring the horizontal displacement of the wave on the photographic record of the two oscilloscope traces of the wave. In all of the experiments the speed of movement of the film in the oscillograph-record camera was 600 in. per min. Hence, if $\Delta\tau$ is the time in seconds and δ is the horitontal displacement, then

$$\Delta\tau = 0.1\ \delta \qquad \text{(E-10)}$$

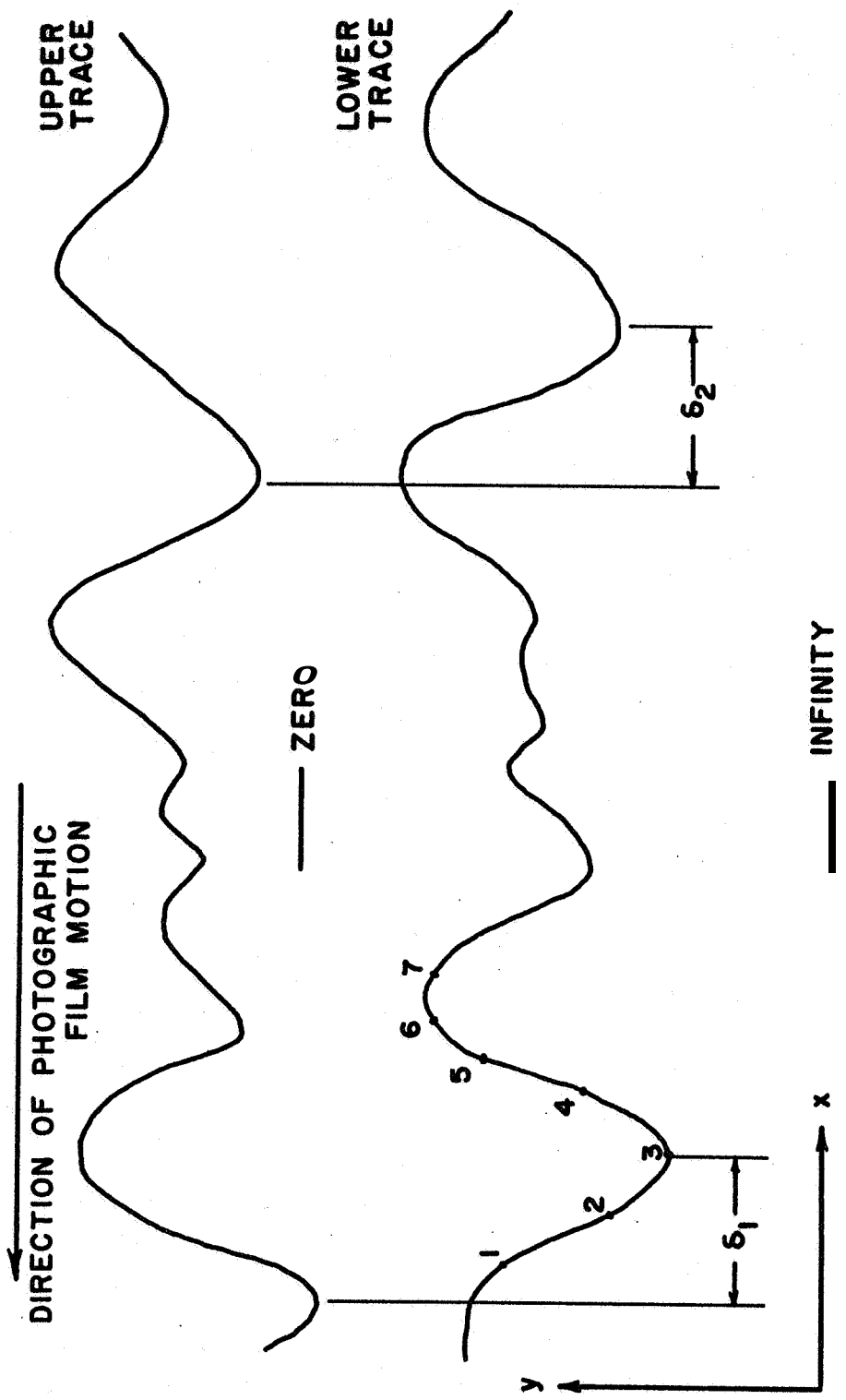

Fig 32 Schematic Diagram of an Oscillograph-Record Camera Trace

where

δ = displacement for a given wave on the two traces, in.

Accordingly, the wave velocity is given by

$$V_W = 0.208/\delta \qquad \text{(E-11)}$$

If the traces are enlarged so that they can be more easily read, as was done in the subject investigation, the numerator in Equation E-11 must be adjusted accordingly. The original 35mm film was projected onto the screen of a Recordak Library Film Reader Model C (Eastman Kodak) with an enlargement ratio of 1:15.2. The projected profiles were traced on rectangular coordinate graph paper having 10 lines per cm. The corresponding equation for determining the wave velocity is

$$V_W = 80.3/\delta_e \qquad \text{(E-12)}$$

where

δ_e = wave displacement on the enlarged tracing in mm. On each length of negative examined, it was possible to measure the displacements of several waves. The displacements for each length of negative examined were averaged, and the average value of the displacement was employed for calculating the average wave velocity for that particular length, employing equation E-12.

E.3 Surface Area

The enlarged traces of the waves, referred to in the previous section, were also employed for determining the surface area of the liquid film, The method employed for calculating that surface area was based on the following two assumptions:

1. All points of the surface of the liquid film move with the same velocity; the film velocity being the average wave velocity as determined in the previous section.

2. The surface of the liquid is two-dimensional; i.e., at a given time, the geometry of the surface for any section of the liquid film intersected by a plane passing through the axis of the test section is identical to the geometry of the surface as determined herein.

Assumption 1 is necessary for converting the distance on the photographic trace of a wave to distance on the liquid film. Assumption 2 results in the fractional increase in surface area being equal to the fractional increase in the length of the profile of the surface of the liquid film.

To determine the shape of the surface of the liquid film, the scale of the photographic trace presented in Fig. 32 had to be changed; that is, the ordinate which measures the output voltage from the photomultiplier tube had to be converted into the units for measuring the thickness of the liquid film, and the horizontal scale had to be converted from the distance of the trace of the oscillograph-record to distance along the liquid film.

To facilitate the calculations, a trace, such as that presented in Fig. 32, was approximated by a series of straight line segments. The end points of the segments, lying on the trace, were given x and y coordinate values, as read from the graph paper on which the enlarged tracing was made. The y coordinates of zero and infinity readings (see Section C.2) were also read from the graph paper. They are denoted by y_0 and y_i, respectively.

Refer to Fig. 32 and consider point 1, having the coordinates x_1 and y_1 on the enlarged trace. The transformed ordinate y_1', which is the film thickness in inches for point 1, is determined by the method of Section E.1. Thus

$$y_1' = - \frac{\ln\left(\frac{y_1 - y_i}{y_o - y_i}\right)}{bc} \qquad \text{(E-13)}$$

where bc is determined as before.

The transformed abscissa x_1', measured from some arbitrary reference, is determined as follows: First, based upon the photographic film speed and the scale factor, the coordinate x_1 is converted to a time, measured from a reference corresponding to the reference of x_1. Thus

$$\tau_1 = \frac{x_1}{3860} \qquad \text{(E-14)}$$

where

τ_1 = time coordinate of point 1, sec

The time scale is then converted to a scale corresponding to the distance in inches along the liquid film. That conversion makes use of the averaqe wave velocity, Thus

$$x_1' = 12\, V_W\, \tau_1 \qquad \text{(E-15)}$$

Hence the transformation from x_1 *to* x_1' becomes

$$x_1' = \frac{V_W\, x_1}{322} \qquad \text{(E-16)}$$

Each coordinate point describing the oscillograph-record trace was transformed to an equivalent point describing the geometric profile of the liquid film. The result of that transformation was a series of end points of line segments, approximating the surface of the liquid film. The increase in the surface area of the liquid film was then obtained by determining the increase in the length of the line segments, compared with the axial straight line distance they represented. The surface area factor ΔA for the segment between points 1 and 2 is given by

$$\Delta A_{12} = \sqrt{(x_2'-x_1')^2 + (y_2'-y_1')^2} \qquad \text{(E-17)}$$

Hence for a given oscillograph-record camera trace,

$$\Delta A = \sum_{i=1}^{N} \frac{\sqrt{(x_{i+1}'-x_i')^2 + (y_{i+1}'-y_i')^2}}{x_{i+1}'-x_i'} \qquad \text{(E-18)}$$

where

N = the number of straight line segments approximating the trace

APPENDIX F

SAMPLE CALCULATIONS

The sample calculations presented here illustrate the procedures employed in calculating the pertinent paramenters from experimental data. The calculations given are those for determining the measured and calculated values of the Sherwood number, the mean film thickness, the wave velocity, and the interfacial surface area.

F.1 Measured Sherwood Number

The following subscripts are employed in this section:

a air

v vapor

w water

i inlet

o outlet

All of the symbols employed here are either self-explanatory or are presented in Appendix A.

For the calculation of the dimensionless groups the properties were evaluated at the following temperatures:

Re_a: $(T_{ai} + T_{ao})/2$

Re_w: $(T_{wi} + T_{wo})/2$

Sc, Sh: $(T_{ai} + T_{ao} + T_{wi} + T_{wo})/4$

The values of μ_a, μ_w, and D were taken from the references indicated below.

μ_a: Reference 34

μ_w: Reference 35

D: Reference 56

The following measured variables were employed in the calculations; for example, from Run No. 623. Thus

Test section diameter, d	1.500 in.
Test section length, L	23.53 in.
Metering orifice pressure drop, ΔP_{or}	10.2 cm H_2O
Metering orifice upstream static pressure, P_{or}	8.5 cm Hg gage
Inlet air sample dry bulb temperature, T_{dbi}	25.6 C
Inlet air sample wet bulb temperature, T_{wbi}	8.9 C
Outlet air sample dry bulb temperature, T_{dbo}	35.25 C
Outlet air sample wet bulb temperature, T_{wbo}	18.6 C
Metering orifice air temperature, T_{or}	376.4 F
Inlet air temperature, T_{ai}	226.6 F
Outlet air temperature, T_{ao}	195.4 F
Inlet water temperature, T_{wi}	83.8 F
Outlet water temperature, T_{wo}	90.9 F
Test section average static pressure, P_{av}	15.93 psia
Atmospheric pressure, P_{atm}	29.43 in. Hg abs
Inlet water weight rate of flow, W_{wi}	0.00418 lb/sec

Air weight flow rate (Reference 53):

$$W_a = K A_2 Y F\sqrt{2g \gamma_{or} (\Delta P_{or})}$$

where

K = flow coefficient

A_2 = orifice area, ft^2

Y = velocity of approach factor

F = thermal expansion factor

γ_{or} = specific weight of the air upstream from the orifice, lb/ft^3

$$W_a = 0.07997 \left(1 - \frac{0.004243\ \Delta P_{or}}{0.1934\ P_{or} + 0.4912 P_{atm}}\right) [1 + 0{,}000018\ (T_{or} - 70)]$$

$$\sqrt{\frac{\Delta P_{or}(0.1934\ P_{or} + 0.4912 P_{atm})}{T_{or} + 460}}$$

$$= 0.0378\ lb/sec$$

Inlet air specific humidity (Reference *63):*

$$\omega = \frac{c_{pa}\ (t_2 - t_1) + \dfrac{h_{fg2}\ R_a\ T_2}{(p_m - p_{g2}) v_{g2}}}{h_{g1} - h_{f2}}$$

where

1 = at the dry-bulb temperature

2 = at the wet-bulb temperature

$$\omega = \frac{0.4315\ (T_{wb} - T_{db}) + \dfrac{53.35\ (1.8 T_{wb} + 491.7)\ (h_{fg})_{wb}}{(v_g)_{wb}\ [70.73\ P_{atm} - 144\ (p_v)_{wb}]}}{(h_g)_{db} - (h_f)_{wb}}$$

$$\omega_i = \frac{0.4315(8.9-25.6) + \frac{53.35(1.8^\circ 8.9 + 491.7)1066.7}{1829(70.73^\circ 29.43\text{-}1\ 44^\circ 0.165)}}{1095.6\text{-}16.0} = 0{,}000443 \text{ lb/lb}$$

Outlet air specific humidity:

$$\omega o = \frac{0.4315(18.6-35.25) + \frac{53.35(1.8^\circ 18.6 + 491.7)1056.7}{1005\ 70.73^\circ 29.43 - 144^\circ 0.311)}}{1103.1 - 33.5} = 0.006800 \text{ lb/lb}$$

Vapor weight flow rate:

$$W_{vi} = \frac{\omega_i W_a}{1 + \omega_i} = 0.000017 \text{ lb/sec}$$

$$W_{vo} = \frac{\omega_o W_a}{1 + \omega_i} = 0.000257 \text{ lb/sec}$$

Weight flow rate of evaporation:

$$W_{ev} = W_{vo} - W_{vi} = 0.000240 \text{ lb/sec}$$

Inlet vapor concentration difference:

$$\Delta C = \left(\frac{p_v}{R_v\ (T_v + 460)}\right)_w - \frac{\omega p_m}{(R_v \omega + R_a)\ (T_a + 460)}$$

$$\Delta C = \frac{1.679\ (p_v)_w}{T_w + 460} - \frac{144\ \omega\ (P_{av})}{(85.78\omega + 53.35)\ (T_a + 460)}$$

$$\Delta C_i = \frac{1.679(0.5734)}{83.8 + 460} - \frac{144(0.000443)15.93}{(85.78^\circ 0.000443 + 53.35)\ \ (226.6 + 460)}$$

$$= 0.00176 \text{ lb/ft}^3$$

Outlet vapor concentration difference:

$$\Delta C_o = \frac{1.679(0.7182)}{90.9 + 460} - \frac{144(0.006800)\ 15.93}{(85.78 \cdot 0.006800 + 53.35)\ (195.4 + 460)}$$

$$= 0{,}00169\ \text{lb/ft}^3$$

Log mean vapor concentration difference:

$$\Delta C_m = \frac{\Delta C_i - \Delta C_o}{\ln(\Delta C_i / \Delta C_o)} = 0.00173\ \text{lb/ft}^3$$

Mass transfer coefficient (equation D-2):

$$h_M = \frac{45.83\ W_{ev}}{d\ L\ (\Delta C_m)} = 0.1805\ \text{ft/sec}$$

Measured Sherwood number (equation D-1)

$$Sh = \frac{h_M d}{12D} = \frac{0.1805(1.500)}{12(0.000326)} = 69.2$$

Air Reynolds number (equation 4):

$$Re_a = \frac{0.475\ W_a}{\mu_a d} = \frac{0.475(0.0378)}{0.000000447\ (1.500)} = 26{,}350$$

Schmidt number (equation 4):

$$Sc = \frac{\mu_a}{\rho_a D_a} = \frac{0.000000423}{0.00220(0.000327)} = 0.589$$

Mass transfer group:

$$Sh/Re^{0.83}\ Sc^{0.44} = 0.0188$$

Water Reynolds number (equation 7):

$$Re_W = \frac{1.491\ (W_{wi} - 0.5\ W_{ev})}{\pi d \mu_W} = \frac{1.491(0.00418 - 0.5'0.000240)}{3.1416\ (1.500)\ 0.00001646}$$

$$= 78.0$$

F.2 Calculated Sherwood Number

Due to the large number of computations involved in the step-by-step calculation, it is not practical to give a complete example here, Therefore only the results of the calculation for Run Nbk 623 are presented, including a comparison of the results with the experimentally measured values.

Parameter	Measured Value	Calculated Value
T_{ao}	195.4 F	195.7 F
T_{wo}	90.9 F	91.0 F
W_{ev}	0.000240 lb/sec	0.000239 lb/sec
Sh	69.2	67.8

The Sherwood number ratio R_{Sh} is then (equation D-23):

$$R_{Sh} = Sh / Sh_{calc} = 1.020$$

The agreement between the measured and calculated values of air and water temperatures for Run No. 623 is somewhat better than that obtained for most of the runs. Generally the values agreed within approximately 2 F.

F.3 Mean Film Thickness

The calculations presented in Sections F.3 through F.5 are based

upon Run No. 5525. The nomenclature is the same as that employed in Appendix E.

The pertinent data for the calculation of the mean film thickness are as follows:

Distance from test section inlet to point of measurement	20.25 in.
Inlet air temperature	242.2 F
Inlet water flow rate	0.00996 lb/sec
Outlet water flow rate (calculated)	0.00976 lb/sec
Calibration cell thickness	0.00984 in.
Calibration galvanometer readings:	i_r = 8.90
	= 14.34
	i_i = 1.20
	i_{rc} = 12.80
	i_{oc} = 14.48
	i_{ic} = 1.20
Run galvanometer readings:	i_{rr} = 8.80
	i_{or} = 10.95
	i_{ir} = 1.05

Inlet calibration factor (equation E-7):

$$bc_i = -\frac{\ln \frac{(i_r-i_i)\,(i_{oc}-i_{ic})}{(i_o-i_i)\,(i_{rc}-i_{ic})}}{t} = -\frac{\ln \frac{(8.90-1.20)\,(14.48-1.20)}{(14.34-1.20)\,(12.80-1.26)}}{0.00984}$$

$$= 40.7 \text{ in.}^{-1}$$

Calibration factor at point of measurement (equation E-8):

$$bc = bc_i \ (W_{Li}/W_L) = 40.7 \ (0.00996/0.00976) = 41.5 \text{ in.}^{-1}$$

Mean film thickness (equation E-4):

$$\delta = -\frac{\ln \frac{i_{rr}-i_{ir}}{i_{or}-i_{ir}}}{bc} = -\frac{\ln \frac{8.80-1.05}{10.95-1.05}}{41.5} = 0.0059 \text{ in.}$$

F.4 Wave Velocity

The following values of wave displacements were measured on the enlarged tracing of Run No. 525a:

54, 63, 50, 52, 50, 57, and 53 mm

The average value of the wave displacement is then 54.1 mm.

Wave velocity (equation E-12):

$$V_W = 80.3 \ / \ \delta_e = 80.3 \ / \ 54.1 = 1\text{-}48 \text{ fps}$$

F.5 Surface Area

The surface area factor will be calculated for a single segment only. The segment between points 42 and 43 of Run No, 525a will be employed. The pertinent data are:

y_o = 161.0 mm

y_i = - 7.0 mm

y_{42} = 105.0 mm

y43 = 123.5 mm

x_{42} = 254.0 mm

x_{43} = 275.0 mm

V_W = 1.48 fps

bc = 41.5 $in.^{-1}$

Transformed y coordinates (equation E-13):

$$y_{42}' = -\frac{\ln\left(\frac{y_{42}-y_i}{y_o-y_i}\right)}{bc} = -\frac{\ln\frac{105.0+7.0}{(161.0+7.0)}}{41.5} = 0.00976 \text{ in.}$$

$$y_{43}' = -\frac{\ln\frac{123.5+7.0}{(161.0+7.0)}}{41.5} = 0.00608 \text{ in.}$$

Transformed x coordinates (equation E-16):

$$x_{42}' = \frac{V_W x_{42}}{322} = \frac{1.48\ (254.0)}{322} = 1.168 \text{ in.}$$

$$x_{43}' = \frac{1.48\ (275.0)}{322} = 1.304 \text{ in.}$$

Surface area increase factor for segment 42-43 (equation E-17):

$$\Delta A_{42,43} = \frac{\sqrt{(x_{43}'-x_{42}')^2 + (y_{43}'-y_{42}')^2}}{x_{43}'-x_{42}'} = \frac{\sqrt{(0.136)^2 + (0.00368)^2}}{0.136}$$

$$= 1.0004$$

APPENDIX G

TABULATED DATA

Table 2 presents the experimental data and the pertinent calculated parameters for the mass transfer experiments.

TABLE 2

Data for Mass Transfer Experiments

RUN NO.	TEST SECTION LENGTH (IN.)	AIR VEL. (FPS)	AIR RE. NO.	AIR INLET TEMP. (F)	AIR OUTLET TEMP. (F)	AIR INLET HUMIDITY (LB/LB)	AIR OUTLET HUMIDITY (LB/LB)	STATIC PRESS. (PSIA)	WATER INLET RATE (LB/SEC)	WATER RE. NO.	WATER INLET TEMP. (F)	WATER OUTLET TEMP. (F)	SHER. NO.	SHER. NO. RATIO
210	8.5	47.4	36492.	103.	99.	0.00040	0.00175	16.3	0.00152	24.	80.	63.	96.6	1.051
211	8.5	47.3	36239.	105.	101.	0.00044	0.00179	16.3	0.00188	29.	80.	64.	94.6	1.007
212	8.5	47.4	36394.	104.	100.	0.00044	0.00184	16.3	0.00285	45.	80.	65.	96.7	0.988
213	8.5	47.4	36406.	104.	100.	0.00044	0.00193	16.3	0.00418	67.	79.	67.	102.4	1.023
214	8.5	47.4	36219.	105.	102.	0.00039	0.00197	16.3	0.00609	99.	78.	70.	103.6	1.027
215	8.5	47.3	36225.	105.	101.	0.00039	0.00205	16.3	0.00996	164.	78.	72.	104.2	1.025
216	8.5	47.4	36319.	105.	101.	0.00043	0.00206	16.3	0.01573	263.	78.	74.	99.9	0.978
217	8.5	47.4	36226.	105.	102.	0.00043	0.00206	16.3	0.02649	444.	77.	75.	98.6	0.966
218	8.5	47.3	36017.	107.	102.	0.00039	0.00211	16.3	0.04355	730.	77.	75.	103.6	1.020
219	8.5	47.3	36057.	107.	102.	0.00038	0.00205	16.3	0.07182	1199.	76.	75.	101.2	0.995
220	8.5	48.3	26076.	228.	210.	0.00048	0.00346	15.9	0.00152	28.	86.	91.	79.5	0.989
221	8.5	48.1	25880.	230.	211.	0.00048	0.00341	15.9	0.00188	35.	85.	90.	78.8	0.990
222	8.5	48.1	25901.	230.	211.	0.00046	0.00332	15.9	0.00285	53.	84.	89.	80.7	1.025
223	8.5	48.0	25866.	230.	210.	0.00048	0.00319	15.9	0.00418	77.	82.	88.	79.3	1.020
224	8.5	48.4	26263.	226.	207.	0.00047	0.00301	15.9	0.00609	110.	80.	85.	82.6	1.057
225	8.5	48.3	26309.	225.	206.	0.00047	0.00282	15.9	0.00996	179.	80.	83.	78.2	1.006
226	8.5	48.3	26264.	225.	207.	0.00049	0.00274	15.9	0.01573	276.	79.	81.	79.5	1.027
227	8.5	47.9	26022.	227.	207.	0.00047	0.00259	15.9	0.02649	460.	78.	80.	76.5	0.997
228	8.5	47.9	26143.	225.	205.	0.00051	0.00245	15.9	0.04355	750.	78.	79.	72.3	0.939
229	8.5	47.7	26012.	225.	205.	0.00051	0.00241	15.9	0.07182	1228.	77.	78.	71.6	0.934
230	8.5	49.5	20276.	350.	321.	0.00049	0.00555	15.7	0.00152	32.	94.	107.	66.1	0.946
231	8.5	49.5	20269.	350.	320.	0.00051	0.00536	15.7	0.00188	39.	91.	106.	67.1	0.957
232	8.5	49.4	20227.	351.	321.	0.00051	0.00503	15.7	0.00285	59.	88.	106.	66.1	0.979
233	8.5	49.4	20198.	351.	321.	0.00051	0.00454	15.7	0.00418	85.	85.	103.	64.4	0.985
234	8.5	49.3	20192.	350.	319.	0.00053	0.00419	15.7	0.00609	119.	84.	95.	67.5	1.062
235	8.5	49.1	20160.	350.	318.	0.00050	0.00368	15.7	0.00996	190.	83.	91.	63.1	1.013
236	8.5	49.1	20157.	350.	317.	0.00050	0.00333	15.7	0.01573	289.	80.	87.	62.5	1.013
237	8.5	48.9	19987.	353.	319.	0.00050	0.00313	15.7	0.02649	478.	80.	85.	60.6	0.993
238	8.5	48.8	19970.	352.	317.	0.00050	0.00298	15.7	0.04355	768.	79.	82.	60.6	0.995
239	8.5	48.4	19755.	354.	319.	0.00050	0.00290	15.7	0.07182	1248.	78.	80.	60.5	1.003
310	16.5	47.5	36046.	107.	101.	0.00008	0.00212	16.1	0.00152	23.	79.	63.	75.4	0.994
311	16.5	47.5	36011.	107.	100.	0.00008	0.00221	16.1	0.00188	29.	79.	63.	79.0	1.009
312	16.5	47.5	36086.	106.	100.	0.00010	0.00230	16.1	0.00285	44.	78.	64.	82.9	1.007
313	16.5	47.5	35992.	106.	101.	0.00012	0.00245	16.1	0.00418	65.	77.	65.	87.2	1.025
314	16.5	47.5	35939.	107.	101.	0.00014	0.00257	16.1	0.00609	96.	76.	67.	89.0	1.026

Table 2 (Continued)

RUN NO.	TEST SECTION LENGTH (IN.)	AIR VEL. (FPS)	AIR RE NO	AIR INLET TEMP. (F)	AIR OUTLET TEMP. (F)	AIR INLET HUMIDITY (LB/LB)	AIR OUTLET HUMIDITY (LB/LB)	STATIC PRESS. (PSIA)	WATER INLET RATE (LB/SEC)	WATER RE. NO.	WATER INLET TEMP. (F)	WATER OUTLET TEMP. (F)	SHER. NO.	SHER. NO. RATIO
315	16.5	47.5	35897.	107.	101.	0.00014	0.00274	16.1	0.00996	159.	76.	69.	91.7	1.044
316	16.5	47.5	35969.	107.	101.	0.00014	0.00276	16.1	0.01573	254.	76.	71.	90.6	1.023
317	16.5	47.5	35905.	107.	101.	0.00018	0.00286	16.1	0.02649	429.	76.	72.	91.7	1.035
318	16.5	47.4	35754.	108.	102.	0.00020	0.00293	16.1	0.04355	708.	75.	73.	92.7	1.049
319	16.5	47.5	35857.	107.	102.	0.00029	0.00298	16.1	0.07182	1174.	75.	73.	90.4	1.020
320	16.5	48.3	26348.	228.	205.	0.00023	0.00507	15.8	0.00152	28.	88.	90.	67.2	0.948
321	16.5	48.4	26401.	228.	205.	0.00023	0.00507	15.8	0.00188	35.	86.	90.	69.5	0.971
322	16.5	48.4	26454.	228.	204.	0.00023	0.00497	15.8	0.00285	53.	83.	90.	71.5	0.996
323	16.5	48.4	26424.	228.	204.	0.00023	0.00474	15.8	0.00418	76.	81.	88.	71.6	1.011
324	16.5	48.2	26349.	228.	203.	0.00020	0.00449	15.8	0.00609	109.	80.	85.	73.8	1.059
325	16.5	48.2	26318.	229.	203.	0.00020	0.00414	15.8	0.00996	176.	79.	84.	70.4	1.027
326	16.5	48.1	26330.	229.	202.	0.00026	0.00395	15.8	0.01573	273.	77.	81.	70.5	1.035
327	16.5	48.0	26252.	229.	202.	0.00024	0.00378	15.8	0.02649	453.	76.	80.	70.0	1.036
328	16.5	48.1	26454.	227.	200.	0.00028	0.00361	15.8	0.04355	731.	76.	77.	70.2	1.033
329	16.5	47.9	26261.	228.	201.	0.00028	0.00349	15.8	0.07182	1187.	75.	76.	70.3	1.041
330	16.5	48.8	20485.	348.	301.	0.00022	0.00877	15.6	0.00152	30.	91.	107.	62.8	0.959
331	16.5	48.7	20518.	347.	300.	0.00022	0.00844	15.6	0.00188	38.	88.	106.	63.2	0.955
332	16.5	48.7	20491.	348.	300.	0.00022	0.00806	15.6	0.00285	57.	84.	106.	64.3	0.993
333	16.5	48.6	20474.	347.	299.	0.00022	0.00753	15.6	0.00418	84.	83.	104.	62.8	1.022
334	16.5	48.6	20494.	346.	298.	0.00025	0.00676	15.6	0.00609	119.	80.	101.	61.1	1.039
335	16.5	48.6	20489.	348.	297.	0.00025	0.00586	15.6	0.00996	189.	78.	96.	58.9	1.044
336	16.5	48.5	20457.	348.	297.	0.00029	0.00512	15.6	0.01573	291.	78.	92.	55.0	0.998
337	16.5	48.4	20514.	346.	295.	0.00029	0.00454	15.6	0.02649	473.	76.	87.	53.9	0.986
338	16.5	48.4	20494.	347.	295.	0.00029	0.00420	15.6	0.04355	751.	76.	81.	54.7	1.006
339	16.5	48.5	20555.	346.	294.	0.00029	0.00389	15.6	0.07182	1203.	74.	78.	54.9	1.008
610	23.5	47.6	36083.	111.	103.	0.00031	0.00297	16.3	0.00152	24.	83.	65.	65.4	0.974
611	23.5	47.4	35936.	111.	103.	0.00031	0.00311	16.3	0.00188	30.	83.	65.	68.7	0.994
612	23.5	47.5	36004.	111.	102.	0.00031	0.00320	16.3	0.00285	45.	83.	65.	71.3	0.969
613	23.5	47.5	36098.	110.	102.	0.00023	0.00331	16.3	0.00418	67.	82.	67.	75.9	0.979
614	23.5	47.6	36159.	109.	102.	0.00031	0.00353	16.3	0.00609	99.	81.	68.	79.5	0.990
615	23.5	47.4	35858.	111.	103.	0.00031	0.00371	16.3	0.00996	164.	80.	71.	80.7	0.985
616	23.5	47.5	36001.	110.	102.	0.00027	0.00385	16.3	0.01573	262.	79.	73.	83.8	1.007
617	23.5	47.5	36163.	108.	102.	0.00035	0.00396	16.3	0.02649	443.	78.	74.	84.0	0.999
618	23.5	47.5	35985.	110.	102.	0.00035	0.00394	16.3	0.04355	733.	78.	75.	81.6	0.973
619	23.5	47.4	36011.	109.	102.	0.00040	0.00398	16.3	0.07182	1206.	78.	75.	82.5	0.983

Table 2 (Continued)

RUN NO.	TEST SECTION LENGTH (IN.)	AIR VEL. (FPS)	AIR RE. NO.	AIR INLET TEMP. (F)	AIR OUTLET TEMP. (F)	AIR INLET HUMIDITY (LB/LB)	AIR OUTLET HUMIDITY (LB/LB)	STATIC PRESS. (PSIG)	WATER INLET RATE (LB/SEC)	WATER RUN NO.	WATER INLET TEMP. (F)	WATER OUTLET TEMP. (F)	SHER. NO.	SHER. NO. RATIO
620	23.5	47.7	26408.	229.	199.	0.00045	0.00715	15.9	0.00152	28.	88.	92.	65.8	0.974
621	23.5	48.0	26787.	226.	195.	0.00049	0.00700	15.9	0.00188	34.	85.	91.	68.9	0.992
622	23.5	48.0	26777.	226.	195.	0.00042	0.00695	15.9	0.00285	53.	84.	91.	70.6	1.022
623	23.5	48.0	26753.	227.	195.	0.00044	0.00680	15.9	0.00418	78.	84.	91.	69.2	1.020
624	23.5	47.9	26774.	226.	194.	0.00048	0.00651	15.9	0.00609	113.	83.	89.	68.4	1.022
625	23.5	47.9	26858.	225.	193.	0.00048	0.00613	15.9	0.00996	183.	82.	88.	67.3	1.020
626	23.5	47.8	26777.	225.	193.	0.00048	0.00576	15.9	0.01573	286.	81.	85.	66.0	1.012
627	23.5	47.6	26746.	225.	192.	0.00052	0.00556	15.9	0.02649	475.	79.	84.	65.7	1.014
628	23.5	47.5	26700.	224.	191.	0.00048	0.00530	15.9	0.04355	767.	78.	82.	66.2	1.026
629	23.5	47.1	26478.	225.	192.	0.00050	0.00538	15.9	0.07182	1248.	78.	80.	69.6	1.087
632	23.5	48.5	20859.	349.	287.	0.00029	0.01109	15.7	0.00285	57.	85.	108.	62.8	0.976
633	23.5	48.5	20925.	347.	285.	0.00029	0.01063	15.7	0.00418	85.	84.	107.	61.0	0.996
634	23.5	48.3	20882.	348.	284.	0.00029	0.00981	15.7	0.00609	124.	84.	106.	57.8	0.998
635	23.5	48.4	20925.	347.	283.	0.00025	0.00871	15.7	0.00996	200.	82.	103.	54.9	0.998
636	23.5	48.1	20822.	348.	282.	0.00021	0.00761	15.7	0.01573	305.	81.	97.	54.0	1.016
637	23.5	48.2	20910.	347.	281.	0.00023	0.00666	15.7	0.02649	495.	80.	90.	53.0	1.011
638	23.5	48.0	20804.	348.	281.	0.00021	0.00608	15.7	0.04355	797.	79.	88.	51.2	0.987
639	23.5	47.8	20679.	349.	281.	0.00025	0.00575	15.7	0.07182	1292.	79.	85.	50.0	0.972
710	32.4	47.2	36272.	108.	97.	0.00017	0.00332	16.2	0.00152	23.	78.	65.	61.6	0.938
711	32.4	47.1	36210.	108.	96.	0.00021	0.00344	16.2	0.00188	29.	78.	66.	63.2	0.938
712	32.4	47.0	36455.	104.	94.	0.00015	0.00355	16.2	0.00285	44.	78.	66.	67.7	0.958
713	32.4	47.1	36204.	108.	96.	0.00017	0.00380	16.2	0.00418	64.	76.	66.	73.8	0.992
714	32.4	47.2	36290.	107.	97.	0.00017	0.00400	16.2	0.00609	96.	76.	69.	75.4	0.980
715	32.4	47.1	36070.	108.	97.	0.00021	0.00427	16.2	0.00996	158.	76.	70.	78.5	0.997
716	32.4	47.1	36099.	108.	98.	0.00021	0.00452	16.2	0.01573	254.	76.	72.	81.1	1.016
717	32.4	47.1	35882.	110.	99.	0.00021	0.00473	16.2	0.02649	435.	75.	75.	81.0	1.012
718	32.4	47.2	36018.	109.	99.	0.00021	0.00478	16.2	0.04355	713.	75.	75.	83.1	1.033
719	32.4	47.2	35978.	109.	99.	0.00029	0.00489	16.2	0.07182	1184.	74.	76.	82.3	1.023
720	32.4	47.3	26649.	228.	188.	0.00024	0.00853	15.8	0.00152	26.	82.	92.	67.2	0.963
721	32.4	47.3	26745.	227.	187.	0.00020	0.00850	15.8	0.00188	33.	82.	91.	68.6	0.985
722	32.4	47.3	26687.	228.	187.	0.00019	0.00834	15.8	0.00285	50.	80.	91.	70.3	1.008
723	32.4	47.2	26672.	228.	187.	0.00019	0.00809	15.8	0.00418	75.	78.	92.	67.7	0.993
724	32.4	47.2	26664.	228.	186.	0.00019	0.00775	15.8	0.00609	108.	76.	89.	69.7	1.046
725	32.4	47.2	26691.	228.	186.	0.00019	0.00731	15.8	0.00996	177.	76.	88.	67.3	1.048
726	32.4	47.1	26707.	228.	184.	0.00023	0.00688	15.8	0.01573	272.	74.	85.	69.0	1.095

Table 2 (Comtinued)

RUN NO.	TEST SECTION LENGTH (IN.)	AIR VEL. (FPS)	AIR RE. NO.	AIR INLET TEMP. (F)	AIR OUTLET TEMP. (F)	AIR INLET HUMIDITY (LB/LB)	AIR OUTLET HUMIDITY (LB/LB)	STATIC PRESS. (PSIA)	WATER INLET RATE (LB/SEC)	WATER RE. NO.	WATER INLET TEMP. (F)	WATER OUTLET TEMP. (F)	SHER. NO.	SHER. NO. RATIO
727	32.4	46.9	26509.	230.	185.	0.00023	0.00639	15.8	0.02649	456.	74.	83.	64.5	1.044
728	32.4	46.8	26479.	230.	185.	0.00019	0.00604	15.8	0.04355	738.	74.	80.	64.4	1.048
729	32.4	46.7	26466.	229.	184.	0.00023	0.00585	15.8	0.07182	1201.	74.	78.	64.6	1.055
731	32.4	48.1	21460.	343.	266.	0.00006	0.01468	15.7	0.00188	37.	92.	110.	57.1	0.930
732	32.4	48.0	21304.	345.	267.	0.00008	0.01423	15.7	0.00285	58.	90.	110.	56.0	0.922
733	32.4	48.1	21440.	344.	265.	0.00008	0.01369	15.7	0.00418	85.	86.	109.	58.8	0.965
734	32.4	48.1	21459.	343.	264.	0.00007	0.01283	15.7	0.00609	125.	85.	108.	56.4	0.967
735	32.4	47.7	21286.	345.	263.	0.00005	0.01158	15.7	0.00996	201.	81.	106.	55.1	1.004
736	32.4	47.8	21414.	343.	261.	0.00005	0.01020	15.7	0.01573	311.	80.	102.	52.9	1.001
737	32.4	47.8	21437.	343.	259.	0.00008	0.00878	15.7	0.02649	506.	79.	96.	50.8	0.987
738	32.4	47.6	21369.	343.	258.	0.00008	0.00794	15.7	0.04355	801.	79.	89.	51.6	1.015
739	32.4	47.5	21350.	343.	257.	0.00010	0.00732	15.7	0.07182	1266.	76.	84.	53.6	1.061
914	39.9	47.3	36003.	116.	101.	0.00043	0.00579	16.4	0.00609	105.	84.	76.	68.2	0.954
920	39.9	47.6	27236.	228.	183.	0.00051	0.01059	16.0	0.00152	27.	90.	94.	60.4	0.955
921	39.9	47.8	27519.	225.	181.	0.00053	0.01036	16.0	0.00188	34.	89.	94.	60.5	0.942
922	39.9	47.4	27205.	228.	180.	0.00044	0.01085	16.0	0.00285	53.	88.	94.	64.6	1.010
923	39.9	47.3	27106.	229.	181.	0.00043	0.01073	16.0	0.00418	79.	87.	94.	64.6	1.011
924	39.9	47.2	27005.	230.	181.	0.00042	0.01065	16.0	0.00609	116.	85.	94.	65.3	1.027
925	39.9	47.4	27202.	228.	180.	0.00046	0.01017	16.0	0.00996	191.	85.	92.	64.2	1.026
926	39.9	47.3	27163.	228.	179.	0.00050	0.00956	16.0	0.01573	298.	84.	90.	63.3	1.024
927	39.9	47.2	27184.	228.	178.	0.00043	0.00896	16.0	0.02649	496.	83.	89.	61.9	1.008
928	39.9	46.7	26781.	230.	179.	0.00045	0.00856	16.0	0.04355	804.	82.	87.	60.7	1.006
929	39.9	46.4	26663.	230.	178.	0.00044	0.00816	16.0	0.07182	1304.	80.	86.	60.2	1.003
930	39.9	47.6	21153.	355.	261.	0.00057	0.01771	15.6	0.00152	28.	95.	111.	51.1	0.874
931	39.9	47.6	21180.	353.	261.	0.00057	0.01757	15.6	0.00188	36.	93.	110.	53.4	0.897
932	39.9	47.6	21201.	353.	260.	0.00051	0.01729	15.6	0.00285	57.	91.	110.	54.4	0.905
933	39.9	47.6	21231.	353.	259.	0.00051	0.01697	15.6	0.00418	86.	90.	109.	55.2	0.938
934	39.9	47.6	21248.	353.	258.	0.00053	0.01655	15.6	0.00609	127.	88.	108.	55.7	0.978
935	39.9	47.5	21210.	353.	258.	0.00046	0.01558	15.6	0.00996	207.	87.	106.	55.3	1.029
936	39.9	47.2	21085.	355.	256.	0.00050	0.01385	15.6	0.01573	323.	85.	104.	51.2	1.000
937	39.9	47.2	21123.	354.	255.	0.00055	0.01240	15.6	0.02649	530.	84.	99.	50.3	1.013
938	39.9	46.9	21023.	355.	254.	0.00050	0.01093	15.6	0.04355	850.	83.	95.	47.5	0.973
939	39.9	46.7	20936.	355.	253.	0.00050	0.00989	15.6	0.07182	1346.	82.	89.	48.3	0.999